Chapter 2
Problems in Plane Stress

In many problems of practical interest, it is a reasonable approximation to disregard the elastic component of strain in the theoretical analysis, even when the body is only partially plastic. In effect, we are then dealing with a hypothetical material which is rigid when stressed below the elastic limit, the modulus of elasticity being considered as infinitely large. If the plastically stressed material has the freedom to flow in some direction, the distribution of stress in the deforming zone of the assumed rigid/plastic body would approximate that in an elastic/plastic body, except in a transition region near the elastic/plastic interface where the deformation is restricted to elastic order of magnitude. The assumption of rigid/plastic material is generally adequate not only for the analysis of technological forming processes, where the plastic part of the strain dominates over the elastic part, but also for the estimation of the yield point load when the rate of work-hardening is sufficiently small (Section 1.2). In this chapter, we shall be concerned with problems in plane stress involving rigid/plastic bodies which are loaded beyond the range of contained plastic deformation.

2.1 Formulation of the Problem

A plate of small uniform thickness is loaded along its boundary by forces acting parallel to the plane of the plate and distributed uniformly through the thickness. The stress components σ_z, τ_{xz}, and τ_{yz} are zero throughout the plate, where the z-axis is considered perpendicular to the plane. The state of stress is therefore specified by the three remaining components σ_x, σ_y, and τ_{xy}, which are functions of the rectangular coordinates x and y only. During the plastic deformation, the thickness does not generally remain constant, but the stress state may still be regarded as approximately plane provided the thickness gradient remains small compared to unity.

2.1.1 Characteristics in Plane Stress

For greater generality, we consider a nonuniform plate of small thickness gradient, subjected to a state of generalized plane stress in which σ_x, σ_y, and τ_{xy} denote the

J. Chakrabarty, *Applied Plasticity, Second Edition*, Mechanical Engineering Series,
DOI 10.1007/978-0-387-77674-3_2, © Springer Science+Business Media, LLC 2010

stress components averaged through the thickness of the plate. In the absence of body forces, the equations of equilibrium are

$$\frac{\partial}{\partial x}(h\sigma_x) + \frac{\partial}{\partial y}(h\tau_{xy}) = 0, \quad \frac{\partial}{\partial x}(h\tau_{xy}) + \frac{\partial}{\partial y}(h\sigma_y) = 0, \tag{2.1}$$

where h is the local thickness of the plate. If yielding occurs according to the von Mises criterion, the stresses must also satisfy the equation

$$\sigma_x^2 - \sigma_x\sigma_y + \sigma_y^2 + 3\tau_{xy}^2 = \sigma_1^2 - \sigma_1\sigma_2 + \sigma_2^2 = 3k^2, \tag{2.2}$$

where σ_1 and σ_2 are the principal stresses in the xy-plane, and k is the yield stress in pure shear equal to $1/\sqrt{3}$ times the uniaxial yield stress Y. In the (σ_1, σ_2)-plane, (2.2) represents an ellipse having its major and minor axes bisecting the axes of reference.

Suppose that the stresses are given along some curve C in the plastically deforming region. The thickness h is regarded as a known function of x and y at the instant under consideration. Through a generic point P on C, consider the rectangular axes (x, y) along the normal and tangent, respectively, to C. If we rule out the possibility of a stress discontinuity across C, the tangential derivatives $\partial\sigma_x/\partial y$,$\partial\sigma_y/\partial y$, and $\partial\tau_{xy}/\partial y$ must be continuous. Since $\partial h/\partial x$ and $\partial h/\partial y$ are generally continuous, the equilibrium equation (2.1) indicates that $\partial\sigma_x/\partial x$ and $\partial\tau_{xy}/\partial x$are also continuous across c. For given values of these derivatives, the remaining normal derivative $\partial\sigma_y/\partial x$ can be uniquely determined from the relation

$$(2\sigma_x - \sigma_y)\frac{\partial\sigma_x}{\partial x} + (2\sigma_y - \sigma_x)\frac{\partial\sigma_y}{\partial x} + 6\tau_{xy}\frac{\partial\tau_{xy}}{\partial x} = 0 \tag{2.3}$$

obtained by differentiating the yield criterion (2.2), unless the coefficient $2\sigma_y - \sigma_x$ is zero. When $\sigma_x = 2\sigma_y$, the above equation gives no information about $\partial\sigma_y/\partial x$, which may therefore be discontinuous across C. It follows that S is a characteristic when the stress components are given by

$$\sigma_x = \sigma, \quad \sigma_y = \frac{1}{2}\sigma, \quad \tau_{xy} = \tau,$$

where σ is the normal stress, and τ the shear stress transmitted across C. In view of the yield criterion (2.2), the relationship between σ and τ is

$$\sigma^2 + 4\tau^2 = 4k^2 \tag{2.4}$$

which defines an ellipse E in the (σ, τ)-plane, as shown in Fig. 2.1. If ψ denotes the angle of inclination of the tangent to E with the σ-axis, reckoned positive when τ decreases in magnitude with increasing σ, then

$$\tan\psi = \mp\frac{d\tau}{d\sigma} = \pm\frac{\sigma}{4\tau} = \pm\left(\frac{\sigma_x - \sigma_y}{2\tau_{xy}}\right). \tag{2.5}$$

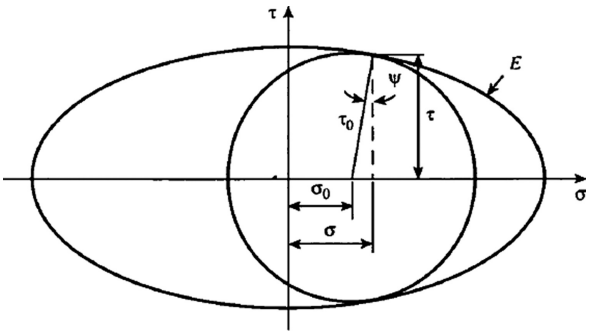

Fig. 2.1 Yield envelope for an element in a state of plane plastic stress including the associated Mohr circle for stress

The expression in the parenthesis is the cotangent of twice the counterclockwise angle made by either of the two principal stresses with the x-axis. It follows that there are two characteristic directions at each point, inclined at an angle $\pi/4 + \psi/2$ on either side of the algebraically greater principal stress direction. The two characteristics are identified as α- and β-lines following the convention indicated in Fig. 2.2, when $\sigma_1 > \sigma_2$. The two characteristics coincide when $\psi = \pm\pi/2$.

The normal and shear stresses acting across the characteristics are defined by the points of contact of the envelope E with Mohr's circle for the considered state of stress. The locus of the highest and lowest points of the circle is an ellipse representing the yield criterion (2.2), which may be written as

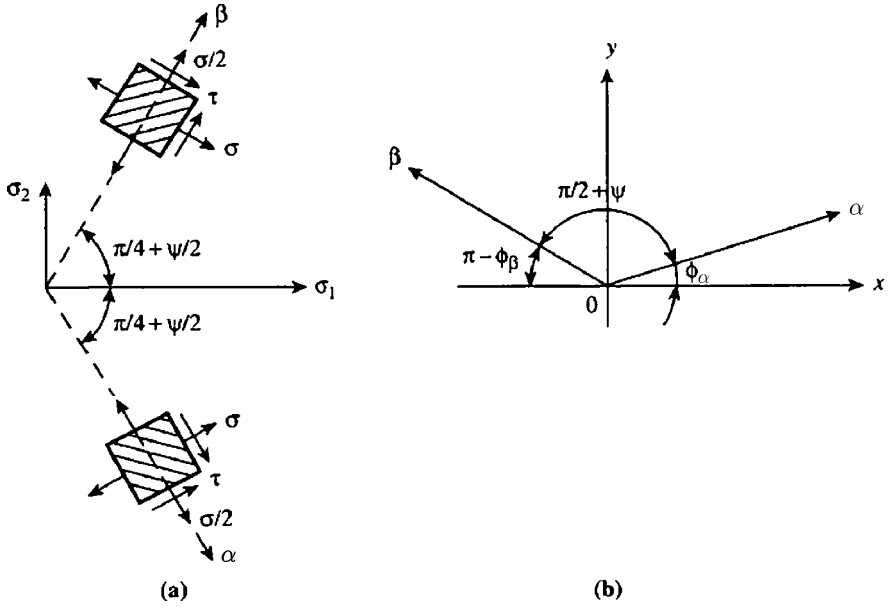

Fig. 2.2 Characteristics directions in plane stress ($\sigma_1 > \sigma_2 > 0$), designated by α- and β-lines

$$F(\sigma_0,\tau_0) = \sigma_0^2 + 3\tau_0^2 = 3k^2,$$

where

$$\sigma_0 = \frac{1}{2}(\sigma_1 + \sigma_2) = \frac{3}{4}\sigma, \quad \tau_0 = \frac{1}{2}(\sigma_1 - \sigma_2). \tag{2.6}$$

Thus, τ_0 is numerically equal to the maximum shear stress and σ_0 the mean normal stress in the plane. Since σ cannot exceed $2k$ in magnitude, the material being ideally plastic, σ_0 be numerically less than $3k/2$ and τ_0 numerically greater than $k/2$ for the characteristics to be real. Since $d\tau/d\sigma_0$ is equal to $-r\sin\psi$ in view of (2.6) and Fig. 2.1, the acute angle which the tangent to the yield locus makes with the σ-axis must be less than $\pi/4$ for the stress equations to be hyperbolic. When τ_0 is numerically less than $k/2$, there is no real contact between the Mohr circle and the envelope E, and the stress equations then become elliptic.

In the limiting case of $|\tau_0| = k/2$, the characteristics are coincident with the axis of the numerically lesser principal stress, the values of the principal stresses being $\pm(2k, k)$ in the limiting state.

2.1.2 Relations Along the Characteristics

When the equations are hyperbolic, it is convenient to establish equations giving the variation of the stresses along the characteristics. Following Hill (1950a), we take the axes of reference along the normal and tangent to a typical characteristic C at a generic point P as before. Setting $2\sigma_y = \sigma_x \tan\psi$ in (2.3), we get

$$\frac{\partial \tau_{xy}}{\partial x} \pm \tan\psi \frac{\partial \sigma_x}{\partial x} = 0,$$

where the upper sign corresponds to the β-line and the lower sign to the α-line, respectively. The substitution of $\partial\sigma_x/\partial x$ from above into the first equation of (2.1) gives

$$h\frac{\partial \tau_{xy}}{\partial x} \pm \tan\psi \frac{\partial \tau_{xy}}{\partial y} = \pm\left(\sigma_x \frac{\partial h}{\partial x} + \tau_{xy}\frac{\partial h}{\partial y}\right)\tan\psi.$$

Regarding the curve C as a β-line, we observe that the space derivatives along the σ and β-lines at P are

$$\frac{\partial}{\partial s_\alpha} = \cos\psi \frac{\partial}{\partial x} - \sin\psi \frac{\partial}{\partial y}, \quad \frac{\partial}{\partial s_\beta} = \frac{\partial}{\partial y},$$

and the preceding equation therefore reduces to

$$h\frac{\partial \tau_{xy}}{\partial s_\alpha} = \frac{\partial h}{\partial s_\alpha}\tan\psi + (\sigma\tan\psi + \tau)\sin\psi \frac{\partial h}{\partial s_\beta} \tag{2.7}$$

since $\sigma_x = \sigma$ and $\tau_{xy} = \tau$ at the considered point. To obtain the derivative $\partial\tau_{xy}/\partial s_\alpha$ at P, let ϕ_β denote the counterclockwise angle made by the tangent to C with an arbitrary fixed direction. If the x-axis is now taken in this direction, then

$$\tau_{xy} = -\frac{1}{4}\sigma \sin 2\phi_\beta - \tau \cos 2\phi_\beta .$$

Differentiating this expression partially with respect to s_α and then setting $\phi_\beta = \pi/2$. we obtain

$$\frac{\partial \tau_{xy}}{\partial s_\alpha} = \frac{1}{2}\sigma \frac{\partial \phi_\beta}{\partial s_\alpha} - \frac{\partial \tau}{\partial s_\alpha} = \tan\psi \left(2\tau \frac{\partial \phi_\beta}{\partial s_\alpha} - \frac{\partial \sigma}{\partial s_\alpha} \right)$$

in view of (2.5). Inserting in (2.7) and rearranging, the result can be expressed in the form

$$d(h\sigma) - 2h\tau d\phi_\beta = -(\sigma \sin\psi + \tau \cos\psi) \frac{\partial h}{\partial s_\beta} ds_\alpha \tag{2.8}$$

along an α-line. Similarly, considering the curve C to be an α-line, it can be shown that

$$d(h\sigma) + 2h\tau d\phi_\alpha = -(\sigma \sin\psi + \tau \cos\psi) \frac{\partial h}{\partial s_\alpha} ds_\beta \tag{2.9}$$

along a β-line, where ϕ_α is the counterclockwise orientation of the α-line with respect to the same fixed direction. Evidently, $d\phi_\beta$ - $d\phi_\alpha$=$d\psi$. If the thickness distribution is given, (2.8) and (2.9) in conjunction with (2.4) would enable us to determine the stress distribution and the characteristic directions in the hyperbolic part of the plastic region. When the thickness is uniform, (2.8) and (2.9) reduce to the relations

$$\left.\begin{aligned} d\sigma - 2\tau d\phi_\beta = 0 \quad \text{along an } \alpha - \text{line}, \\ d\sigma + 2\tau d\phi_\alpha = 0 \quad \text{along an } \beta - \text{line}, \end{aligned}\right\} \tag{2.10}$$

which are analogous to the well-known Hencky equations in plane strain. In the solution of physical problems, it is usually convenient to express the yield criterion parametrically through the angle ψ, or a related angle θ such that

$$\tan\theta = \sqrt{3}\sin\psi, \quad -\frac{\pi}{2} \le \psi \le \frac{\pi}{2}, \quad -\frac{\pi}{3} \le \theta \le \frac{\pi}{3}. \tag{2.11}$$

The angle θ denotes the orientation of the stress vector in the deviatoric plane with respect to the direction representing pure shear in the plane of the plate. Indeed, it follows from (2.4), (2.5), and (2.11) that

$$\left.\begin{aligned}\frac{\sigma}{k} &= \frac{4\sin\psi}{\sqrt{1+3\sin^2\psi}} = \frac{4}{\sqrt{3}}\sin\theta,\\ \frac{\tau}{k} &= \frac{\cos\psi}{\sqrt{1+3\sin^2\psi}} = \sqrt{1-\frac{4}{3}\sin^2\theta}.\end{aligned}\right\} \tag{2.12}$$

Since $2(\sigma_1+\sigma_2) = 3\sigma$ and $2(\sigma_1-\sigma_2) = \sqrt{\sigma^2+16\tau^2}$, we immediately get $\sigma_1+\sigma_2 = \sqrt{3}k\sin\theta$ and $\sigma_1-\sigma_2 = 2k\cos\theta$, and the principal stresses become

$$\sigma_1 = 2k\sin\left(\theta+\frac{\pi}{6}\right), \quad \sigma_2 = 2k\sin\left(\theta-\frac{\pi}{6}\right) \tag{2.13}$$

It is also convenient at this stage to introduce a parameter λ *w*hich is defined in the incremental form

$$d\lambda = \frac{1}{2}\left(\frac{d\sigma}{\tau} - d\psi\right) = 2\frac{d\sigma}{\sigma}\tan\psi - \frac{1}{2}d\psi$$

which is assumed to vanish with ψ or θ. Substituting from (2.12) and integrating, we get

$$\begin{aligned}\lambda &= \tan^{-1}(2\tan\psi) - \frac{1}{2}\psi\\ &= \sin^{-1}\left(\frac{2}{\sqrt{3}}\sin\theta\right) - \frac{1}{2}\sin^{-1}\left(\frac{1}{\sqrt{3}}\tan\theta\right).\end{aligned} \tag{2.14}$$

Evidently, $-\pi/4 \le \lambda \le \pi/4$ over the relevant range. If ω denotes the counterclockwise angle made by a principal stress axis with respect to a fixed axis, then

$$d\omega = d\left(\phi_\alpha + \frac{1}{2}\psi\right) = d\left(\phi_\beta + \frac{1}{2}\psi\right).$$

Dividing (2.8) and (2.9) by $h\sigma$ throughout, and substituting for $d\sigma/\sigma$, σ/τ, $d\phi_\alpha$, and $d\phi_\beta$, we finally obtain the relations

$$\left.\begin{aligned}d(\lambda-\omega) + 2\tan\psi\frac{dh}{h} &= -\left(\frac{1+3\sin^2\psi}{2h\cos\psi}\right)\frac{\partial h}{\partial s_\beta}ds_\alpha,\\ d(\lambda-\omega) + 2\tan\psi\frac{dh}{h} &= -\left(\frac{1+3\sin^2\psi}{2h\cos\psi}\right)\frac{\partial h}{\partial s_\alpha}ds_\beta.\end{aligned}\right\} \tag{2.15}$$

along the α- and β-lines, respectively. Similar equations may be written in terms of θ using (2.11). Numerical values of λ are given in Table 2.1 for the whole range of values of ψ and θ. When h is a constant, (2.15) reduces to

Table 2.1 Parameters for plane strees characteristics

Ψ degrees	Ψ Radians	λ radians	θ degrees	Ψ degrees	λ radians
0	0	0	0	0	0
10	0.17453	0.25177	10	5.843	0.15089
20	0.34907	0.4570	20	12.130	0.30013
30	0.52360	0.59527	30	19.471	0.44556
40	0.89813	0.68435	35	23.845	0.51581
50	0.87266	0.73722	40	28.977	0.58352
60	1.04720	0.76616	45	35.264	0.64757
70	1.22173	0.77992	50	55.542	0.75558
80	1.39626	0.78473	55	55.542	0.75558
90	1.57080	0.78540	60	90.000	0.78540

$$\left.\begin{aligned} \lambda - \omega &= \text{constant along an } \alpha\text{-line,} \\ \lambda - \omega &= \text{constant along a } \beta\text{-line,.} \end{aligned}\right\} \tag{2.16}$$

In analogy with Hencky's first theorem, we can state that the difference in values of both λ *a*nd ω between a pair of points, where two given characteristics of one family are cut by a characteristic of the other family, is the same for all intersecting characteristics. It follows that if a segment of one characteristic is straight, then so are the corresponding segments of the other members of the same family, the values of λ and ω being constant along each straight segment. If both families of characteristics are straight in a certain portion of the plastic region, the state of stress is uniform throughout this region.

2.1.3 The Velocity Equations

Let (v_x, v_y) denote the rectangular components of the velocity averaged through the thickness of the plate. The material is assumed as rigid/plastic, obeying the von Mises yield criterion and the Lévy–Mises flow rule. In terms of the stresses σ_x, σ_y, and τ_{xy}, the flow rule may be written as

$$\frac{\partial v_x/\partial x}{2\sigma_x - \sigma_y} = \frac{\partial v_y/\partial x}{2\sigma_y - \sigma_x} = \frac{\partial v_x/\partial y + \partial v_y/\partial x}{6\tau_{xy}}. \tag{2.17}$$

Consider a curve C along which the stress and velocity components are given, and let the x- and y-axes be taken along the normal and tangent, respectively, to C at a typical point P. Assuming the velocity to be continuous across C, the tangential derivatives dv_x/dy and dv_y/dy are immediately seen to be continuous. From (2.17), the normal derivatives dv_x/dx and dv_y/dx can be uniquely determined unless $2\sigma_y - \sigma_x = 0$, which corresponds to $dv_y/dy = 0$. Thus, C is a characteristic for the velocity field if it coincides with a direction of zero rate of extension. There are two such directions at each point and they are identical to those of the stress characteristics.

Since the characteristics are inclined at an angle $\pi/4+\psi/2$ to the direction of the algebraically greater principal strain rate $\dot{\varepsilon}_1$, the condition $\dot{\varepsilon} = 0$ along a characteristic gives

$$\sin\psi = \frac{\dot{\varepsilon}_1 + \dot{\varepsilon}_2}{\dot{\varepsilon}_1 - \dot{\varepsilon}_2} = \frac{1}{3}\left(\frac{\sigma_1 + \sigma_2}{\sigma_1 - \sigma_2}\right) = \frac{1}{\sqrt{3}}\tan\theta. \tag{2.18}$$

The range of plastic states for which the characteristics are real corresponds to $|\sigma_0| \leq 3|\tau_0|$ and are represented by the arcs AB and CD of the von Mises ellipse shown in Fig. 2.3. The numerically lesser principal strain rate vanishes in the limiting states, represented by the extremities of these arcs, where the tangents make an acute angle of $\pi/4$ with the σ_0-axis.

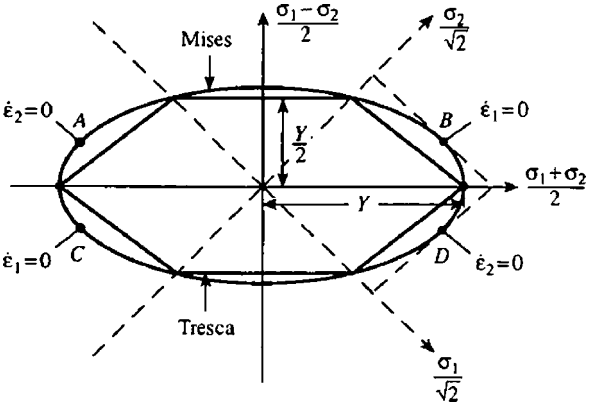

Fig. 2.3 Plane stress yield loci according to Tresca and von Mises for a material with a uniaxial yield stress Y

The velocity of a typical particle is the resultant of its rectangular components v_x and v_y. The resolved components of the velocity vector along the α and β-lines, denoted by u and v, respectively, are related to the rectangular components as

$$u = v_x\cos\phi_\alpha + v_y\sin(\psi + \phi_\alpha), \quad v = -v_x\sin\phi_\alpha + v_y\cos(\psi + \phi_\alpha),$$

where ϕ_α denotes the counterclockwise angle made by the α-line with the x-axis. The preceding relations are easily inverted to give

$$\left.\begin{aligned} v_x &= [u\cos(\psi + \phi_\alpha) - v\sin\phi_\alpha]\sec\psi, \\ v_y &= [u\sin(\psi + \phi_\alpha) - v\cos\phi_\alpha]\sec\psi. \end{aligned}\right\} \tag{2.19}$$

Differentiating v_x partially with respect to x, and using the fact that $dv_x/dx = 0$ when $\phi_\alpha = -\psi$, we obtain

$$\frac{\partial v}{\partial s_\alpha} - (u\tan\psi + v\sec\psi)\frac{\partial\phi_\alpha}{\partial s_\alpha} = 0.$$

Similarly, equating dv_y/dy to zero after setting $\phi_\alpha = -\psi$ in the expression for the partial derivative of v_y with respect to y, we get

$$\frac{\partial v}{\partial s_\beta} + (u \sec\psi + v \tan\psi)\frac{\partial \phi_\beta}{\partial s_\beta} = 0$$

in view of the relation $d\phi_\beta - d\phi_\alpha = d\psi$ The velocity relations along the characteristics therefore become

$$\left.\begin{aligned} du - (u \tan\psi + v\sec\psi)\, d\phi_\alpha = 0 \text{ along an } \alpha\text{-line,} \\ dv + (u \sec\psi + v\tan\psi)\, d\phi_\beta = 0 \text{ along an } \beta\text{-line,} \end{aligned}\right\} \tag{2.20}$$

When the characteristic directions are known at each point of the field, the velocity distribution can be determined from (2.20). For $\psi = 0$, these equations reduce to the well-known Geiringer equations in plane plastic strain.

Since the thickness strain rate has the same sign as that of $-(\sigma+\sigma_2)$, a thinning of the sheet corresponds to $\sigma_0 > 0$ and a thickening to $\sigma_0 < 0$. If the rate of change of thickness following the element is denoted by h, it follows from the associated flow rule that

$$\frac{\dot{h}}{h} = \frac{1}{h}\left(\frac{\partial h}{\partial t} + \omega\frac{\partial h}{\partial s}\right) = -\left(\frac{\sigma_\mathrm{n} + \sigma_1}{2\sigma_1 - \sigma_\mathrm{n}}\right)\frac{\partial \omega}{\partial s}, \tag{2.21}$$

where w is the speed of a typical particle, s is the arc length along the momentary flow line, and (σ_n, σ_t) are the normal stress components along the normal and tangent, respectively, to the flow line. The change in thickness during a small interval can be computed from (2.21). Evidently, whenever there is a discontinuity in the velocity gradient, there is also a corresponding jump in $\partial h/\partial t$, leading to a discontinuity in the surface slope of an initially uniform sheet.

2.1.4 Basic Relations for a Tresca Material

If the material yields according to Tresca's yield criterion with a given uniaxial yield stress $Y = 2k$, the yield locus is a hexagon inscribed in the von Mises ellipse. When the principal stresses σ_1 and σ_2 have

opposite signs, the greatest shear stress occurs in the plane of the sheet, and the yield criterion becomes

$$(\sigma_1 - \sigma_2)^2 = \left(\sigma_x - \sigma_y\right)^2 + 4\tau_{xy}^2 = 4k^2, \quad \left|\sigma_x + \sigma_y\right| \le 2k. \tag{2.22}$$

As in the case of plane strain, the stress equations are hyperbolic, and the characteristics are sliplines bisecting the angles between the principal stress axes. Since the shear stresses acting across the characteristics are of magnitude k, the envelope

of the Mohr's circles then coincides with the yield locus. The variation of the normal stress σ along the characteristics is obtained from (2.8) and (2.9) by setting $\tau = k$, $\psi = 0$, and $d\phi_\alpha = d\phi_\beta = d\phi$, the expression in each parenthesis being then equal to k.

For a uniform sheet, these relations reduce to the well-known Hencky equations in plane strain. Since the thickness strain rate vanishes by the associated flow rule, the velocity equations are also hyperbolic and the characteristics are again the slip-lines, the velocity relations along the characteristics being given by the familiar Geiringer equations in plane strain.

When the principal stresses σ_1 and σ_2 have the same sign, the greatest shear stress occurs out of the plane of the applied stresses, and the numerically greater principal stress must be of magnitude $2k$ for yielding to occur. On the (σ_0, τ_0)-plane, the yield criterion is defined by the straight lines $\sigma_0 \pm \tau_0 = \pm 2k$. In terms of the principal stresses, the yield criterion may be written as

$$(\sigma_1 + 2k)\,(\sigma_2 \pm 2k) = 0, \quad \sigma_1\sigma_2 \geq 0.$$

This equation can be expressed in terms of the (x, y) components of the stress, using the fact that $\sigma_1 + \sigma_2 = \sigma_x + \sigma_y$ and $\sigma_1\sigma_2 = \sigma_x\sigma_y - \tau^2_{xy}$ the result being

$$\tau_{xy}^2 - \sigma_x\sigma_y + 2k\left|\sigma_x + \sigma_y\right| = 4k^2, \;\; 2k \leq \left|\sigma_x + \sigma_y\right| \leq 4k. \tag{2.23}$$

The partial differentiation of (2.23) with respect to x reveals that the stress derivatives are uniquely determined unless $\sigma_x = \pm 2k$. Hence, there is a single characteristic across which the normal stress is of magnitude $2k$. In other words, the stress equations are parabolic with the characteristic coinciding with the direction of the numerically lesser principal stress, whose magnitude is denoted by σ. When the x- and y-axes are taken along the normal and tangent, respectively, to the characteristic, we have

$$\sigma_x = \pm\, 2k \text{ and } \sigma_y = \pm\sigma,\, \tau_{xy} = \mp\left(k - \frac{\sigma}{2}\right)\sin 2\omega. \tag{2.24}$$

where ω denotes the counterclockwise angle made by the characteristic with a fixed direction which is temporarily considered as the x-axis. Inserting (2.24) into the equilibrium equation (2.1), and setting $\omega = \pi/2$ after the differentiation, we get

$$\left(1 - \frac{\sigma}{2k}\right)\frac{\partial\omega}{\partial s} = -\frac{1}{h}\frac{\partial h}{\partial n}, \;\; \frac{\partial}{\partial s}\left(\frac{h\sigma}{2k}\right) = -\left(1 - \frac{\sigma}{2k}\right)h\frac{\partial\omega}{\partial n}, \tag{2.25}$$

where ds and dn are the line elements along the characteristic and its orthogonal trajectory, forming a right-handed pair of curvilinear axes.

When the thickness is uniform, ω is constant along each characteristic, which is therefore a straight line defined by $y = x\tan\omega + f(\omega)$, where $f(\omega)$ is a function of ω to be determined from the stress boundary condition. The curvature of the numerically greater principal stress trajectory is

$$\frac{\partial \omega}{\partial n} = \frac{\partial \omega}{\partial x}\sin\omega - \frac{\partial \omega}{\partial y}\cos\omega = -\frac{\cos\omega}{x + f'(\omega)\cos^2\omega}. \tag{2.26}$$

Inserting from (2.26) into the second equation of (2.25), and using the fact that $ds = sec\ \omega\ dx$ along a characteristic, the above equation is integrated to give (Sokolovsky, 1969),

$$1 - \frac{\sigma}{2k} = \frac{g(\omega)}{x + f'(\omega)\cos^2\omega}, \tag{2.27}$$

where $g(\omega)$ is another function to be determined from the boundary condition. Since the numerically lesser principal strain rate vanishes according to the associated flow rule, it follows that the velocity equations are also parabolic, and the characteristic direction coincides with the direction of zero rate of extension. The tangential velocity v remains constant along the characteristic, and the normal velocity u follows from the condition of zero ate of shear associated with these two orthogonal directions.

2.2 Discontinuities and Necking

2.2.1 Velocity Discontinuities

In a nonhardening rigid/plastic solid, the velocity may be tangentially discontinuous across certain surfaces where the shear stress attains its greatest magnitude k. For a thin sheet of metal, it is also necessary to admit a necking type of discontinuity involving both the tangential and normal components of velocity. To be consistent with the theory of generalized plane stress, the strain rate is considered uniform through the thickness of the neck, whose width b is comparable to the sheet thickness h. Since plastic deformation is confined in the neck, the rate of extension vanishes along its length, and the neck therefore coincides with a characteristic. The relative velocity vector across the neck must be perpendicular to the other characteristic in order that the velocity becomes continuous across it. Localized necking cannot occur, however, when the stress state is elliptic.

Let v denote the magnitude of the relative velocity vector which is inclined at an angle ψ to the direction of the neck, Fig. 2.4a. The rate of extension in the direction perpendicular to the neck is $(v/b)\ sin\ \psi$, and the rate of shear across the neck is $(v/2b)\ cos\ \psi$. The condition of the zero rate of extension along the neck therefore gives the principal strain rates as (Hill, 1952).

$$\dot{\varepsilon}_1 = \frac{v}{2b}(1 + \sin\psi),\ \dot{\varepsilon}_2 = -\frac{v}{2b}(1 - \sin\psi),\ \dot{\varepsilon}_3 = -\frac{v}{b}\sin\psi, \tag{2.28}$$

irrespective of the flow rule. These relations imply that the axis of $\dot{\varepsilon}_1$ is inclined at an angle $\pi/4 + \psi/2$ to the neck. For a von Mises material, ψ is related to the stress according to (2.18), while for a Tresca material, $\psi = 0$ when the stress state

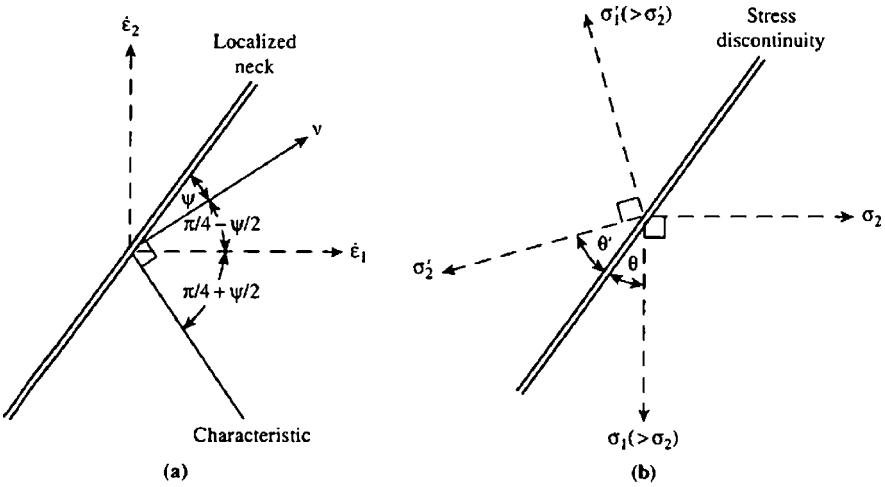

Fig. 2.4 Velocity and stress discontinuities in plane stress including the associated principal directions

is hyperbolic. In the case of a uniaxial tension, $\dot{\varepsilon}_1 = -2\dot{\varepsilon}_2$ for any regular yield function, giving $\psi = \sin^{-1} 1/3 \approx 19.47°$, the angle of inclination of the neck to the direction of tension being $\beta = \pi/4 + \psi/2 = \tan^{-1}\sqrt{2} \approx 54.74°$. For a Tresca material, on the other hand, ψ can have any value between 0 and $\pi/2$ under a uniaxial state of stress.

When the material work-hardens, a localized neck is able to develop only if the rate of hardening is small enough to allow an incremental deformation to remain confined in the incipient neck. For a critical value of the rate of hardening, the deformation is just able to continue in the neck, while the stresses elsewhere remain momentarily unchanged. Since the force transmitted across the neck remains momentarily constant, we have

$$-\frac{dh}{h} = \frac{d\sigma}{\sigma} = \frac{dY}{Y} = \frac{H}{Y} d\varepsilon,$$

where σ is the normal stress across the neck, Y the current yield stress, H the rate of hardening, and $d\varepsilon$ the equivalent strain increment. If the Lévy–Mises flow rule is adopted, then

$$-\frac{dh}{h} = \left(\frac{\sigma_1 + \sigma_2}{2Y}\right) d\varepsilon = \frac{3\sigma}{4Y} d\varepsilon.$$

The last two equations reveal that the critical rate of hardening is equal to $3\sigma/4$ or $(\sigma_1 + \sigma_2)/2$. Using (2.12), the condition for localized necking to occur may therefore be expressed as

$$\frac{H}{Y} \leq \frac{\sigma_1 + \sigma_2}{2Y} = \frac{\sqrt{3}\sin\psi}{\sqrt{1+3\sin^2\psi}}. \tag{2.29}$$

It is also necessary to have $-1 \leq \sigma_1/\sigma_2 \leq 2$ for the equations to be hyperbolic. As ψ increases from 0 to $\pi/2$, the critical value of H/Y increases from 0 to $\sqrt{3}/2$. In the case of a uniaxial tension ($3 \sin \psi = 1$), localized necking can occur only if $H/Y \leq 0.5$. Thus, for a sheet of metal with a rounded stress–strain curve, a gradually increasing uniaxial tensile stress a produces a diffuse neck when $H = \sigma$, and eventually a localized neck when $H = \sigma/2$. A microstructural model for the shear band type of strain localization has been examined by Lee and Chan (1991).

2.2.2 Tension of a Grooved Sheet

Consider a uniform rectangular sheet of metal whose thickness is locally reduced by cutting a pair of opposed grooves in an oblique direction across the width, Fig. 2.5a. The grooves are deep enough to ensure that plastic deformation is localized there when the sheet is pulled longitudinally in tension. The width of the sheet is large compared to the groove width b, which is slightly greater than the local sheet thickness h so that a uniform state of plane stress exists in the grooves. The material in the grooves is prevented from extending along its length by the constraint of the adjacent nonplastic material. The principal strain rates in the grooves are therefore given by (2.28) in terms of the angle of inclination of the relative velocity with which the sides of the grooves move apart. If the material is isotropic, the directions of the principal stresses σ_1 and σ_2 are inclined at angles $\pi/4 + \psi/2$ and $\pi/4 - \psi/2$, respectively, to the direction of the grooves, where $\sigma_1 > \sigma_2$, the principal axes of stress and strain rate being coincident.

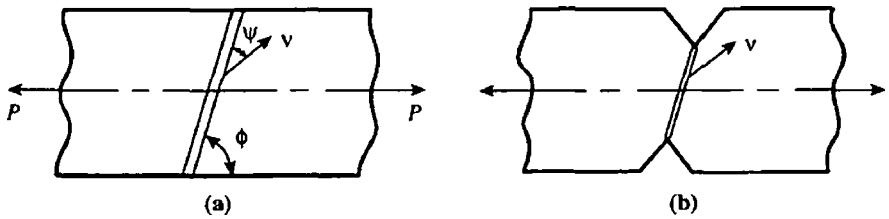

Fig. 2.5 Necking of grooved and notched metal strips under longitudinal tension

Let ϕ denote the counterclockwise angle made by the prepared groove with the direction of the applied tensile force P. Then the normal and shear stresses acting across the grove are $P \sin\phi/lh$ and $P \cos \phi/lh$, respectively, where l is the length of the groove. By the transformation relations for the stress, we have

$$(\sigma_1 + \sigma_2) + (\sigma_1 - \sigma_2)\sin\psi = (2P/lh)\sin\phi,$$
$$(\sigma_1 - \sigma_2)\cos\psi = (2P/lh)\cos\phi.$$

These equations can be solved for the principal stresses in terms of the angles ϕ and ψ, giving

$$\sigma_1 = \frac{P\,[\sin(\phi-\psi)+\cos\phi]}{hl\cos\psi},\ \sigma_2 = \frac{P\,[\sin(\phi-\psi)-\cos\phi]}{hl\cos\psi}. \tag{2.30}$$

From (2.28) and (2.30), Lode's well-known stress and strain parameters are obtained as

$$\left.\begin{aligned}\mu &= \frac{2\sigma_2-\sigma_1-\sigma_3}{\sigma_1-\sigma_3} = -\frac{3\cos\phi-\sin(\phi-\psi)}{\sin(\phi-\psi)+\cos\phi},\\ \nu &= \frac{2\dot{\varepsilon}_2-\dot{\varepsilon}_1-\dot{\varepsilon}_3}{\varepsilon_1-\varepsilon_3} = -\frac{3\,(1-\sin\psi)}{(1+3\sin\psi)}.\end{aligned}\right\} \tag{2.31}$$

Equation (2.31) form the basis for establishing the (μ, ν) relationship for a material using the measured values of ϕ and ψ. The ends of the sheet must be supported in such a way that they are free to rotate in their plane to accommodate the relative movement necessary to permit the localized deformation to occur. The shape of the deviatoric yield locus may be derived from the fact that the length of the deviatoric stress vector is

$$s = \sqrt{\frac{2}{3}}\left(\sigma_1^2-\sigma_1\sigma_2+\sigma_2^2\right)^{1/2} = \frac{P}{hl}\frac{\sqrt{2\left[\sin^2(\phi-\psi)+3\cos^2\psi\right]}}{\sqrt{3}\cos\psi}, \tag{2.32}$$

and the angle made by the stress vector is $\theta = \tan^{-1}(-\mu/\sqrt{3})$ with the direction representing pure shear. If the yield locus and plastic potential have a sixfold symmetry required by the isotropy and the absence of the Bauschinger effect, it is only necessary to cover a 30° segment defined by the direction of pure shear ($\mu = \nu = 0$) and that of uniaxial tension ($\mu = \nu = -1$). This is accomplished by varying ϕ between 90° and $\tan^{-1}\sqrt{2} \approx 54.7°$, and measuring ψ for each selected value of ϕ. It may be noted that according to the Lévy–Mises flow rule ($\mu = \nu$), the relationship $\tan\phi = 4\tan\psi$ always holds.

The preceding analysis, due to Hill (1953), is equally applicable to the localized necking caused by the tension of a sheet provided with a pair of asymmetrical notches as shown in Fig. 2.5b. If the notches are deep and sharp, and the rate of work-hardening is sufficiently low, plastic deformation is localized in a narrow neck joining the notch roots. This method may be used for the determination of the yield criterion and the plastic potential for materials with sufficient degrees of pre-strain, provided it is reasonably isotropic. The method has been tried with careful experiments by Hundy and Green (1954), and by Lianis and Ford (1957), using specimens which can be effectively tested to ensure that they are actually isotropic. These investigations have confirmed the validity of the von Mises yield criterion and the associated plastic potential for several engineering materials, as indicated in Fig. 1.8.

2.2.3 Stress Discontinuities

We begin by considering the normal and shear stresses acting over a surface which coincides with a characteristic. When the state of stress is hyperbolic, there is only one stress circle that can be drawn through the given point on the Mohr envelope without violating the yield criterion. Since the stress states on both sides of the characteristic are represented by the same circle, all components of the stress are continuous. When the stress state is parabolic, and the yield criterion is that of Tresca, the principal stress acting along the tangent to the characteristic can have any value between 0 and ±2 k, permitting a discontinuity in the numerically lesser principal stress. When the considered surface is not a characteristic, a stress discontinuity is always possible with two distinct plastic states separated by a line of stress discontinuity.

Let σ_1, σ_2 be the principal stresses on one side of the discontinuity ($\sigma_1 \geq \sigma_2$), and σ'_1, σ'_2, those on the other side ($\sigma'_1 \geq \sigma'_2$) . The angles of inclination of σ_1 and σ'_2 with the line of discontinuity are denoted by θ and θ', respectively, reckoned positive as shown in Fig. 2.4b. Since the normal and shear stresses across the line of discontinuity must be continuous for equilibrium, we have

$$\left.\begin{aligned}(\sigma_1+\sigma_2)-(\sigma_1-\sigma_2)\cos 2\theta &= \left(\sigma'_1+\sigma'_2\right)+\left(\sigma'_1-\sigma'_2\right)\cos 2\theta',\\ (\sigma_1-\sigma_2)\sin 2\theta &= \left(\sigma'_1-\sigma'_2\right)\sin 2\theta'.\end{aligned}\right\} \tag{2.33}$$

If the von Mises yield criterion is adopted, the stresses on each side of the discontinuity must satisfy (2.2). Considering the stress components along the normal and tangent to the discontinuity, specified by n and t, respectively, and using the continuity conditions $\sigma_n = \sigma'_n$ and $\tau_{nt} = r'_{nl}$, it is easily shown from (2.2) that $\sigma'_n - \sigma'_t = \sigma_t$ giving

$$2\cot 2\theta' = \cot 2\theta + \left(\frac{\sigma_1+\sigma_2}{\sigma_1-\sigma_2}\right)\operatorname{cosec} 2\theta. \tag{2.34}$$

The elimination of $\sigma'_1 - \sigma'_2$ between the two equations of (2.33), and the substitution from (2.34), lead to the relation

$$2\left(\sigma'_1-\sigma'_2\right) = (\sigma_1+\sigma_2) - 3\,(\sigma_1-\sigma_2)\cos 2\theta. \tag{2.35}$$

Since $\sigma'_1 - \sigma'_2$ is then given by the yield criterion, the principal stresses and their directions are known on one side of the discontinuity when the corresponding quantities on the other side are given.

Considering the Tresca criterion for yielding, suppose that (σ_1, σ_2) represents a hyperbolic state, so that $\sigma_1 - \sigma_2 = 2k$ and $|\sigma_1 + \sigma_2| \leq 2k$. If the ($\sigma'_1$, σ'_2) state is also hyperbolic, then $\sigma'_1 - \sigma'_2 = 2$k by the yield criterion, and the continuity conditions (2.33) furnish $\theta' = \theta$, and

$$\sigma_1' = \sigma_1 - 2k\cos 2\theta \geq 0, \quad \sigma_2' = \sigma_2 - 2k\cos 2\theta \leq 0.$$

If the (σ'_1, σ'_2) state is parabolic, the yield criterion is either $\sigma'_1 = 2k(\sigma'_2 \geq 0)$ or $\sigma'_2 = -2k(\sigma'_1 \leq 0)$. In the first case, (2.33) gives

$$\left.\begin{aligned} \tan\theta' &= \left(1 + \cos 2\theta - \frac{\sigma_2}{k}\right)\operatorname{cosec} 2\theta, \\ \frac{\sigma_2'}{2k} &= -\frac{\sigma_2}{k}\left(\frac{\sigma_2}{2k} - \cos 2\theta\right)\Big/\left(1 + \cos 2\theta - \frac{\sigma_2}{k}\right), \end{aligned}\right\} \frac{\sigma_2}{2k} \leq \cos 2\theta. \qquad (2.36)$$

The corresponding results for the second case are obtained from (2.36) by replacing σ_2 and σ'_2 with $-\sigma_1$ and σ'_1, respectively, $\tan\theta$ with $\cos\theta$, and reversing the sign of $\cos 2\theta$. Exceptionally, when the stress normal to the discontinuity is $\pm 2k$, the other principal stress on either side can have any value between 0 and $\pm 2k$. Such a discontinuity may be considered as the limit of a narrow zone of a continuous sequence of plastic states.

When yielding occurs according to the von Mises criterion, all the stress components must be continuous across a line of velocity discontinuity. This is evident for a necking type of discontinuity (since the neck must coincide with a characteristic), across which the stress is necessarily continuous. For a shearing discontinuity, the shear stress across the line of discontinuity is of magnitude k, and since the normal stress is continuous for equilibrium, the remaining stress must also be continuous in view of the yield criterion. As a consequence of this restriction, the velocity must be continuous across a line of stress discontinuity. The rate of extension along a line of stress discontinuity, which is the derivative of the tangential velocity, is evidently continuous. Since the flow rule predicts opposite signs for this component of the strain rate on the two sides of the stress discontinuity, the rate of extension must vanish along its length. The discontinuity may therefore be regarded as the limit of a narrow zone of elastic material through which the stress varies in a continuous manner.

2.2.4 Diffuse and Localized Necking

It is well known that the deformation of a bar subjected to a longitudinal tension ceases to be homogeneous when the rate of work-hardening of the material is less than the applied tensile stress. At the critical rate of hardening, the load attains its maximum, and the subsequent extension of the bar takes place under a steadily decreasing load. Plastic instabilities of this sort, leading to diffuse local necking, also occur when a flat sheet is subjected to biaxial tension in its plane. The strain-hardening characteristic of the material is defined by the equivalent stress $\overline{\sigma}$, and the equivalent total strain $\overline{\varepsilon}$, related to one another by the true stress–strain curve in uniaxial tension. Using the Lévy–Mises flow rule in the form

$$\frac{d\varepsilon_1}{2\sigma_1-\sigma_2}=\frac{d\varepsilon_2}{2\sigma_2-\sigma_1}=-\frac{d\varepsilon_3}{\sigma_1+\sigma_2}=\frac{\overline{d\varepsilon}}{2\overline{\sigma}}, \tag{2.37}$$

and the differential form of the von Mises yield criterion (2.2) where $3k^2$ is replaced by $\overline{\sigma}^2$, it is easily shown that the stress and strain increments in any element must satisfy the relation

$$d\sigma_1 d\varepsilon_1 + d\sigma_2 d\varepsilon_2 = d\overline{\sigma}\, d\overline{\varepsilon}.$$

Consider a rectangular sheet whose current dimensions are b_1 and b_2 along the directions of σ_1 and σ_2, respectively. If the applied loads $hb_2\sigma_1$ and $hb_2\sigma_2$ attain stationary values at the onset of instability, where h denotes the current thickness, then

$$\frac{d\sigma_1}{\sigma_1}=\frac{db_1}{b_1}=d\varepsilon_1, \quad \frac{d\sigma_2}{\sigma_2}=\frac{db_2}{b_2}=d\varepsilon_2,$$

in view of the constancy of the volume hb_1b_2 of the sheet material. Combining the preceding two relations, we have

$$\frac{d\overline{\sigma}}{\overline{d\varepsilon}}=\sigma_1\left(\frac{d\varepsilon_1}{\overline{d\varepsilon}}\right)^2+\sigma_2\left(\frac{d\varepsilon_2}{\overline{d\varepsilon}}\right)^2.$$

Substituting from (2.37), and using the expression for $\overline{\sigma}^2$, and setting $\sigma_2/\sigma_1 = p$, the condition for plastic instability is obtained as (Swift, 1952; Hillier, 1966)

$$\frac{H}{\overline{\sigma}}=\frac{(1+\rho)\left(4-7\rho+4\rho^2\right)}{4\left(1-\rho+\rho^2\right)^{3/2}}, \tag{2.38}$$

where $H = d\overline{\sigma}/d\overline{\varepsilon}$ denotes the critical rate of hardening. The quantity on the left-hand side of (2.38) is the reciprocal of the subtangent to the generalized stress–strain curve. The variation of the critical subtangent with stress ratio ρ is shown in Fig. 2.6 for both localized and diffuse necking. If the stress ratio is maintained constant throughout the loading, the total equivalent strain at instability is obtained directly from (2.38), if we adopt the simple power law $\overline{\sigma} = C\,\overline{\varepsilon}^n$, which gives $H/\overline{\sigma} = n/\overline{\varepsilon}$. In the case of variable stress ratio, the instability strain will evidently depend on the prescribed loading path.

In the biaxial tension of sheet metal, failure usually occurs by strain localization in a narrow neck following the onset of instability. The phenomenon can be explained by considering the development of a pointed vertex on the yield locus, which allows the necessary freedom of flow of the plastic material in the neck. When both the principal strains are positive, experiments seem to indicate that the neck coincides with the direction of the minimum principal strain ε_2 in the plane of the sheet. The incremental form of the Hencky stress–strain relations may be assumed to hold at the incipient neck, where the subsequent deformation remains

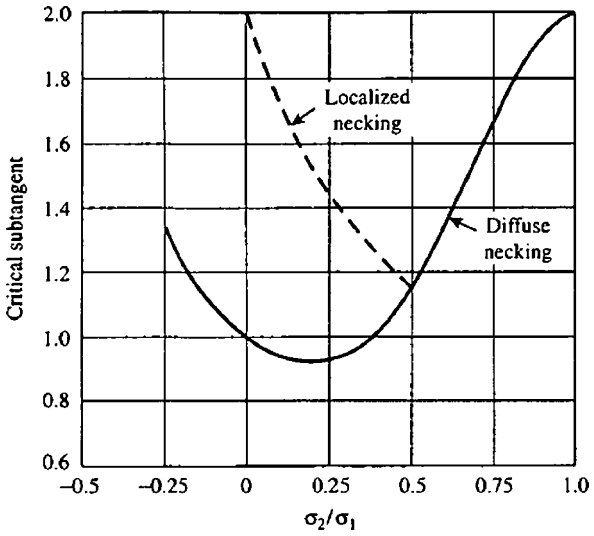

Fig. 2.6 Critical subtangent to the effective stress–strain curve as a function of the stress ratio

confined (Stören and Rice, 1975). The principal surface strains in the neck may therefore be written as

$$\varepsilon_1 = \overline{\varepsilon}\left(\frac{2\sigma_1 - \sigma_2}{2\overline{\sigma}}\right),\ \varepsilon_2 = \overline{\varepsilon}\left(\frac{2\sigma_2 - \sigma_1}{2\overline{\sigma}}\right),$$

where $\overline{\sigma}$ and $\overline{\varepsilon}$ are the equivalent stress and total strain, respectively. The elimination of σ_2 and $\sigma 1$ in turn between these two relations gives the principal stresses

$$\sigma_1 = (2\varepsilon_1 + \varepsilon_2)\,\frac{2\overline{\sigma}}{3\overline{\varepsilon}},\ \sigma_2 = (2\varepsilon_2 + \varepsilon_1)\,\frac{2\overline{\sigma}}{3\overline{\varepsilon}}.$$

Assuming the power law $\overline{\sigma} = C\,\overline{\varepsilon}^n$ for the generalized stress–strain curve, the incremental form of the first equation above at the inception of the neck is found as

$$\frac{d\,\sigma_1}{\sigma_1} = \frac{2d\,\varepsilon_1 + d\,\varepsilon_2}{(2+\alpha)\,\varepsilon_1} - (1-n)\,\frac{d\,\overline{\varepsilon}}{\overline{\varepsilon}}, \tag{2.39}$$

where $\alpha \geq 0$ denotes the constant strain ratio $\varepsilon_2/\varepsilon_1$, prior to the onset of necking. The quantity de is the increment of the equivalent total strain $\overline{\varepsilon}$. Since $\overline{\varepsilon}^2 = \frac{4}{3}\left(\varepsilon_1^2 + \varepsilon_1\varepsilon_2 + \varepsilon_2^2\right)$ according to the Hencky theory, we get

$$\frac{d\,\overline{\varepsilon}}{\overline{\varepsilon}} = \frac{(2+\alpha)\,d\,\varepsilon_1 + (1+2\alpha)\,d\,\varepsilon_2}{2\left(1+\alpha+\alpha^2\right)\varepsilon_1}.$$

The neck is characterized by a discontinuity in $d\varepsilon_1$, but $d\varepsilon_2$ must be regarded as continuous across the neck. Since the material outside the neck undergoes neutral loading at its inception, we set $d\varepsilon_2 = 0$. Combining the last two equations, and using

the fact that $d\sigma_1/\sigma_1 = d\varepsilon_1$ for the load across the neck to be stationary, the condition for localized necking is obtained as

$$\left\{\varepsilon_1 + \frac{(1-n)(2+\alpha)}{2\left(1+\alpha+\alpha^2\right)} - \frac{2}{2+\alpha}\right\}\frac{d\varepsilon_1}{\varepsilon_1} = 0.$$

Since $d\varepsilon_1 \neq 0$ for the development of the neck, the expression in the curly brackets must vanish, giving the limit strain over the range $0 < \alpha < 1$ in the form

$$\varepsilon_1 = \frac{3\alpha^2 + n(2+\alpha)^2}{2(2+\alpha)\left(1+\alpha+\alpha^2\right)} = \frac{(2-\rho)\left[(2\rho-1)^2+3n\right]}{6\left(1-\rho+\rho^2\right)}, \tag{2.40}$$

where ρ is the stress ratio σ_2/σ_1, equal to $(1 + 2\alpha)/(2 + \alpha)$. The value of ε_1 given by (2.40) may be compared with that predicted by (2.38) for a material with a given value of n. The limit strain is seen to be higher than the instability strain except when $\alpha = 0$, for which both the conditions predict $\varepsilon_1 = n$.

For $\alpha < 0$, the neck forms along the line of zero extension, which is inclined at angle $\tan^{-1}\sqrt{-\alpha}$ to the direction of the minimum principal strain in the plane of the sheet. The strain ratio then remains constant during the incremental deformation, and the onset of necking is given by (2.29), with Y = a, the limit strain being easily shown to be

$$\varepsilon_1 = n\left(\frac{2-\rho}{1+\rho}\right) = \frac{n}{1+\alpha}, \quad -\tfrac{1}{2} \leq \alpha \leq 0.$$

The curve obtained by plotting ε_1 against ε_2 corresponding to localized necking in a given material is called the forming limit diagram, which represents the failure curve in sheet stretching. This will be discussed in Section 6.5 on the basis of a different physical model including anisotropy of the sheet metal.

2.3 Yielding of Notched Strips

2.3.1 V-Notched Strips in Tension

Consider the longitudinal extension of a rectangular strip having a pair of symmetrical V-notches of included angle 2α in the plane of the strip. The material is assumed to be uniformly hardened, obeying the von Mises yield criterion and the associated Lévy–Mises flow rule. When the load attains the yield point value, the region of incipient plastic flow extends over the characteristic field shown in Fig. 2.7. The triangular region *OAB* is under a uniaxial tension $\sqrt{3}\,k$ parallel to the notch face, and the characteristics are straight lines inclined at an angle $\beta = \tan^{-1}\sqrt{2}$ to the notch face. Within the fan *OBC*, one family of characteristics are straight lines passing through the notch root, and the state of stress expressed in polar coordinates (r, ϕ) is given by

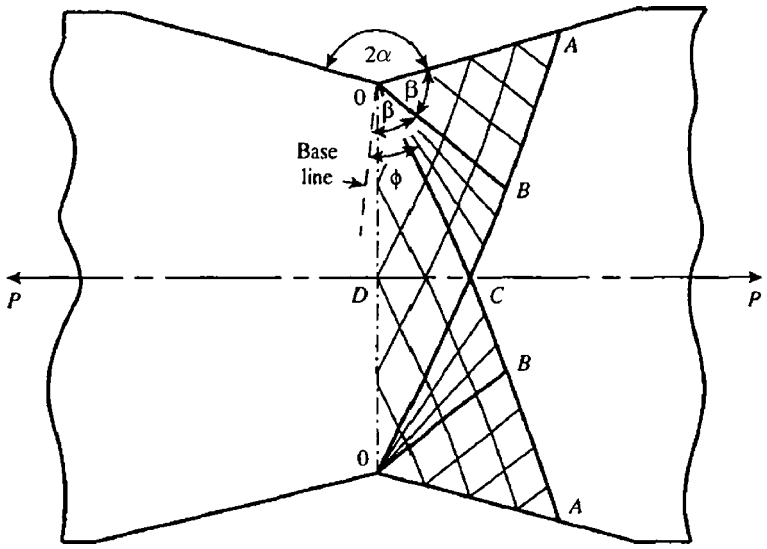

Fig. 2.7 Characteristic field in a sharply notched metal strip under longitudinal tension ($\alpha \geq 70.53$)

$$\sigma_r = k \cos \phi, \ \sigma_\phi = 2k \cos \phi, \ \tau_{r\phi} = k \sin \phi, \tag{2.41}$$

so that the equilibrium equations and the yield criterion are identically satisfied. It follows from (2.5) that $\cos \psi = 2\tan \phi$ within the fan. Along the line *OB*, $\psi = \sin^{-1} \frac{1}{3}$, giving $\phi = \beta = \tan^{-1} \sqrt{2}$. The baseline from which ϕ is measured therefore makes an angle 2β with the notch face. The curved characteristics in *OBC* are given by

$$r\,(d\phi/dr) = -\cos \psi = -2 \tan \phi, \ \ or \quad r^2 \sin \phi = \text{constant}.$$

The curved characteristics approach the baseline asymptotically, if continued, and are inflected where $\phi = \pi/2 - \beta$. The region *OCO* is uniformly stressed, and the principal stress axes coincide with the axes of symmetry. From geometry, angle *COD* is equal to $\phi_0 - (2\beta + \alpha - \pi)$, where ϕ_0 is the value of ϕ along *OC*, the corresponding value of ψ being denoted by ψ_0. Since the algebraically lesser principal stress direction in *OCO* is parallel to *00*, angle *COD* is also equal to $\pi/4 - \psi_0/2$. The relation $\cot \psi 0 = 2\tan \phi_0$ therefore gives

$$2 \tan \phi_0 + \tan 2\,(\alpha + 2\beta - \phi_0) = 0, \tag{2.42}$$

which can be solved for ϕ_0 when α lies between $\pi - 2\beta$ and $\pi/2$, the limiting values of ϕ_0 being 0 and β, respectively. Since $\sigma_1 + \sigma_2 = 3k \cos \phi_0$ and $\sigma_1 - \sigma_2 = k\sqrt{1 + 3 \sin^2 \phi_0}$ within *OCO* in view of (2.41), the constraint factor is

$$f = \frac{\sigma_1}{\sqrt{3}k} = \frac{3\cos\phi_0 + \sqrt{1 + 3\sin^2\phi_0}}{2\sqrt{3}},\ \pi - 2\beta \le \alpha \le \pi/2. \tag{2.43}$$

The field of Fig. 2.7, which is due to Hill (1952), has been extended by Bishop (1953) in a statically admissible manner to show that the solution is in fact complete. As α decreases from $\pi/2$, the constraint factor increases from unity to reach its highest value of $2/\sqrt{3}$ when $\alpha = \pi - 2\beta \approx 70.53°$. The field in this case shrinks to a coincident pair of characteristics along the transverse axis of symmetry. In general, the constraint factor is closely approximated by the empirical formula

$$f = 1 + 0.155\sin\left\{4.62\left(\frac{\pi}{2} - \alpha\right)\right\},\ \pi - 2\beta \le \alpha \le \pi/2. \tag{2.44}$$

For all sharper notches, the characteristic field and the constraint factor are identical to those for $\alpha = \pi - 2\beta$. Indeed, by the maximum work principle, the constraint factor cannot decrease when material is added to reduce the notch angle, while the value of f certainly cannot exceed $2/\sqrt{3}$ since no stress component can exceed $2k$ in magnitude.

The yield point load can be associated with a deformation mode consisting of localized necking along both characteristics through the center D of the minimum section. If the ends of the strip are moved longitudinally with a unit speed relative to D, the particles on the transverse axis of symmetry must move inward with a speed equal to $\tan(\pi/4 - \psi/2)$. The vector representing the relative velocity of particles across the neck is then perpendicular to the other characteristic as required. Strictly speaking, there is no opportunity for the deformation to occur outside the localized necks.

2.3.2 Solution for Circular Notches

Consider, now, the longitudinal tension of a strip with symmetrical circular notches of radius c, the roots of the notch being at a distance 2α apart. For sufficiently small values of the ratio a/c, the characteristic field is radially symmetric as shown in Fig. 2.8, and the stress distribution is defined by (2.13) where σ_2 and σ_1 represent the radial and circumferential stresses denoted by σ_r and $\sigma\phi$, respectively. The substitution into the equation of radial equilibrium gives

$$\frac{d\sigma_r}{dr} = \frac{\sigma_\phi - \sigma_r}{r} = \frac{2k\cos\theta}{r},\ \text{or}\ r\frac{d\theta}{dr} = \frac{2}{\sqrt{3} + \tan\theta},$$

where r is the radius of a generic point in the field. The boundary condition $\sigma_r = 0$ at the notch surface is equivalent to $\theta = \pi/6$ at $r = c$, and the integration of the above equation results in

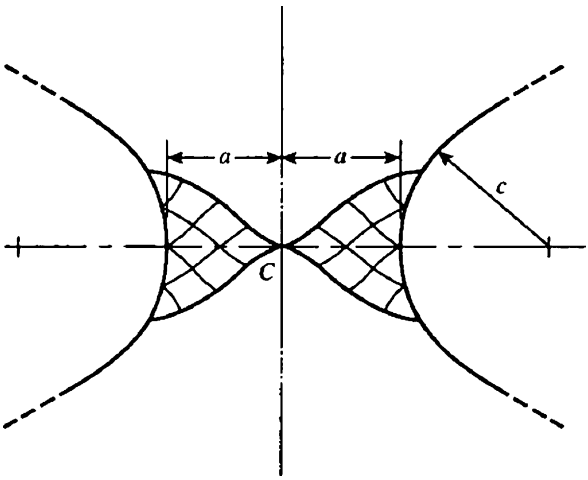

Fig. 2.8 Characteristic field in a circularly notched strip under longitudinal tension ($a/c \leq 1.071$)

$$\frac{r^2}{c^2} = \frac{\sqrt{3}}{2} \sec\theta \exp\left[\sqrt{3}\left(0 - \frac{\pi}{6}\right)\right], \ \frac{\pi}{6} \leq \theta \leq \frac{\pi}{3}. \tag{2.45}$$

The characteristics coincide when $\theta = \pi/3$, and this corresponds to $r/c \approx 2.071$. The angular span of the circular root covered by the field in this limiting case is $4\beta - \pi \approx 38.96°$, which is obtained from (2.14) as twice the difference between the values of λ corresponding to $\theta = \pi/3$ and $\theta = \pi/6$. The characteristic field is easily constructed using (2.45) and (2.14), and the fact that the polar angle ϕ measured from the transverse axis is, by (2.16), equal to the decrease in the value of λ from that on the transverse axis. The resultant longitudinal force per unit thickness across the minimum section is

$$P = 2\int_c^{a+c} \sigma_\phi dr = 2\int_c^{a+c} \frac{d}{dr}(r\sigma_r)\, dr = 4k\,(a+c)\sin\left(\theta_0 - \frac{\pi}{6}\right),$$

where θ_0 is the value of θ at the center of the minimum section where $r = a + c$, and is directly given by (2.45). The constraint factor is

$$f = \frac{P}{2\sqrt{3}ka} = \frac{2}{\sqrt{3}}\left(1 + \frac{c}{a}\right)\sin\left(\theta_0 - \frac{\pi}{6}\right), \ 0 \leq \frac{a}{c} \leq 1.071. \tag{2.46}$$

The value of f computed from (2.46) exceeds unity by the amount $0.226a/(a + c)$ to a close approximation. For higher values of a/c, the characteristics coincide along a central part of the transverse axis, and the longitudinal force per unit thickness is $4k(a - 1.071c)$ over the central part, and $2k(2.071c)$ over the remainder of the minimum section, giving the constraint factor

$$f = \frac{1}{\sqrt{3}}\left(2 - 0.071\frac{c}{a}\right), \quad \frac{a}{c} \geq 1.071.$$

As a/c increases, f approaches its asymptotic value of $2/\sqrt{3}$, which is the ratio of the maximum shear stresses in pure shear and simple tension. Localized necking would occur at the yield point along the characteristics through C if the rate of work-hardening of the material is not greater than the uniaxial yield stress of the material.

Consider, now, the solution for Tresca's yield criterion and its associated flow rule. Since no stress can exceed $2k$, which is now equal to the uniaxial yield stress, the constraint factor f cannot exceed unity. On the other hand, f is unity for a strip of width $2a$. Hence, the actual constraint factor is $f = 1$, whatever the shape of the notch. A localized neck forms directly across the minimum section when the yield point is attained, provided the rate of work-hardening is not greater than $2k$.

2.3.3 Solution for Shallow Notches

The preceding solutions hold only when the notches are sufficiently deep. In the case of shallow notches, the deformation originating at the notch roots spreads across to the longitudinal free edges. Considering a sharply notched bar with an included angle 2α, a good approximation to the critical notch depth may be obtained by extending the characteristic field further into the specimen. With reference to Fig. 2.9, which shows one-quarter of the construction, the solution involves the extension $ABCEFG$ of the basic field $OABC$. The extended field is bounded by a stress-free boundary AG generated from a point on the notch face, the material lying beyond AG being assumed unstressed. The construction begins with the consideration of the curvilinear triangle CBE, which is defined by the β-line CB and the conditions of symmetry along CE. Since $\cot\phi = 2\tan\psi$ along CB, the boundary conditions are

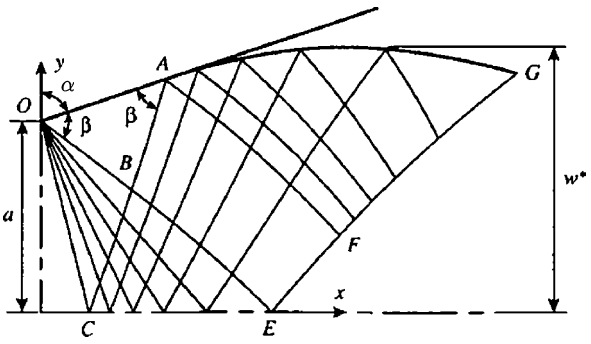

Fig. 2.9 Critical width of a V-notched strip subjected to longitudinal tension

$$\lambda = \frac{\pi}{2} - \phi - \tfrac{1}{2}\tan^{-1}\left(\tfrac{1}{2}\tan\phi\right),\ \omega = -\gamma + \phi + \tfrac{1}{2}\tan^{-1}\left(\tfrac{1}{2}\tan\phi\right),$$

along *CB* in view of (2.14), where ω denotes the counterclockwise angle made by the algebraically greater principal stress with the longitudinal axis of symmetry, while $\gamma = \sigma + 2\beta - 3\,\pi/4$. Since $\omega = 0$ along *CE* by virtue of symmetry, the values of λ and ω are easily obtained throughout the field *CBE* using the characteristic relations (2.16). Starting with the known coordinates of the nodal points along CB, and using the fact that

$$\phi_\alpha = \omega - \left(\frac{\pi}{4} + \frac{\psi}{2}\right), \quad \phi_\beta = \omega + \left(\frac{\pi}{4} + \frac{\psi}{2}\right), \tag{2.47}$$

where ψ is obtained from (2.14), the coordinates of each point of the field can be determined numerically by the mean slope approximation for small arcs considered along the characteristics,

Since *AB* is a straight characteristic, all the β-lines in the field *ABEF* are also straight, though not of equal lengths. The angles ψ, ω, and λ. along *AF* are therefore identical to those along *BE*. The known values of ϕ_β and ϕ_α along *BE* and *AF* furnish the coordinates of the nodal points of *AF* by simple geometry and the tangent approximation. Since all characteristics meet the stress-free boundary *OAG* at a constant angle $\beta = 54.74°$, we have the boundary conditions $\psi = 19.47°$ and $\lambda = 25.53°$ along *AG*. Starting from point *A*, where $\omega = \pi/2 - \alpha$, and using (2.16), the values of λ and ω throughout the field *AFG* are easily determined. The angles ϕ_α and ϕ_β at the nodal points of the field are then computed from (2.47), and the rectangular coordinates are finally obtained by the mean slope approximation. The stress-free boundary *AG* generated as a part of the construction has a maximum height ω^*, which is the critical semiwidth of the strip. The numerical computation carried out by Ewing and Spurr (1974) suggests the empirical formula

$$\frac{a}{\omega^*} = 1 - 0.286\sin\left\{4.62\left(\frac{\pi}{2} - \alpha\right)\right\}, \tag{2.48}$$

which is correct to within 0.5% over the range $70.5° \le \alpha \le 90°$. This formula actually provides an upper bound on the critical semiwidth, since all specimens wide enough to contain the extended field are definitely not overstressed, as may be shown by arguments similar to those used for the corresponding plane strain problem (Chakrabarty, 2006).

When the semiwidth w of the notched bar is less than w^*, we can find an angle $\alpha^* > \alpha$ such that $w^*(\alpha^*) = w$. Then, the corresponding constraint factor $f(\alpha^*)$ calculated from (2.46) would provide a lower bound on the yield point load. Indeed, the yield point load cannot be lowered by the addition of material required to reduce the notch angle from $2\alpha^*$ to the actual value 2α. The constraint factor for subcritical widths is closely approximated by the lower bound value, which may be expressed empirically as

$$f = 1 + 0.54\left(1 - \frac{a}{w}\right), \quad a \le w \le w^*.$$

In the case of an unnotched bar, the above formula reduces to $f = 1$. The deformation mode then consists of a localized neck inclined at an angle $\beta = 54.74°$ to the tension axis. Such a neck is also produced in a tensile strip with either a single notch or a symmetric central hole (Fig. 2.10). The tension of single-notched strips has been investigated by Ewing and Richards (1973), who also produced some experimental evidence in support of their theoretical prediction.

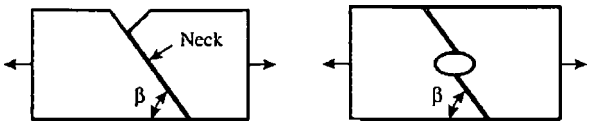

Fig. 2.10 Initiation of a localized neck in a flat sheet inclined at an angle β to the direction of tension

2.4 Bending of Prismatic Beams

2.4.1 Strongly Supported Cantilever

A uniform cantilever of narrow rectangular cross section carries a load kF per unit thickness at the free end, just sufficient to cause plastic collapse, the weight of the cantilever itself being negligible. The material is assumed to obey the von Mises yield criterion and the Lévy–Mises flow rule. Consider first the situation where the cantilever is rigidly held at the built-in end. If the ratio of the length l of the beam to its depth d is not too large, the characteristic field in the yield point state will be that shown in Fig. 2.11. The deformation mode at the incipient collapse consists of rotation of the rigid material about a center C on the longitudinal axis of symmetry. The solution involves localized necking along EN and localized bulging along NF, together with a simple shear occurring at N. The vector representing the relative velocity of the material is inclined to EF at an angle ψ which varies along the discontinuity. Although a local bulging can only occur in a strain-softening material, the solution may be accepted as a satisfactory upper bound on the collapse load (Green, 1954a) for ideally plastic materials.

In the triangular regions ABD and GHK, the state of stress is a uniform longitudinal tension and compression, respectively, of magnitude $\sqrt{3}\,k$, the characteristics being straight lines inclined at an angle $\beta = \tan^{-1}\sqrt{2}$ to the free edge. The region ADE is an extension of the constant stress field round the singularity A, the corresponding stresses being given by (2.41), where the polar angle ϕ is measured from a baseline that is inclined at an angle 2β to the free edge AB. The curved characteristics in ADE have the equation $r^2 \sin\phi = \text{constant}$, while the relation $\cot\psi = 2\tan\phi$ holds for the characteristic angle ψ. The normal stresses vanish at N, and the stress components along the curve ENF in plane polar coordinates are

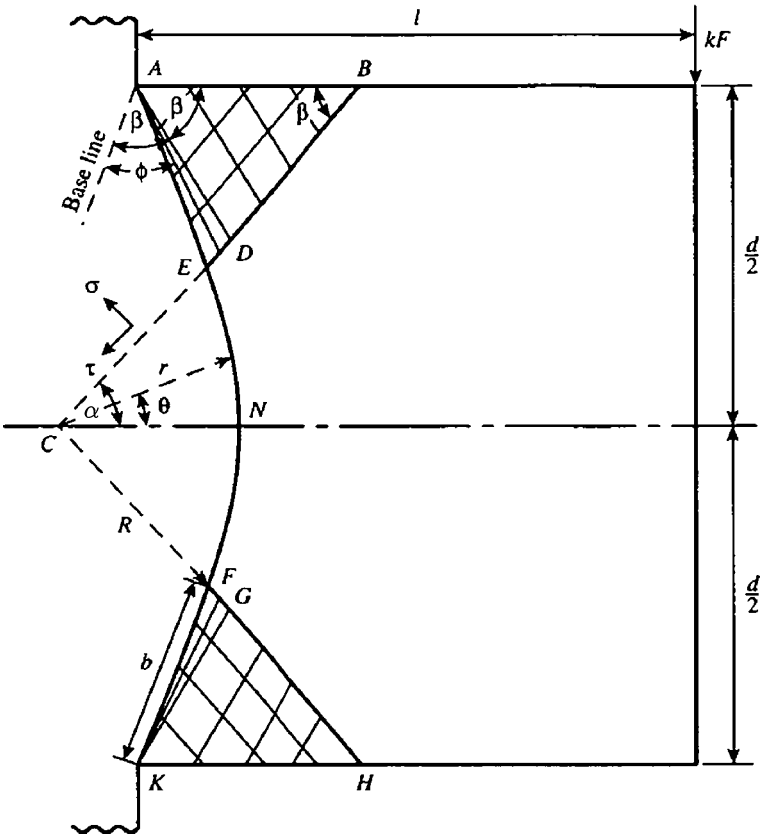

Fig. 2.11 Characteristic fields for an end-loaded cantilever with strong support ($i/d \leq 5.65$)

$$\sigma_r = k \sin\theta,\ \sigma_\theta = 2k \sin\theta,\ \tau_{r\theta} = -k \cos\theta, \tag{2.49}$$

so that the equilibrium equations and the yield criterion are identically satisfied, the polar angled being measured counterclockwise with respect to the longitudinal axis. The relation $\cot\psi = 2\cot\theta$ immediately follows from (2.5) and (2.49). The polar equation to the curve *ENF*, referred to *C* taken as the origin, is given by

$$r\,(d\theta/dr) = \cot\psi = 2\cot\theta, \quad \text{or} \quad r^2 \cos\theta = \text{constant}$$

Since the characteristic directions are everywhere continuous, the value of ψ at *E* may be written as

$$\psi_0 = \tan^{-1}\left(\frac{1}{2}\cot\phi_0\right) = \tan^{-1}\left(\frac{1}{2}\tan\alpha\right),$$

where ϕ_0 and α are the values of ϕ and θ, respectively, at E. It follows that $\phi_0 = \pi/2 - \alpha$. From geometry, angle AEC is $2\beta - \phi_0 + \alpha$, which must be equal to $\pi/2 + \psi_0$, and substituting for ϕ_0 and ψ_0 in terms of α, we obtain

$$2\alpha - \tan^{-1}\left(\tfrac{1}{2}\tan\alpha\right) = \pi - 2\beta. \tag{2.50}$$

The solution to this transcendental equation is $\alpha \approx 51.20°$, which gives $\psi_0 \approx 31.88°$. The fan angle EAD is $\delta = \alpha + \beta - \pi/2 = \psi_0/2$. It is interesting to note that the state of stress in the deforming region in plane stress bending varies from pure tension at the upper edge to pure shear at the center, whereas in plane strain bending the stress state is pure shear throughout the region of deformation.

The geometry of the field is completely defined by the dimensions b and R, representing the lengths AE and CE, respectively. The ratios b/d and R/d depend on the given ratio l/d, and are determined in terms of F/d from the conditions:

(a) the sum of the vertical projections of AE and CE is equal to $d/2$; and
(b) the resultant vertical force transmitted across $AENFK$ per unit thickness is equal to kF.

The resultant force acting across ENF is most conveniently obtained by regarding $CENF$ as a fully plastic region, the normal and shear stresses across CE and CF being of magnitudes σ and τ directed as shown. The pair of conditions (a) and (b) furnishes the relations

$$\left.\begin{aligned} &R\sin\alpha + b\cos\lambda = d/2, \\ &R\,(\sigma\cos\alpha - \tau\sin\alpha) + b\,(\tau\sin\lambda - \sigma\cos\lambda) = kF/2, \end{aligned}\right\} \tag{2.51}$$

where $\sigma = 2k \sin\alpha$ and $\tau = \mathrm{k}\cos\alpha$ in view of (2.49), while $\lambda = \alpha + 2\beta - \pi/2 \approx 70.68°$. Substituting for σ and τ, and inserting the values of σ and λ, equations of (2.51) are easily solved for b/d and R/d as

$$\frac{b}{d} = 0.6075 - 0.9696\frac{F}{d}, \quad \frac{R}{d} = -0.0941 + 1.1741\frac{F}{d}. \tag{2.52}$$

The ratio F/d at the yield point is finally determined from the condition that the resultant moment of the forces acting on $AENFK$ about the center of rotation C is equal to the moment of the applied force about the same point. Thus

$$KF\,(l + R\cos\alpha - b\cos\lambda) = \sigma\left(R^2 + b^2 + 2Rb\sin\psi_0\right) + 2\tau Rb\,\cos\,\psi_0.$$

Substituting for σ and τ, using the values of σ, λ, and ψ_0 inserting the expressions for b/d and R/d from (2.52), the above equation may be rearranged into the quadratic

$$0.4342 - \left(\frac{1}{d} - 0.2600\right)\frac{F}{d} - 0.5288\frac{F^2}{d^2} = 0, \tag{2.53}$$

when *F/d* has been calculated from (2.53) for a given value of *l/d*, the ratios *b/d* and *R/d* follow from (2.52). Since $R = 0$ when $F/d \approx 0.080$, the proposed field applies only for $l/d \leq 5.65$. For higher *l/d* ratios, the characteristic field is modified in the same way as that in the corresponding plane strain problem, the collapse load being closely approximated by the empirical formula

$$\frac{d}{F} = 0.20 + 2.18\frac{1}{d}, \ \frac{1}{d} \geq 5.65.$$

The values of *F/d*, *b/d*, and *R/d* corresponding to a set of values of $l/d < 5.65$ are given in Table 2.2. The plane stress values of *F/d* are found to be about 14% lower than the corresponding plane strain values (Chakrabarty, 2006) over the

Table 2.2 Results for an end-loaded cantilever

Strong support				Work support			
l/d	*F/d*	*b/d*	*R/d*	*l/d*	*F/d*	*b/d*	*δ*
1.33	0.346	0.272	0.313	0.328	0.492	0.536	54.74
1.62	0.287	0.329	0.243	0.275	0.482	0.531	49.06
2.00	0.233	0.382	0.180	0.255	0.477	0.527	43.26
2.55	0.182	0.431	0.120	0.177	0.477	0.523	37.53
3.36	0.137	0.475	0.067	0.134	0.482	0.518	31.82
4.72	0.086	0.514	0.019	0.095	0.492	0.515	26.07
5.65	0.80	0.530	0	0.079	0.498	0.512	23.49

whole range of values of *l/d*. The yield point load for a tapered cantilever has been discussed by Ranshi et al. (1974), while the influence of an axial force has been examined by Johnson et al. (1974).

Let M denote the bending moment at the built-in end under the collapse load *ktF*, where *t* is the thickness of the cantilever. Since the fully plastic moment under pure bending is $M_0 = \sqrt{3}\,ktd^2$, the ratio M/M_0 is equal to $4Fl/\sqrt{3}\,d^2$, and (2.53) may be written in the form

$$\frac{M}{M_0} \approx 1 + 1.23\frac{F}{d}\left(0.49 - \frac{F}{d}\right) \tag{2.54}$$

which is correct to within 0.3% for $F/d \leq 0.62$. The elementary theory of bending assumes $M/M_0 \approx 1$ irrespective of the shearing force. The results for the end-loaded cantilever are directly applicable to a uniformly loaded cantilever if we neglect the effect of surface pressure on the region of deformation. Since the resultant vertical load now acts halfway along the beam, the collapse load for a uniformly loaded cantilever of length $2l$ is identical to that for an end-loaded cantilever of length l.

2.4.2 Weakly Supported Cantilever

Consider a uniform cantilever of depth d, which fits into a horizontal-slot in a rigid vertical support. The top edge of the beam is clear of the support, so that the adjacent plastic region is able to spread into the slot under the action of a load kF per unit thickness at the free end. The length of the cantilever is l, measured from the point where the bottom edge is strongly held. The characteristic field, due to Green (1954b), is shown in Fig. 2.12. It consists of a pair of triangles ABN and CEF, under uniaxial tension and compression, respectively, and a singular field CEN where one family of characteristics is straight lines passing through C. The characteristics in the uniformly stressed triangles are inclined at an angle $\beta - \tan^{-1}\sqrt{2}$ to the respective free edges. The curved characteristics in CEN are given by the polar equation $r^2 \sin\phi = \text{constant}$, where ϕ is measured from a datum making an angle 2β to the bottom edge CF. The stresses in this region are given by (2.41) with an overall reversal of sign.

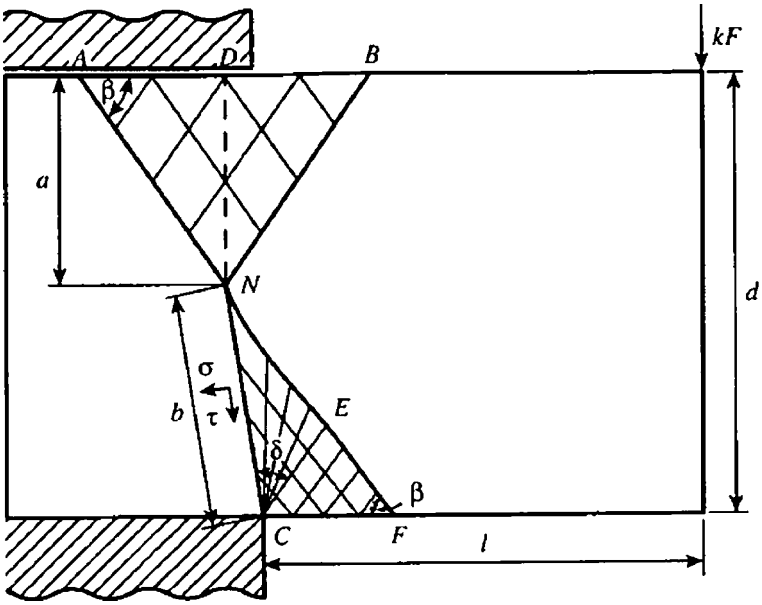

Fig. 2.12 Characteristic field for an end-loaded cantilever with weak support ($l/d \geq 1.33$)

For a given depth of the cantilever, the field is defined by the angle δ at the stress singularity, and the length b of the characteristic CN. The height of the triangle ABN is

$$a = d - b\sin(\beta + \delta)\,. \tag{2.55}$$

The stress is discontinuous across the neutral point N, about which the cantilever rotates as a rigid body at the incipient collapse. The normal and shear stresses over CN are

$$\sigma = -2k\cos(\beta - \delta), \quad \tau = \sin(\beta - \delta).$$

Since the tensile stress across the vertical plane DN is $\sqrt{3}k$ parallel to AB, the condition of zero resultant horizontal force across CND and the fact that the resultant vertical force per unit thickness across this boundary is equal to kF furnish the relations

$$b[\tau\ \cos\ (\beta + \delta) - \sigma \sin(\beta + \delta)] = \sqrt{3}ka,$$
$$b[\tau\ \sin\ (\beta + \delta) + \sigma \cos(\beta + \delta)] = kF.$$

Substituting for σ and τ, and using the value of β, these relations can be simplified to

$$\frac{F}{d} = \sin^2\delta, \quad \sqrt{3}\frac{a}{b} = \frac{2\sqrt{2}}{3} + \left(\frac{1}{3} - \frac{F}{b}\right)\tan(\beta + \delta) \tag{2.56}$$

When F/b and a/b have been calculated from (2.56) for a selected value of δ, the ratio d/b follows from (2.55), while l/b is obtained from the condition of overall moment equilibrium. Taking moment about N of the applied shearing force kF and also of the tractions acting over CND, we get

$$\frac{l}{b} = \cos(\beta + \delta) + \frac{b}{F}\left[\cos(\beta + \delta) + \frac{\sqrt{3}a^2}{2b^2}\right]. \tag{2.57}$$

Numerical values of l/d, F/d, b/d, and a/d for various values of δ are given in Table 2.2. As l/d decreases, δ increases to approach the limiting value equal to β. The angle between the two characteristics CN and EN decreases with decreasing l/d, becoming zero in the limit when the triangle $\underline{CEF}$ shrinks to nothing. The ratios F/d and l/d attain the values 0.328 and 1.332, respectively, in the limiting state.

The ratio M/M_0 at the built-in section (through C), which is equal to $4Fl/\sqrt{3}\mathrm{d}^2$, can be calculated from the tabulated values of l/d and F/d. The results can be expressed by the empirical formula

$$\frac{M}{M_0} \approx 1 + 1.45\frac{F}{d}\left(0.34 - \frac{F}{d}\right), \tag{2.58}$$

which is correct to within 0.5% for $F/d < 0.33$. Equations (2.54) and (2.58) are represented by solid curves in Fig. 2.13, the corresponding relations for plane strain bending being shown by broken curves. Evidently, M exceeds M_0 over the whole practical range, indicating that the constraining effect of the built-in condition outweighs the weakening effect of the shear except for very short cantilevers. In the case of a strong support, the maximum value of M/M_0 is about 1.121 in plane strain and 1.074 in plane stress, corresponding to F/d equal to about 0.28 and 0.25, respectively.

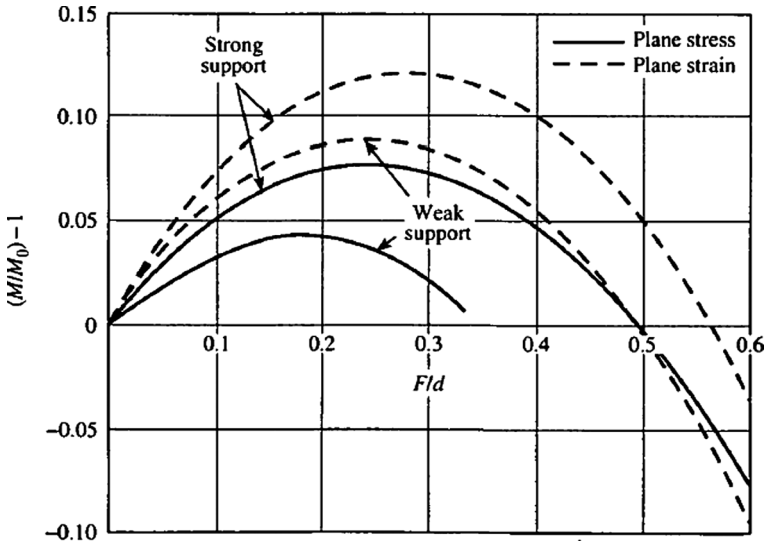

Fig. 2.13 Influence of transverse shear on the yield moment in the plane stress and plane strain bending of beams

2.4.3 Bending of I-Section Beams

Consider an I-beam, shown in Fig. 2.14a, whose transverse section has an area A_ω for the web and A_f for each flange including the fillets. The depth of the web is denoted by d, and the distance between the centroids of the flanges is denoted by *h.* It is assumed that the flanges yield in simple tension or compression, while the

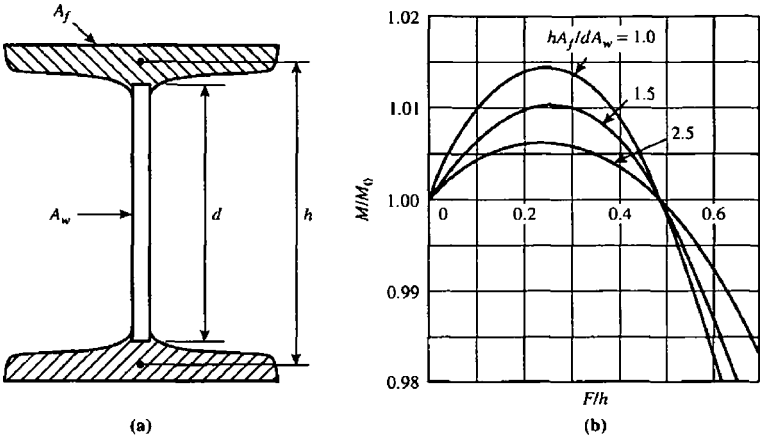

Fig. 2.14 Yield point states for I-section beams subjected to combined bending and shear

web yields under combined bending and shear. The bending moment carried by the flanges is $M_f = \sqrt{3}\,khA_f$, since one flange is in tension and the other in compression with a stress of magnitude $\sqrt{3}\,k$. For a uniform cantilever of length l, carrying a load ktF at the free end, where t is the web thickness, the bending moment existing at the fixed end is $M = ktFl$. Hence the bending moment shared by the web is

$$M_\omega = M - M_f = k\left(tFl - \sqrt{3}hA_f\right)$$

giving

$$\frac{M_\omega}{M'_0} = \frac{4Fl}{\sqrt{3}d^2} - \frac{4\,h}{d}\left(\frac{A_f}{A_w}\right),$$

where M'_0 is the fully plastic moment of the web under pure bending, equal to $\sqrt{3}\,kd^2t/4 = \sqrt{3}\,kA\omega d/4$. When the cantilever is strongly supported at the built-in end, $M\omega/M'_0$ is given by the right-hand side of (2.54), and the collapse load is given by

$$1.23\frac{F^2}{d^2} + \left(2.31\frac{l}{d} - 0.60\right)\frac{F}{d} - \frac{4h}{d}\left(\frac{A_f}{A_w}\right) - 1 = 0. \tag{2.59a}$$

For a weak end support, $M\omega/M'_0$ is given by the right-hand side of (2.58), and the equation for the collapse load becomes

$$1.45\frac{F^2}{d^2} + \left(2.31\frac{l}{d} - 0.49\right)\frac{F}{d} - \frac{4h}{d}\left(\frac{A_f}{A_w}\right) - 1 = 0. \tag{2.59b}$$

Equation (2.59), due to Green (1954b), is certainly valid over the practical range of values of l/d for standard I-beams. Since the flanges do not carry any shearing load, $M_f = M_0 - M'_0$, where M_0 is the fully plastic moment of the I-beam under pure bending. The relation $M_f = M - M_w$ therefore gives

$$\frac{M}{M_0} = 1 + \left(\frac{M_w}{M'_0} - 1\right)\frac{M'_0}{M_0}, \quad \frac{M_0}{M'_0} = 1 + \frac{4h}{d}\left(\frac{A_f}{A_w}\right).$$

The relationship between the bending moment and the shearing force at the yield point state of an I-beam is now obtained on substitution from (2.54) and (2.58), where M/M_0 is replaced by M_w/M'_0. Considering the strong support, for instance, we have

$$\frac{M}{M_0} = 1 + \left\{1.23\frac{F}{d}\left(0.49 - \frac{F}{d}\right)\right\}\Big/\left(1 + \frac{4h}{d}\frac{A_f}{A_\omega}\right). \tag{2.60}$$

The variation of M/M_0 with F/d is displayed in Fig. 2.14b. A satisfactory lower bound solution for M/M_0 at the yield point of an I-beam has been derived by Neal

(1961). The influence of axial force on the interaction relation, based on the characteristic field in plane stress, has been investigated by Ranshi et al. (1976).

2.5 Limit Analysis of a Hollow Plate

2.5.1 Equal Biaxial Tension

A uniform square plate, whose sides are of length 2α, has a circular hole of radius c at its center. The plate is subjected to a uniform normal stress σ along the edges in the plane of the plate. As the loading is continued into the plastic range, plastic zones spread symmetrically outward from the edge of the hole and eventually meet the outer edges of the plate when the yield point is reached. We begin by considering the von Mises yield criterion and its associated Lévy–Mises flow rule. For a certain range of values of c/a, the characteristic field would be that shown in Fig. 2.15a. The stress distribution within the field is radially symmetrical with the radial and circumferential stresses given by (2.13), where $\sigma_1 = \sigma_\phi$ and $\sigma_2 = \sigma_r$, the spatial distribution of the angle θ being given by (2.45). Assuming $\theta = \alpha$ at the external boundary $r = a$, where $a_r = a$, we obtain

$$\frac{\sigma}{Y} = \frac{2}{\sqrt{3}} \sin\left(\alpha - \frac{\pi}{6}\right), \quad \frac{c^2}{a^2} = \frac{2}{\sqrt{3}} \cos\alpha \exp\left\{-\sqrt{3}\left(\alpha - \frac{\pi}{6}\right)\right\}'. \tag{2.61}$$

The deformation mode at the incipient collapse consists of localized necking along the characteristics through A, permitting the rigid corners to move diagonally

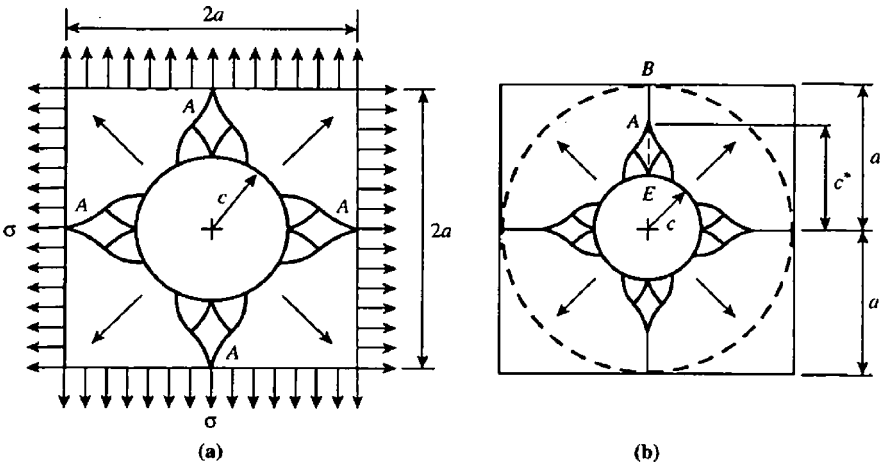

Fig. 2.15 Equal biaxial tension of a square plate with a central circular hole. (**a**) $0.483 \leq c/a \leq$ and (**b**)$0.143 \leq c/a \leq 0.483$

outward. Since the characteristics of stress and velocity exist only over the range $\pi/6 \leq \alpha \leq \pi/3$, the solution is strictly valid for $0.483 \leq c/a \leq 1$. When $\alpha = \pi/3$, the two characteristics coincide at A, and σ attains the value $0.577\,Y$.

For $c/a \leq 0.483$, (2.61) provides a lower bound on the yield point load, since the associated stress distribution is statically admissible in the annular region between the hole and the broken circle of radius a, shown in Fig. 2.15b. The remainder of the plate is assumed to be stressed below the yield limit under balanced biaxial stresses of magnitude σ, a discontinuity in the circumferential stress being allowed across the broken circle. On the other hand, an upper bound solution is obtained by extending the localized necks as straight lines from $r = c^* = 2.071c$ to $r = a$, permitting the same mode of collapse as in (a). Since $\sigma\phi = 2\sigma_r = 2k$ along the straight part of the neck, the longitudinal force per unit thickness across BAE is

$$a\sigma = \int_c^a \sigma_\phi dr = \int_c^{c^*} \frac{d}{dr}(r\sigma_r)dr + 2k\left(a - c^*\right) = \frac{2Y}{\sqrt{3}}\left(a - \frac{c^*}{2}\right),$$

where the second step follows from the equation of stress equilibrium. The upper bound therefore becomes

$$\sigma = \frac{2Y}{\sqrt{3}}\left(1 - 1.035\frac{c}{a}\right), \quad 0.143 \leq \frac{c}{a} \leq 0.483. \tag{2.62a}$$

For $c/a \leq 0.143$, a better upper bound is provided by the assumption of a homogeneous deformation mode in which the rate of plastic work per unit volume is $2U/a$, where U is the normal velocity of each side of the square. Since the rate of external work per unit plate thickness is $8a\sigma U$, we obtain the upper bound

$$\sigma = Y\left(1 - \frac{\pi c^2}{4a^2}\right), \quad 0 \leq \frac{c}{a} \leq 0.143. \tag{2.62b}$$

The difference between the lower and upper bounds, given by (2.61) and (2.62), respectively, is found to be less than 3% over the whole range of values of c/a.

When the material yields according to the Tresca criterion, a lower bound solution is obtained from the stress distribution $\sigma_r = Y(1- c/r)$, $\sigma_\phi = Y$ in the annulus $c \leq r \leq a$, and $\sigma_r = \sigma_\phi = \sigma$ in the region r = a. The continuity of the radial stress across r = a gives the lower bound $a = Y(1 - c/a)$. To obtain an upper bound, we assume localized necking along the axes of symmetry normal to the sides of the square, involving a diagonally outward motion of the four rigid corners with a relative velocity v perpendicular to the necks. For a unit plate thickness, the rate of internal work in the necks is $4(a - c)vY$, while the rate of external work is $4a\sigma v$, giving the upper bound $\sigma = Y(1 - c/a)$. Since the upper and lower bounds coincide, it is in fact the exact solution for the yield point stress.

2.5.2 Uniaxial Tension: Lower Bounds

Suppose that the plate is brought to the yield point by the application of a uniform normal stress σ over a pair of opposite sides of the square. The effect of the circular cutout is to weaken the plate so that the yield point value of σ is lower than the uniaxial yield stress Y. A lower bound solution for the yield point stress may be obtained from the stress discontinuity pattern of Fig. 2.16a, consisting of four uniformly stressed regions separated by straight lines, across which the tangential stress is discontinuous. The material between the circular hole of radius ρa the inner square of side ρa is assumed stress free. The conditions of continuity of the normal and shear stresses across each discontinuity are given by (2.33). If the principal stresses are denoted by the symbols s and t where $s \leq t$, the stress boundary conditions require

$$t_1 = \sigma,\ s_3 = 0,\ t_4 = 0,$$

where the subscripts correspond to the numbers used for identifying the regions of uniform stress. Let α denote the counterclockwise angle which the direction of the algebraically lesser principal stress in region 2 makes with the vertical. Then the clockwise angles made by this principal axis with the discontinuities bordering regions 1, 3, and 4 are

$$\theta_1' = \alpha - \theta_1,\ \theta_3' = \frac{\pi}{2} + \alpha - \theta_3,\ \theta_4' = -\left(\frac{\pi}{4} - \alpha\right).$$

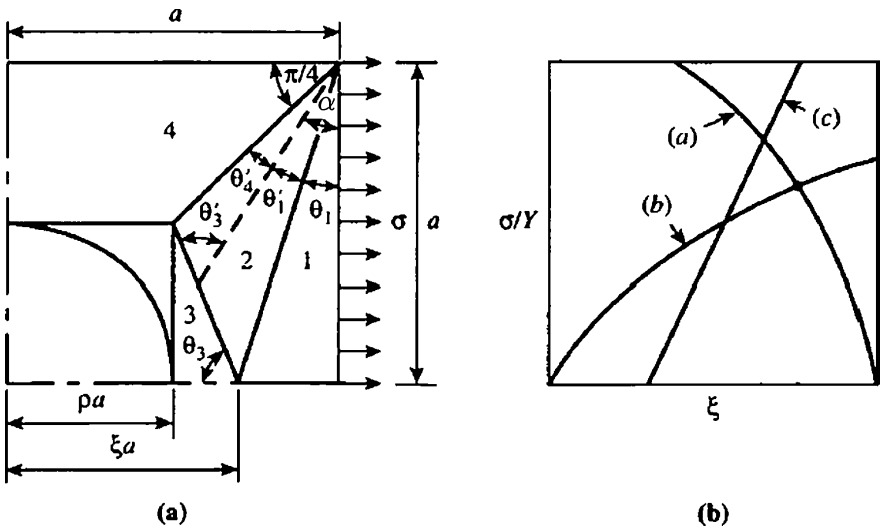

Fig. 2.16 Uniaxial tension of a square plate with a circular hole. (**a**) Stress discontinuities and (**b**) graphical representation of yields equalities

From geometry, the counterclockwise angles made by the algebraically greater principal stress axis with the line of discontinuity in regions 1, 3, and 4 are given by

$$\tan\theta_1 = 1-\xi,\ \ \tan\theta_3 = \rho/(\xi-\rho),\ \ \theta_4 = -\frac{\pi}{4}.$$

Considering the discontinuity between regions 4 and 2, and using (2.33), the quantities $(s_2 + t_2)/s_4$ and $(s_2 - t_2)/s_4$ can be expressed as functions of α. The consideration of the discontinuity between regions 3 and 2 then furnishes α and the ratio t_3/s_4. Finally, the continuity conditions across the boundary between regions 1 and 2 furnish s_4 and s_1 in terms of the applied stress σ. The results may be summarized in the form

$$\left.\begin{aligned} s_1 &= \frac{\rho\sigma}{(1-\rho)(1-\xi)},\ \ \tan 2\alpha = \frac{2\rho}{\xi},\\ s_2+t_2 &= \frac{\sigma(\xi-2\rho)}{\xi(1-\rho)},\ \ s_2-t_2 = \frac{\sigma\sqrt{\xi^2+4\rho^2}}{\xi(1-\rho)},\\ -t_3 &= \frac{\rho\sigma}{(1-\rho)(\xi-\rho)},\ \ s_4 = \frac{\sigma}{1-\rho}. \end{aligned}\right\} \tag{2.63}$$

Since regions 3 and 4 are in uniaxial states of stress, the magnitudes of t_3 and s_4 must not exceed the yield stress Y. For the von Mises criterion, the required inequalities in regions 1 and 2 follow from (2.2) and (2.63). When ρ is sufficiently small, the greatest admissible value of a is that for which region 4 is at the yield limit, giving the lower bound

$$\sigma = Y(1-\rho),\quad 0 \le \rho \le 0.204.$$

For higher values of ρ, region 4 is not critical, and we need to examine the following yield inequalities for the estimation of the lower bound:

$$\frac{\sigma}{Y} \le \frac{(1-\rho)(1-\xi)}{\left[(1-\rho)^2(1-\xi)^2 - \rho(1-\rho)(1-\xi)+\rho^2\right]^{1/2}}, \tag{2.64a}$$

$$\frac{\sigma}{Y} \le \frac{\xi(1-\rho)}{\left(\xi^2-\rho\xi+4\rho^2\right)^{1/2}},\quad \frac{\sigma}{Y} \le \frac{(1-\rho)(\xi-\rho)}{\rho}, \tag{2.64b,c}$$

The parameter ξ must be chosen in the interval $0 \le \xi \le 1$ such that the inequalities (2.64) admit the greatest value of σ. If the right-hand sides of these inequalities are plotted as functions of ξ for a given ρ, the greatest admissible value of σ/Y is the largest ordinate of the region below all the curves, as indicated in Fig. 2.16b. Thus, a/Y is given by the point of intersection of the curves (a) and (b), if this point is below the line (c), and by the point of intersection of (a) and (c), if curve (b) passes above this point. It turns out that the former arises for $0.204 \le \rho \le 0.412$, and the latter for $0.412 \le \mathrm{p} \le 1$.

When the Tresca criterion is adopted, the inequalities corresponding to regions 1 and 2 only are modified, the stress distribution being statically admissible if

$$s_1 \le Y,\ s_2 - t_2 \le Y,\ -t_3 \le Y,\ s_4 \le Y.$$

Since $s_2 - t_2$ is greater than s_4 over the whole range in view of (2.63), it is only necessary to consider the first three of the above inequalities. To obtain the best lower bound, the first two conditions should be taken as equalities for relatively small values of ρ, while the first and third conditions should be taken as equalities for relatively large values of ρ. Using (2.63), the results may be expressed as

$$\left.\begin{aligned} &\rho = \frac{\xi\,(1-\xi)}{(3\xi-2)\sqrt{2-\xi}},\ \frac{\sigma}{Y} = \frac{(1-\xi)\,(1-\rho)}{\rho}, \quad 0 \le \rho \le 0.44, \\ &\xi = \frac{1+\rho}{2},\ \ \frac{\sigma}{Y} = \frac{(1-\rho)^2}{2\rho}, \quad 0.44 \le \rho \le 1. \end{aligned}\right\} \tag{2.65}$$

The lower and upper bound solutions given in this section are essentially due to Gaydon and McCrum (1954), Gaydon (1954), and Hodge (1981). All the bounds discussed here apply equally well to the uniaxial tension of a square plate of side $2a$, containing a central square hole with side $2c$, where $c = \rho a$.

2.5.3 Uniaxial Tension: Upper Bounds

An upper bound on the yield point stress is derived from the velocity field involving straight localized necks which run from the edge of the hole to the stress-free edges of the plate, as shown in Fig. 2.17a. The rigid triangles between the two pairs of neck move away vertically toward each other, while the rigid halves of the remainder of the plate move horizontally at the incipient collapse. Let v denote the velocity of one side of the neck relative to the other, and ψ the angle of inclination of the neck to the relative velocity vector. For a von Mises material, the rate of plastic work per unit volume in the neck is $kv\sqrt{1+3\sin^2\psi}/b$ in view of (2.28), where b is the width

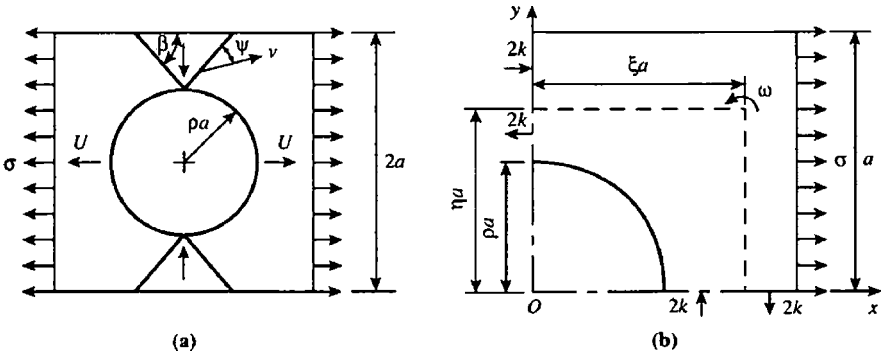

Fig. 2.17 Velocity discontinuity patterns for the plastic collapse of a uniaxially loaded square plate with a circular hole

of the neck. Since the length of each neck is $a(1-\rho)$ cosec β, where β is the angle of inclination of the neck to the free edge of the plate, the rate of internal work in the necks per unit plate thickness is

$$W = 4kva\,(1-\rho)\cos\mathrm{ec}\beta\sqrt{1+3\sin^2\psi}. \tag{2.66}$$

Equating this to the rate of external work, which is equal to $4\sigma aU = 4\sigma avcos\,(\beta-\psi)$ per unit thickness, we obtain the upper bound

$$\frac{\sigma}{Y} = \frac{(1-\rho)\cos\mathrm{ec}\beta\sqrt{1+3\sin^2\psi}}{\sqrt{3}\cos(\beta-\psi)}.$$

Minimizing σ with respect to β and ψ, it is found that the best upper bound corresponds to $\beta = \pi/4 + \psi/2$ and $\psi = \sin^{-1}\frac{1}{3}$, giving

$$\sigma = Y(1-\rho). \tag{2.67}$$

Since the upper bound coincides with the lower bound in the range $0 \le \rho \le 0.204$, the exact yield point stress is $Y(1-\rho)$ for a von Mises material over this range.

For a Tresca material, the rate of plastic work per unit volume in a neck is $kv(1+sin\,\psi)/b$ in view of (2.28), whatever the state of stress in the neck. The upper bound solution is therefore modified to

$$\frac{\sigma}{Y} = \frac{(1-\rho)\cos\mathrm{ec}\beta\,(1+3\sin\psi)}{2\cos(\beta-\psi)}.$$

This has a minimum value for $\beta = \psi = \pi/2$, and the best upper bound is precisely that given by (2.67). The necks coincide with the vertical axis of symmetry, and the two halves of the plate move apart as rigid bodies at the incipient collapse.

For relatively large values of ρ, a better upper bound is obtained by assuming that each quarter of the plate rotates as a rigid body with an angular velocity ω about a point defined by the distances ξa and ηa as shown in Fig. 2.17b. The deformation mode involves localized necking and bulging, with normal stresses of magnitude $2k$ acting along the horizontal and vertical axes of symmetry. Since the normal component of the relative velocity vector is of magnitude $\omega|x-\xi\ a|$ along the x-axis, and to $\omega|y-\eta a|$ along the y-axis, the rate of internal work per unit thickness of the quarter plate is

$$W = 2k\omega\left\{\int_{\rho a}^{a}|x-\xi\mathrm{a}|dx + |\int_{\rho a}^{a}|y-\eta\mathrm{a}|\,dy\right\}.$$

Carrying out the integration, the result may be expressed as

$$W = 2k\omega a^2\left\{\left(1+\rho^2\right)-(1+\rho)(\xi+\eta)+\xi^2+\eta^2\right\}. \tag{2.68}$$

The rate of external work on the quarter plate is σaU, where $U = a\omega(\eta - \frac{1}{2})$ is the normal component of the velocity of the center of the loaded side. Equating the rates of external and internal work done, and setting to zero the partial derivatives of σ with respect to ξ and η, we get

$$2\xi = 1 + \rho, \quad 2\eta = (1 + \rho) + \frac{\sigma}{2k},$$

for the upper bound to be a minimum. The best upper bound on a is therefore given by

$$\left(\frac{\sigma}{2k}\right)^2 + 2\rho\left(\frac{\sigma}{2k}\right) - 2(1 - \rho)^2 = 0.$$

It is easily verified that the conditions for a minimum σ are the same as those required for equilibrium of the quarter plate under the tractions acting along the neck and the external boundaries. The solution to the above quadratic is

$$\frac{\sigma}{2k} = -\rho + \sqrt{2 - 4\rho + 3\rho^2}, \tag{2.69}$$

where $k = Y/\sqrt{3}$ for a von Mises material, and $k = Y/2$ for a Tresca material. Evidently, (2.67) should be used in the range $0 \le \rho \le 0.42$, and (2.69) in the range of $0.42 \le \rho \le 1$ for a von Mises material. The ranges of applicability of (2.67) and (2.69) for a Tresca material are modified to $0 \le \rho \le \frac{1}{3}$ and $\frac{1}{3} \le \rho \le 1$, respectively. The upper and lower bound solutions are compared with one another in Fig. 2.18a and b, which correspond to the von Mises and Tresca materials, respectively.

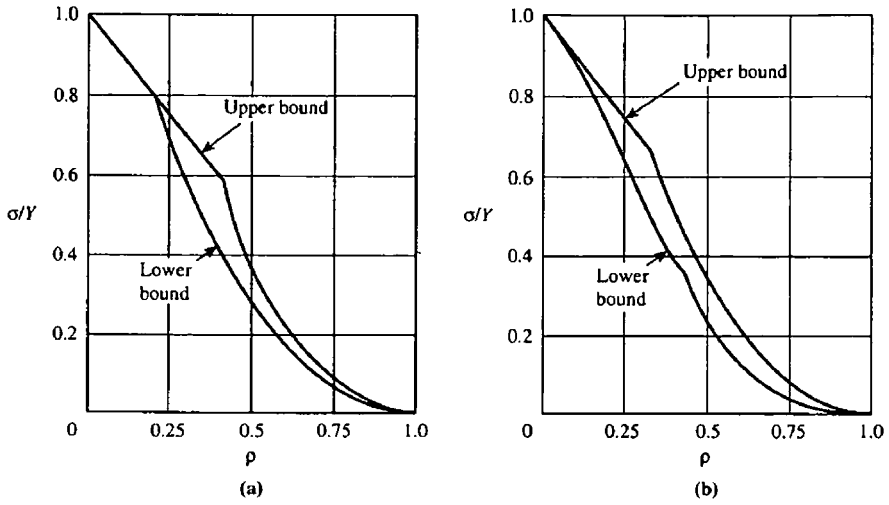

Fig. 2.18 Bounds on the collapse load for a square plate with a circular hole. (**a**) von Mises material and (**b**) Tresca material

2.5.4 Arbitrary Biaxial Tension

Suppose that a uniform normal stress $\lambda\sigma$ $(0 \leq \lambda \leq 1)$ is applied to the horizontal edges of the plate, in addition to the stress σ acting on the vertical edges. For a given value of λ, let σ be increased uniformly to its yield point value. A graphical plot of $\lambda\sigma$ against σ at the yield point state defines a closed interaction curve such that points inside the curve represent safe states of loading. Since such a curve must be convex, a simple lower bound may be constructed by drawing a straight line joining the points representing the lower bounds corresponding to uniaxial and equal biaxial tensions acting on the plate.

Upper bounds on the yield point stress for an arbitrary λ can be derived on the basis of the velocity discontinuity patterns of Fig. 2.17. Considering mode (a), the rate of external work done by the stress $\lambda\sigma$ is obtained from the fact that the speed of the rigid triangle is equal to $-v \sin(\beta - \psi)$, the length of its base being $2a(1 - \rho)\cot\beta$. Equating the total external work rate to the internal work rate given by (2.66), we get

$$\frac{\sigma}{Y} = \frac{(1-\rho)\sqrt{1+\sin^2\psi}}{\sin\beta\cos(\beta-\psi) - \lambda(1-\rho)\cos\beta\sin(\beta-\psi)}$$

for a von Mises material. The upper bound has a minimum value when $\beta = \pi/4 + \psi/2$ and $3\sin\psi = (1+z)/(1-z)$, where $z = \lambda(1-\rho)$, the best upper bound for the considered deformation mode being

$$\frac{\sigma}{Y} = \frac{1-\rho}{\sqrt{(1-\lambda)(1-\rho) + \lambda^2(1-\rho)^2}}, \quad \lambda(1-\rho) \leq 0.5. \tag{2.70}$$

When $\lambda(1-\rho) \geq 0.5$, the best configuration requires $\beta = \pi/2$, giving $\sigma = 2Y(1-\rho)/\sqrt{3}$ as the upper bound. For a Tresca material, the quantity $\sqrt{1+3\sin^2\psi}$ in (2.66) must be replaced by $(1 + \sin\psi)$, and the upper bound is then found to be $\sigma = Y(1-\rho)$, on setting $\beta = \psi = \pi/2$ for all values of λ.

If the rotational mode (b) is considered for collapse, the rate of external work per unit thickness is $\sigma a^2\omega(\eta - \frac{1}{2})$ due to the horizontal stress, and $-\lambda\sigma a^2\omega(\xi - \frac{1}{2})$ due to the vertical stress. Equating the total external work rate to the internal work rate given by (2.68), and minimizing $\sigma/2k$ with respect of ξ and η, we get

$$2\xi = (1+\rho) - \frac{\lambda\sigma}{2k}, \quad 2\eta = (1+\rho) + \frac{\sigma}{2k},$$

and the best upper bound on the yield point stress is then given by

$$\left(1+\lambda^2\right)\left(\frac{\sigma}{2k}\right)^2 + 2\rho(1-\lambda)\left(\frac{\sigma}{2k}\right) - 2(1-\rho)^2 = 0 \tag{2.71}$$

for both the von Mises and Tresca materials with the appropriate value of k. When $\lambda = 0$, E (2.70) and (2.71) coincide with (2.67) and (2.69), respectively. When

$\lambda = 1$, these bounds do not differ appreciably from those obtained earlier for the von Mises material, while coinciding with the exact solution for the Tresca material. For sufficiently small values of ρ, a better bound for the von Mises material is obtained by dividing the right-hand side of (2.62b) by the quantity $\sqrt{1 - \lambda + \lambda^2}$, which is appropriate for an arbitrary λ. The bounds on the collapse load for a square plate with reinforced cutouts have been discussed by Weiss et al. (1952), Hodge and Perrone (1957), and Hodge (1981).

2.6 Hole Expansion in Infinite Plates

2.6.1 Initial Stages of the Process

An infinite plate of uniform thickness contains a circular hole of radius a, and a gradually increasing radial pressure ρ is applied round the edge of the hole, Fig. 2.19. While the plate is completely elastic, the radial and circumferential stresses are the same as those in a hollow circular plate of infinite external radius and are given by

$$\sigma_r = -\frac{\rho a^2}{r^2}, \quad \sigma_\theta = \frac{\rho a^2}{r^2}.$$

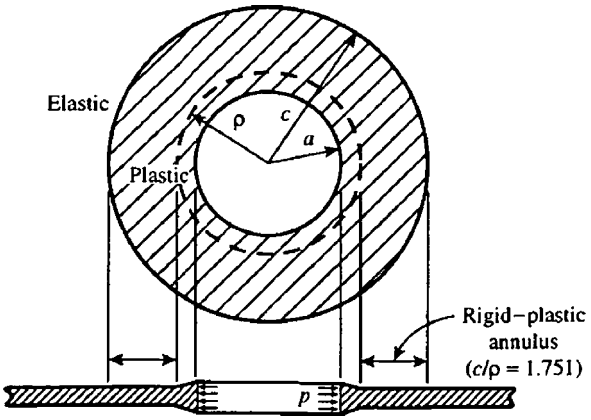

Fig. 2.19 Elastic and plastic regions around a finitely expanded circular hole in an infinite plate

Each element is therefore in a state of pure shear, the magnitude of which is the greatest at $r = a$. Yielding therefore begins at the edge of the hole when ρ is equal to the shear yield stress k. If the pressure is increased further, the plate is rendered plastic within some radius c, the stresses in the nonplastic region being

$$\sigma_r = -\frac{kc^2}{r^2}, \quad \sigma_\theta = \frac{kc^2}{r^2}, \quad r \geq c.$$

Since the stresses have opposite signs, the velocity equations must be hyperbolic in a plastic region near the boundary $r = c$, with the characteristics inclined at an angle $\pi/4$ to the plastic boundary. Over a range of values of c/a, the plastic material would be entirely rigid. The equation of equilibrium is

$$\frac{\partial \sigma_r}{\partial r} = \frac{\sigma_\theta - \sigma_r}{r}.$$

If the von Mises criterion is adopted, the stresses may be expressed in terms of the deviatoric angle ϕ as

$$\sigma_r = -2k \sin\left(\frac{\pi}{6} + \phi\right), \quad \sigma_\theta = 2k \sin\left(\frac{\pi}{6} - \phi\right), \tag{2.72}$$

where $\phi = 0$ at $r = c$. Inserting the relation $\sigma_\theta - \sigma_r > = 2k\, cos\, \phi$ into the equilibrium equation, we have

$$\cos\left(\frac{\pi}{6} + \phi\right) \frac{\partial \phi}{\partial r} = -\frac{\cos \phi}{r}.$$

Using the boundary condition at $r = c$, this equation is readily integrated to give the radial distribution of ϕ as

$$\frac{c^2}{r^2} = e^{\sqrt{3}\phi} \cos \phi.$$

The relationship between the applied pressure ρ and the plastic boundary radius c is given parametrically in the form

$$\rho = 2k \sin\left(\frac{\pi}{6} + \alpha\right), \quad \frac{c^2}{a^2} = e^{\sqrt{3}\alpha} \cos \alpha, \tag{2.73}$$

where α is the value of ϕ at $r = a$. As α increases from zero, ρ increases from k. The pressure attains its greatest value $2k$ when $\alpha = \pi/3$, giving

$$\frac{c}{a} = \left(\frac{1}{2} e^{\pi/\sqrt{3}}\right)^{1/2} \approx 1.751.$$

The characteristics at this stage envelop the edge of the hole, which coincides with the direction of the numerically lesser principal stress, equal to -k. If the hole is further expanded, the plastic boundary continues to move outward, and the inner radius p of the rigid part of the plastic material is such that $c/\rho = 1.751$ throughout the expansion. Since an ideally plastic material cannot sustain a stress greater than $2k$ in magnitude, the plate must thicken to support the load which must increase for continued expansion.

If the material yields according to the Tresca criterion, $\sigma_\theta - \sigma_r = 2k$ in a plastic annulus adjacent to the boundary $r = c$. Substituting in the equilibrium equation and integrating, we obtain the stress distribution

$$\sigma_r = -k\left(1 + 2\mathrm{In}\frac{c}{r}\right), \quad \sigma_\theta = k\left(1 - 2\mathrm{In}\frac{c}{r}\right). \tag{2.74}$$

in view of the continuity of the stresses across $r = c$. The applied pressure attains its greatest value $2k$ when $c/a = \sqrt{e} \approx 1.649$, and the corresponding circumferential stress vanishes at the edge of the hole. A further expansion of the hole must involve thickening of the plate, while a rigid annulus of plastic material exists over the region $\rho \leq r \leq c$, where $c/p = 1.649$ at all stages of the continued expansion.

2.6.2 Finite Expansion Without Hardening

A solution for the finite expansion of the hole will now be carried out on the basis of the Tresca criterion, neglecting work-hardening. The circumferential stress then changes discontinuously across $r = \rho$ from zero to $-k$, the value required by the condition of the zero circumferential strain rate in the presence of thickening. The angle of inclination of the velocity characteristics to the circumferential direction changes discontinuously from $\cot^{-1}\sqrt{2}$ to zero across $r = \rho$. In the plastic region defined by $a \leq r \leq p$, the equations defining the stress equilibrium and the Lévy–Mises flow rule are

$$\left.\begin{aligned} &\frac{\partial}{\partial r}(h\sigma_r) = \frac{h}{r}(\sigma_\theta - \sigma_r), \quad \frac{\partial v}{\partial r} = \left(\frac{2\sigma_r - \sigma_\theta}{2\sigma_\theta - \sigma_r}\right)\frac{v}{r}, \\ &\frac{1}{h}\left(\frac{\partial h}{\partial \rho} + v\frac{\partial h}{\partial r}\right) = -\left(\frac{\sigma_r + \sigma_\theta}{2\sigma_\theta - \sigma_r}\right)\frac{v}{r}, \end{aligned}\right\} \tag{2.75}$$

where h is the local thickness and v the radial velocity with ρ taken as the time scale. These equations must be supplemented by the yield criterion which becomes $\sigma_r = -2k$ in the region $r \leq p$. The set of equations (2.75) is hyperbolic with characteristics $d\rho = 0$ and $dr - vd\rho = 0$ in the (r, ρ)-plane.

The solution for a hole expanded from a finite radius may be obtained from that expanded from zero radius by discarding the part of the solution which is not required. Indeed, it is immaterial whether the pressure at any radius is applied by an external agency or by the displacement of an inner annulus (Hill, 1949). Since the plate is infinite, the stress and velocity at any point must be functions of a single parameter $\xi = r/p$, so that

$$\rho\frac{\partial}{\partial r} = \frac{d}{d\xi}, \quad \rho\frac{\partial}{\partial \rho} = -\xi\frac{d}{d\xi}.$$

Setting $\sigma_r = -2k$ and $\sigma_\theta = -2ks$ in (2.75), where s is a dimensionless stress variable; they are reduced to the set of ordinary differential equations

$$\frac{dh}{d\xi} = (s-1)\frac{h}{\xi}, \quad \frac{dv}{d\xi} = -\left(\frac{2-s}{1-2s}\right)\frac{v}{\xi}, \quad \left(1 - \frac{\xi}{v}\right)\frac{dh}{d\xi} = \left(\frac{1+s}{1-2s}\right)\frac{h}{\xi}. \tag{2.76}$$

The elimination of $dh/d\xi$ between the first and third equations of (2.76) leads to

$$\frac{v}{\xi} = \frac{(1-s)(1-2s)}{2\left(1-s+s^2\right)}, \quad \frac{dv}{d\xi} = -\frac{(1-s)(2-s)}{2\left(1-s+s^2\right)}.$$

Eliminating v between the above pair of equations, we have

$$\xi \frac{d}{d\xi}\left(\frac{2s-s^2}{1-s+s^2}\right) = \frac{3(1-s)^2}{1-s+s^2}. \tag{2.77}$$

In view of the boundary condition $s = \frac{1}{2}$ when $\xi = 1$, the integration of (2.77) results in

$$\text{In}\left(\frac{1}{\xi}\right) = -\frac{1}{3}\left(\frac{1-2s}{1-s}\right) + \frac{1}{2}\text{In}\left\{\frac{3(1-\text{s})^2}{1-s+s^2}\right\} + \frac{1}{\sqrt{3}}\tan^{-1}\left(\frac{1-2s}{\sqrt{3}}\right). \tag{2.78}$$

The elimination of ξ between (2.77) and the first equation of (2.76) gives

$$h\frac{d}{dh}\left(\frac{2s-s^2}{1-s+s^2}\right) = -\frac{3(1-s)}{1-s+s^2}.$$

If the initial thickness of the plate is denoted by h_0, then $h = h_0$ when $s = \frac{1}{2}$, and the above equation is integrated to

$$\frac{h}{h_0} = [2(1-s)]^{-1/3} \exp\left\{\frac{2}{\sqrt{3}}\tan^1\left(\frac{1-2s}{\sqrt{3}}\right)\right\}. \tag{2.79}$$

If r_0 denotes the initial radius to a typical particle, the incompressibility of the plastic material requires $h_0 r_0 dr_0 = hr\,dr$ at any given stage of the expansion. Since $r_0 = \rho$ when $r = p$, we obtain the relation

$$1 - \frac{r^2}{\rho^2} = 2\int_{\xi}^{1}\left(\frac{h}{h_0}\right)\xi d\xi, \tag{2.80}$$

where the integration is carried out numerically using the relations (2.78) and (2.79). As ξ decreases from unity, s decreases from 0.5 and becomes zero at $r = \rho^*$, which is given by

$$\text{In}\frac{\rho}{\rho^*} = -\frac{1}{3} + \frac{1}{2}(\text{In}\,3) + \frac{\pi}{6\sqrt{3}} \approx 0.518, \quad \frac{c}{\rho^{ast}} \approx 2.768,$$

in view of (2.78). The thickness ratio at $r = p^*$ is $h^*/h_0 \approx 1.453$ in view of (2.79). The solution is therefore complete for $c/a \leq 2.768$, where a is the current radius of the hole. For larger expansions of the hole, σ_θ becomes positive when $r/c \leq 0.361$, and the yield criterion reverts to $\sigma_\theta - \sigma_r = 2k$. Equation (2.76) is then modified in such a way that an analytical solution is no longer possible. A numerical solution furnishes $a/c \approx 0.280$ when the hole is expanded from zero radius, the value of h/h_0 at the edge of the hole being 3.84 approximately. This is in close agreement with the value obtained experimentally by Taylor (1948a).

2.6.3 Work-Hardening von Mises Material

When the material work-hardens and obeys the von Mises yield criterion with the Lévy–Mises flow rule, (2.75) must be supplemented by the yield criterion which is written parametrically through an auxiliary angle ϕ as

$$\sigma_r = -\frac{2\sigma}{\sqrt{3}} \sin\left(\frac{\pi}{6} + \phi\right), \qquad \sigma_\theta = -\frac{2\sigma}{\sqrt{3}} \sin\left(\frac{\pi}{6} - \phi\right), \tag{2.81}$$

where σ is the current yield stress in uniaxial tension or compression. We suppose that the uniaxial stress–strain curve is represented by the equation

$$\sigma = \sigma_0 \left(1 - me^{-ne}\right), \tag{2.82}$$

where σ_0 and n are the empirical constants. The initial yield stress is $Y = (1-m)\sigma_0$, and the current slope of the stress–strain curve is $H = n(\sigma_0 - \sigma)$, which decreases linearly with increasing stress.

The material work-hardens only in the region $r \le \rho$, where $\rho = 0.571c$, since the plastic material beyond this radius remains rigid. It is convenient to define the dimensionless quantities

$$\xi = \frac{r}{\rho}, \quad \eta = \frac{h}{h_0}, \quad s = \frac{\sigma}{\sigma_0}.$$

We consider the expansion of a hole from zero radius, so that the stresses and strains in any element depend only on ξ. On substitution from (2.81), the last two equations of (2.75) become

$$\frac{dv}{d\xi} = -\left(\frac{\sqrt{3} + \tan\phi}{\sqrt{3} - \tan\phi}\right)\frac{v}{\xi}, \quad \left(\frac{\xi - v}{\eta}\right)\frac{d\eta}{d\xi} = -\left(\frac{2\tan\phi}{\sqrt{3} - \tan\phi}\right)\frac{v}{\xi}. \tag{2.83}$$

To obtain the differential equation for s, we write the expression for the circumferential strain rate in terms of the material derivative by using the Lévy–Mises flow rule. Thus

$$\frac{v}{r} = \frac{2\sigma_\theta - \sigma_r}{2H\sigma}\left(\frac{\partial\sigma}{\partial\rho} + v\frac{\partial\sigma}{\partial r}\right).$$

Substituting for σ_r, σ_θ, and H, and introducing the parameter $\xi = r/\rho$, this equation is reduced to

$$\left(\frac{\xi - v}{1 - s}\right)\frac{ds}{d\xi} = -\left(\frac{2n\sec\phi}{\sqrt{3} - \tan\phi}\right)\frac{v}{\xi}. \tag{2.84}$$

Inserting the expressions for σ_r and σ_θ from (2.81) into the first equation of (2.75) gives

$$\left(\frac{1}{\eta}\frac{d\eta}{d\xi}+\frac{1}{s}\frac{ds}{d\eta}\right)\tan\left(\frac{\pi}{6}+\phi\right)+\xi\frac{d\phi}{d\xi}=-\frac{2}{\sqrt{3}-\tan\phi}.$$

Eliminating $d\eta/d\xi$ and $ds/d\xi$ from the above equation by means of (2.83) and (2.84), we finally obtain the differential equation for ϕ in the form

$$\begin{aligned}(\xi-v)\left(\sqrt{3}-\tan\phi\right)\frac{d\phi}{d\xi}\\ =\frac{v}{\xi}\left\{\sqrt{3}\sec\phi+n\left(\frac{1-s}{s}\right)\left(1+\sqrt{3}\tan\phi\right)\right\}\sec\left(\frac{\pi}{6}+\phi\right)-2.\end{aligned}\tag{2.85}$$

Equations (2.84), (2.85), and the first equation of (2.83) must be solved simultaneously for the three unknowns v, s, and ϕ, using the boundary conditions $v=0$, $s=1-\mathrm{m}$, and $\phi=\pi/3$ when $\xi=1$. The second equation of (2.83) can be subsequently solved for η under the boundary condition $\eta=1$ when $\xi=1$. The expressions for all the derivatives given by (2.83) to (2.85) become indeterminate at $\xi=1$, but the application of L'Hospital's rule furnishes

$$\frac{d\phi}{d\xi}=\frac{\sqrt{3}}{2},\quad \frac{dv}{d\xi}=\frac{d\eta}{d\xi}=-\frac{1}{2\,(1+\lambda)},\quad \frac{ds}{d\xi}=-\frac{\lambda}{2\,(1+\lambda)},\ \xi=1,$$

where $\lambda=(2/\sqrt{3})mn/(1-\mathrm{m})$. The first derivatives of all the physical quantities are therefore discontinuous across $\xi=1$. For a nonhardening material, it is easy to see that the stress gradients $\partial\sigma_r/\partial\mathrm{r}$ and $\partial\sigma_\theta/\partial_r$ have the values zero and $-3\kappa/2\rho$, respectively, just inside the radius $r=\rho$.

Once the thickness distribution has been found, the initial radius ratio r_0/ρ to a typical element can be calculated from (2.80) for any assumed value of ξ. The current radius σ for a hole expanded from an initial radius σ_0 is obtained from the relation

$$\int_{a/\rho}^{1}\eta\xi\,d\xi=\frac{1}{2}\left(1-\frac{a_0^2}{\rho^2}\right).$$

The stress distribution is shown graphically in Fig. 2.20 for a material with $m=0.60$ and $n=9.0$. The thickness distribution is displayed in Fig. 2.21 for both work-hardening and nonhardening materials. The selected material is similar to that used by Alexander and Ford (1954), who analyzed the corresponding elastic/plastic problem using the Prandtl–Reuss theory. A rigid/plastic analysis for a plate of variable thickness has been given by Chern and Nemat-Nasser (1969).

From the known variations of r_0/ρ, s, and ϕ with ξ, the internal pressure necessary to expand a circular hole from an internal radius a_0 to a final radius a is found by using the first equation of (2.81). On releasing an amount q of the expanding pressure, the plate is left with a certain distribution of residual stresses. This is obtained by adding the quantities $q(a^2/r^2)$ and $-q(a^2/r^2)$ to the values of σ_r, and σ_θ, respectively, at the end of the expansion, so long as the unloading is elastic. For sufficiently large values of q, secondary yielding would occur on unloading, and the

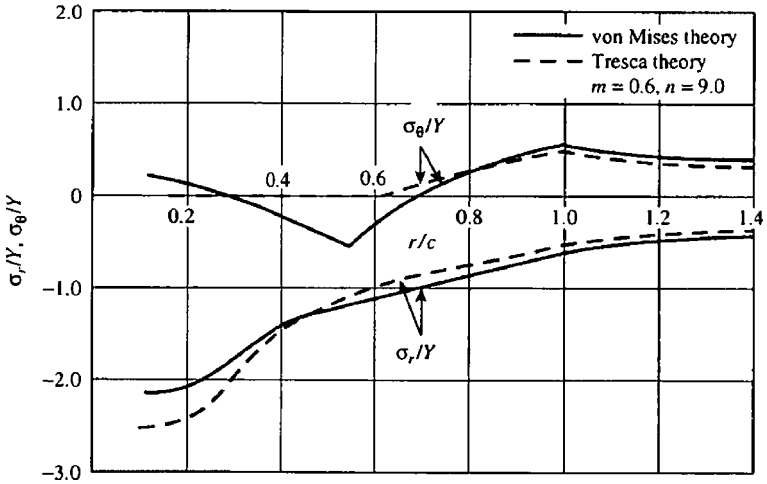

Fig. 2.20 Stress distribution in the finite expansion of a circular hole in an infinite plate of work-hardening material

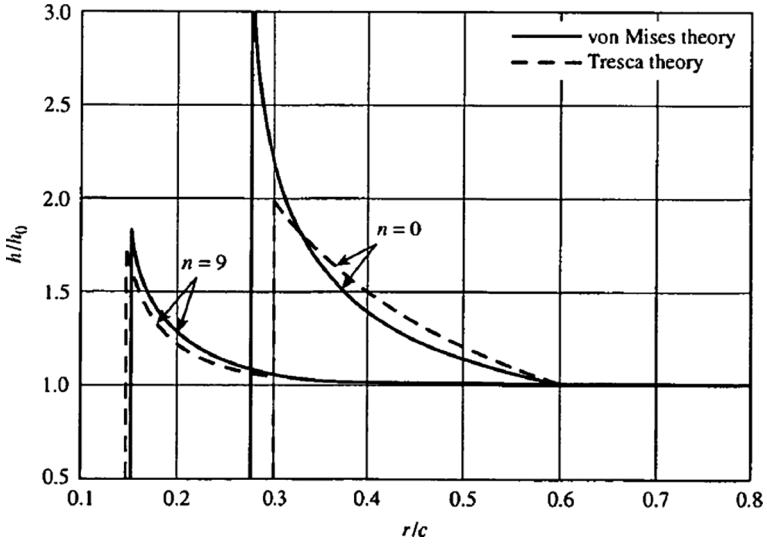

Fig. 2.21 Thickness variation in an infinite plate containing a finitely expanded circular hole

analysis becomes quite involved. A complete analysis of the unloading process for $c/a \leq 1.751$, taking secondary yielding into account, has been given by Alexander and Ford (1954) and by Chakrabarty (2006).

2.6.4 Work-Hardening Tresca Material

Suppose, now, that the material obeys Tresca's yield criterion and its associated flow rule, the stress–strain curve of the material is given by (2.82). For $\rho \leq r \leq c$, where $p = 0.607c$, the stress distribution is still given by (2.74), where $k = Y/2$, since there is no strain hardening in this region. Indeed, the flow rule corresponding to the yield condition $\sigma_\theta - \sigma_r - Y$ implies the thickness strain to be zero, and the velocity vanishes identically in view of the incompressibility condition and the boundary condition. For $r \leq \rho$, the stresses over a certain finite region would be $\sigma_r = -\sigma$ and $\sigma_\theta = 0$, corresponding to a corner of the yield hexagon. The associated flow rule gives

$$\dot{\varepsilon}_r < 0, \quad \dot{\varepsilon}_\theta > 0, \quad \dot{\varepsilon}_z > 0.$$

The sum of the three strain rates must vanish by the condition of plastic incompressibility. The rate of plastic work per unit volume is $\sigma\ \dot{\varepsilon}$, where $\varepsilon = -\varepsilon_r$, indicating that the relationship between σ and ε is the same as that in uniaxial tension or compression. It follows from the plastic incompressibility equation written in the integrated form that

$$\frac{hr}{h_0 r_0} = e^{\varepsilon} = \left(\frac{1-s}{m}\right)^{-1/n} \tag{2.86}$$

in view of (2.82), with $s = \sigma/\sigma_0$. Since $\sigma_\theta = 0$, the first equation of (2.75) reveals that $hr\sigma = h_0 \rho Y$ in view of the boundary conditions at $r = \rho$. Equation (2.86) therefore gives

$$\frac{r_0}{\rho} = \frac{Y}{\sigma} e^{-\varepsilon} = \left(\frac{1-m}{s}\right)\left(\frac{1-s}{m}\right)^{1/n}. \tag{2.87}$$

Differentiating (2.87) partially with respect to r, and noting the fact that $\varepsilon = ln(\partial r_0/\partial r)$, we have

$$-\left(\frac{1-m}{s}\right)\left\{\frac{1}{s} + \frac{1}{n(1-s)}\right\}\left(\frac{1-s}{m}\right)^{2/n}\frac{\partial s}{\partial r} = \frac{1}{\rho}.$$

Integration of this equation under the boundary condition $s = 1-m$ at $r = \rho$, and using the integration by parts, furnishes the result

$$\xi = \left(\frac{1-m}{s}\right)\left(\frac{1-s}{m}\right)^{2/n} + \frac{1-m}{mn}\int_{1-m}^{s}\left(\frac{1-s}{m}\right)^{2/n-1}\frac{ds}{s} \tag{2.88}$$

where $\xi = r/p$. The integral can be evaluated exactly for $n = 2$ and $n = 4$, but the numerical integration for an arbitrary value of n is straightforward. The thickness change can be calculated from the relation

$$\frac{h}{h_0} = \frac{\rho Y}{r\sigma} = \frac{1-m}{\xi s}. \tag{2.89}$$

This solution will be valid so long as the thickness strain rate is positive. Since the strain is a function of ξ only, this condition is equivalent to $dh/d\xi < 0$, which gives $-ds/d\xi < s/\xi$ in view of (2.89). Using the expression for $\partial_s/\partial r$, the condition for the validity of the solution may be written as

$$\xi \leq \left(\frac{1-m}{s}\right)\left\{1 + \frac{s}{n\,(1-s)}\right\}\left(\frac{1-s}{m}\right)^{2/n}.$$

This condition will be satisfied for most engineering materials for all values of $r_0/\rho \geq 0$. For a nonhardening material, $h_0/h = \xi$ and $r_0/\rho = \sqrt{2\xi - 1}$, giving $a/c = 0.303$ for a hole expanded from zero radius. For a work-hardening material with $m = 0.6$ and $n = 9.0$, it is found that $h/h_0 \approx 1.69$ and $r/c \approx 0.143$ at the edge of the hole when its initial radius is zero. The computed results for the Tresca theory are plotted as broken curves in Figs. 2.20 and 2.21, which provide a visual comparison with the results corresponding to the von Mises theory.

The Tresca theory for a hypothetical material with an exponentially rising stress–strain curve has been discussed by Prager (1953), Hodge and Sankaranarayanan (1958), and Nemat-Nasser (1968). A rigid/plastic analysis for the hole expansion under combined radial pressure and twisting moment has been given by Nordgren and Naghdi (1963). An elastic/plastic analysis for the finite expansion of a hole in a nonhardening plate of variable thickness has been presented by Rogers (1967). An elastic/plastic small strain analysis for a linearly work-hardening Tresca material has been given by Chakrabarty (1971).

2.7 Stretch Forming of Sheet Metals

2.7.1 Hydrostatic Bulging of a Diaphragm

A uniform plane sheet is placed over a die with a circular aperture and is firmly clamped around the periphery. A gradually increasing fluid pressure is applied on one side of the blank to make it bulge through the aperture. If the material is isotropic in the plane of the sheet, the bulge forms a surface of revolution, and the radius of curvature at the pole can be estimated at any stage from the measurement of the length of the chord to a neighboring point and its corresponding sagitta. The polar hoop strain can be estimated from the radial expansion of a circle drawn from the center of the original blank. The stress–strain curve of the material under balanced biaxial tension obtained in this way is capable of being continued up to fairly large strains before instability. The process has been investigated by Hill (1950b), Mellor (1954), Ross and Prager (1954), Weil and Newmark (1955), Woo (1964), Storakers (1966), Wang and Shammamy (1969), Chakrabarty and Alexander (1970), Ilahi et al. (1981), and Kim and Yang (1985a), among others.

Let r denote the current radius to a typical particle, and r_0 the initial radius, with respect to the vertical axis of symmetry. The local thickness of the bulged sheet is denoted by t, and the inclination of the local surface normal to the vertical by ϕ, as shown in Fig. 2.22. The ratio of the initial blank thickness t_0 to the blank radius a is assumed small enough for the bending stress to be disregarded. The circumferential and meridional stresses, denoted by σ_θ and σ_ϕ, respectively, must satisfy the equations of equilibrium which may be written in the form

$$\frac{\partial}{\partial r}\left(rt\sigma_\phi\right) = t\sigma_\theta, \quad \sigma_\phi \sin\phi = \frac{pr}{2t}, \tag{2.90}$$

where ρ is the applied fluid pressure. If the meridional and circumferential radii of curvature are denoted by ρ_ϕ and ρ_θ, respectively, the equations of normal and tangential equilibrium may be expressed as

$$\frac{\sigma_\theta}{\rho_\theta} + \frac{\sigma_\phi}{\rho_\phi} = \frac{p}{t}, \quad \frac{\sigma_\phi}{\rho_\theta} = \frac{P}{2t}, \tag{2.90a}$$

where

$$\rho\theta = r \cos \mathrm{ec}\phi, \quad \rho_\phi = \frac{\partial r}{\partial \phi} \sec\phi.$$

The elimination of p/t between the two equations of (2.90a) immediately furnishes

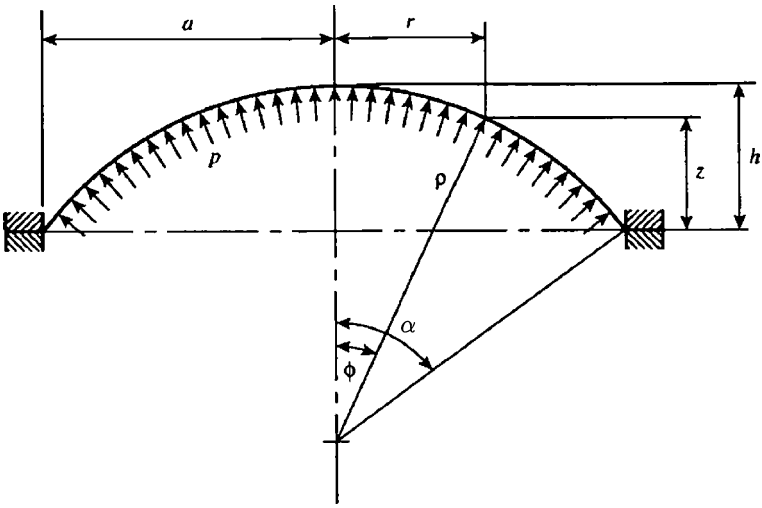

Fig. 2.22 Bulging of a circular diaphragm by the application of a uniform fluid pressure

$$\frac{\sigma_\theta}{\sigma_\phi} = 2 - \frac{\rho_\theta}{\rho_\phi}.$$

This equation indicates that $\sigma\theta \lessgtr \sigma\phi$ for $\rho_\theta \gtrless \rho_\theta$. The principal surface strains ε_θ,ε_ϕ and the thickness strain ε_t at any stage are

$$\varepsilon_\theta = \ln\left(\frac{r}{r_0}\right),\ \varepsilon_\phi = \ln\left(\frac{\partial r}{\partial r_0}\sec\phi\right),\ \varepsilon_t = \ln\left(\frac{t}{t_0}\right). \tag{2.91}$$

The condition for incompressibility requires $\varepsilon_t = -(\varepsilon_\theta + \varepsilon_\phi)$. If the radial velocity is denoted by v the components of the strain rates may be expressed as

$$\dot{\varepsilon}_\theta = \frac{v}{r},\ \dot{\varepsilon}_\phi = \frac{\partial v}{\partial r} + \dot{\phi}\tan\phi,\ \dot{\varepsilon}_t = \frac{\dot{t}}{t},$$

where the dot denotes rate of change following the particle. Eliminating v between the first two of the above relations, we obtain the equation of strain rate compatibility

$$\frac{\partial}{\partial r}(r\dot{\varepsilon}_\theta) = \dot{\varepsilon}_\phi - \dot{\phi}\tan\phi. \tag{2.92}$$

It will be convenient to take the initial radius r_0 as the independent space variable, and the polar compressive thickness strain ε_0 as the time scale, to carry out the analysis.

Introducing an auxiliary angle ψ, representing the angle made by the deviatone stress vector with the direction representing pure shear, the von Mises yield criterion and the associated Lévy–Mises flow rule can be simultaneously satisfied by writing

$$\left.\begin{aligned} &\sigma_\theta = \tfrac{2}{\sqrt{3}}\sigma\sin\left(\tfrac{\pi}{6}+\psi\right),\quad \sigma_\phi = \tfrac{2}{\sqrt{3}}\sigma\cos\psi,\\ &\dot{\varepsilon}_\theta = \dot{\varepsilon}\ \sin\ \psi,\ \dot{\varepsilon}_\phi = \dot{\varepsilon}\cos\left(\tfrac{\pi}{6}+\psi\right), \end{aligned}\right\} \tag{2.93}$$

where σ and $\dot{\varepsilon}$ are the equivalent stress and strain rate, respectively. Introducing dimensionless variables

$$\xi = \frac{r_0}{a},\ s = \frac{\sigma}{c},\ q = \frac{pa}{t_0 C},$$

where C is a constant stress, and using the fact that $\partial r/\partial r_0 = \cos\phi\ \exp(\varepsilon_\phi)$, $r = \mathrm{r}_\phi\ \exp(\varepsilon_\phi)$, and $t = t_0\ \exp(\varepsilon_1)$ in view of (2.91), (2.90) and (2.92) can be combined with (2.93) to obtain the set of differential equations

$$\frac{\partial}{\partial\xi}\left[\xi s\cos\psi\ \exp\left(-\varepsilon_\phi\right)\right] = s\cos\phi\sin\left(\frac{\pi}{6}+\psi\right)\exp\left(-\varepsilon_\theta\right),$$

$$s\ \sin\ \phi = \frac{\sqrt{3}}{4}q\xi\sec\psi\exp\left(2\varepsilon_\theta + \varepsilon_\phi\right), \tag{2.95}$$

$$\frac{\partial}{\partial \xi}\left[\xi \dot{\varepsilon} \sin \psi \exp\left(\varepsilon_\theta\right)\right] = \left[\dot{\varepsilon}\cos\phi\cos\left(\frac{\pi}{6}+\psi\right) - \dot{\phi}\sin\phi\right]\exp\left(-\varepsilon_\phi\right), \quad (2.96)$$

These equations must be supplemented by the strain-hardening law $\sigma = Cf(\varepsilon)$, where ε is the equivalent total strain. Since $\sigma_\theta = \sigma_\phi = \sigma$ at the pole ($\xi = 0$), while $\dot{\varepsilon} = 0$ at the clamped edge ($\xi = 1$), the boundary conditions may be written as

$$\psi = \frac{\pi}{6} \text{ and } \dot{\varepsilon} = 1 \text{ at } \xi = 0; \quad \psi = 0 \text{ at } \xi = 1.$$

When the distributions of the relevant physical parameters have been found for any given polar strain ε_0, the shape of the bulge can be determined by the integration of the equation

$$\frac{\partial z}{\partial r_0} = -\tan\phi\frac{\partial r}{\partial r_0} = -\sin\phi\exp\left(\varepsilon_\phi\right).$$

Using (2.95), this equation may be written in the more convenient form

$$\frac{\partial}{\partial \xi}\left(\frac{z}{a}\right) = -\frac{\sqrt{3}}{4}\left(\frac{q}{s}\right)\xi \sec\psi \exp\left(2\varepsilon_\theta + 2\varepsilon_\phi\right), \quad (2.97)$$

which must be solved numerically under the boundary condition $z = 0$ at $\xi = 1$. The polar height h is finally obtained as the value of z at $\xi = 0$. The polar radius of curvature ρ is given by

$$\frac{\rho}{a} = \left(\frac{2\sigma_0 t_0}{pa}\right)\exp\left(-\varepsilon_0\right) = \left(\frac{2s_0}{q}\right)\exp\left(-\varepsilon_0\right),$$

where σ_0 is the value of σ_θ or σ_ϕ the pole $\xi = 0$. Plastic instability occurs when the pressure attains a maximum, and this corresponds to $d\rho/\rho$ being equal to $d\sigma_0/\sigma_0 - d\varepsilon_0$ during an incremental deformation of the bulge. This condition can be used to establish the point of tensile instability in the bulging process.

Suppose that the values of s, ψ, and ϕ are known at each point for the mth stage of the bulge. In order to continue the solution, we must find the corresponding distribution of $\dot{\varepsilon}$. Using the boundary condition $\dot{\varepsilon} = 1$ at $\xi = 0$, (2.96) is therefore solved numerically for $\dot{\varepsilon}$, the quantity ϕ being found from the values of ϕ in the previous and current stages of the bulge. The values of ε_θ and ε_ϕ for the $(m + 1)$th stage are then obtained from their increments, using (2.93) and an assigned change in ε_0. It is convenient to adopt the power law of hardening

$$\sigma = C\varepsilon^n.$$

Since s is a known function of ε, (2.94) can be solved for ψ, assuming a value of q for the $(m + 1)$th stage, and using (2.95). The correct value of q is obtained when the boundary conditions $\psi = 0$ at $\xi = 1$ and $\psi = \pi/6$ at $\xi = 0$ are both satisfied.

If, for a certain stage of the bulge, $\dot{\varepsilon}$ is found to vanish at $\xi = 1$, indicating neutral loading of the clamped edge, the condition $\dot{\varepsilon} = 0$ at $\xi = 1$ must be satisfied at all subsequent stages. The material rate of change of (2.95) gives

$$\dot{\phi} = \left\{ \frac{\dot{q}}{q} + \left[\sqrt{3} \sin \left(\frac{\pi}{6} + \psi \right) - \frac{n}{\varepsilon} \right] \dot{\varepsilon} + \dot{\psi} \tan \psi \right\} \tan \phi$$

in view of (2.93). The ratio $\dot{q}/q$ in this case should be found by substituting the above expression for ϕ into (2.96), and integrating it under the boundary conditions $\dot{\varepsilon} = 1$ at $\xi = 0$, and $\dot{\varepsilon} = 0$ at $\xi = 1$, the quantity $\dot{\psi}$ being given by the previous and current values of ψ.

Initially, however, it is reasonable to assume $\sqrt{3} \tan\psi \approx 1 - n\xi^2$ as a first approximation, which is appropriate over the whole bulge except at $\xi = 1$ (when $n \neq 0$). Since changes in geometry are negligible, (2.94) reduces in this case to

$$\frac{\partial}{\partial \xi} (s \cos \psi) + \frac{1}{2\xi} \left(1 - \sqrt{3} \tan \psi \right) (s \cos \psi) = 0.$$

This equation is readily integrated under the boundary condition $s = s_0$ at $\xi = 0$, resulting in

$$s \cos \psi = \frac{\sqrt{3}}{2} s_0 \exp \left(-\frac{n}{4} \xi^2 \right), \quad \phi = \frac{q\xi}{2s_0} \exp \left(\frac{n}{4} \xi^2 \right), \tag{2.98}$$

in view of (2.95). The power law of hardening permits the Lévy–Mises flow rule to be replaced by the Hencky relations, so that the strain rates in (2.93) are replaced by the strains themselves. Substituting for the strain ratio $\varepsilon_\phi / \varepsilon_\theta$ into the equation of strain compatibility, obtained by eliminating r between the first two relations of (2.91), we get

$$\frac{\partial \varepsilon_\theta}{\partial \xi} - \frac{\sqrt{3}}{2\xi} \left(\cot \psi - \sqrt{3} \right) \varepsilon_\theta = -\frac{\phi^2}{2\xi} \tag{2.99}$$

to a sufficient accuracy. Inserting the expressions for $\cot \psi$ and ϕ, this equation can be integrated under the boundary condition $\varepsilon_\theta = 0$ at $\xi = 1$. Since $\varepsilon_\theta = \varepsilon_\theta / 2$ at $\xi = 0$, we obtain

$$\frac{q}{s_0} = 2\sqrt{2\varepsilon_0} \left\{ \int_0^1 (1 - nx)^{3/4} \exp \left(\frac{nx}{2} \right) dx \right\}^{-1/2} \approx \sqrt{[8]} \frac{\varepsilon_0}{8 - n}.$$

Using the above expression for q, the hoop strain $\varepsilon_\theta = \varepsilon \sin \psi$ can be expressed as a function of ε_θ and ξ. It is sufficiently accurate to put the result in the form

$$\varepsilon \sin \psi \approx \tfrac{1}{2} \varepsilon_0 \left(1 - \xi^2 \right) \left(1 - \frac{n\xi^2}{8 - n} \right) \left(1 - n\xi^2 \right)^{-3/4}. \tag{2.100}$$

Since $s/s_0 = (\varepsilon/\varepsilon_0)^n$, the distributions of s, ε, ψ, and ϕ can be determined from (2.98) and (2.100) for any small value of $\varepsilon 0$. The shape of the bulge and the polar height are obtained from the integration of the equation $\partial z/\partial \xi = -a\phi$, the result being

$$\frac{z}{a} \approx \frac{q}{4s_0}\left(1-\xi^2\right)\left\{1+\frac{n}{32}\left(1+\xi^2\right)\right\}, \quad \frac{h}{a} \approx \frac{1}{2}\left\{\left(\frac{16+n}{8-n}\right)\varepsilon_0\right\}^{1/2}.$$

The initial shape of the bulge is therefore approximately parabolic for all values of n. Since ϕ changes at the rate $\dot{\phi} = \phi/2\varepsilon_0$ in view of (2.98), the solution for the von Mises material can proceed by integrating (2.96) as explained earlier. Figure 2.23 shows the surface strain distribution for various values of ε_0 in a material with $n = 0.2$, the variation of ε_0 with the polar height being displayed in Fig. 2.24. The theoretical predictions are found to agree reasonably well with available experimental results on hydrostatic bulging. A detailed analysis for the initial deformation of the diaphragm has been given by Hill and Storakers (1980).

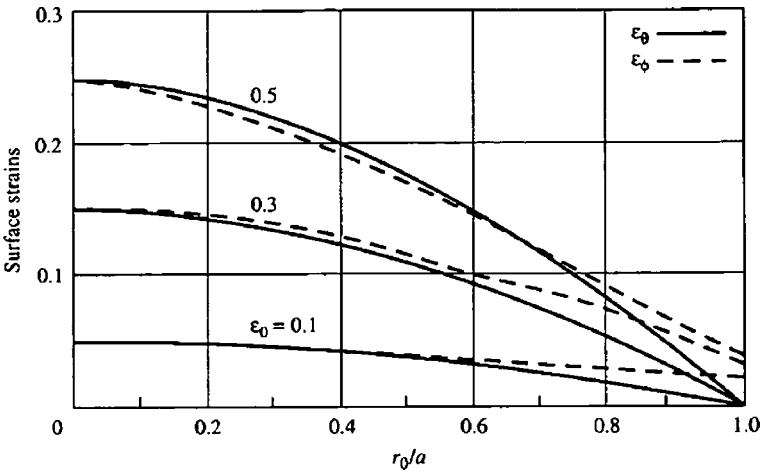

Fig. 2.23 Distribution of circumferential and meridional true strains in the hydrostatic bulging process when $n = 0.2$ (after Wang and Shammamy, 1969)

2.7.2 Stretch Forming Over a Rigid Punch

A flat sheet of metal of uniform thickness t_0 is clamped over a die with a circular aperture of radius a, and the material is deformed by forcing a rigid punch with a hemispherical head. The axis of the punch passes through the center of the aperture and is normal to the plane of the sheet. The deformed sheet forms a surface of revolution with its axis coinciding with that of the punch. Due to the presence of friction between the sheet and the punch, the greatest thinning does not occur at the

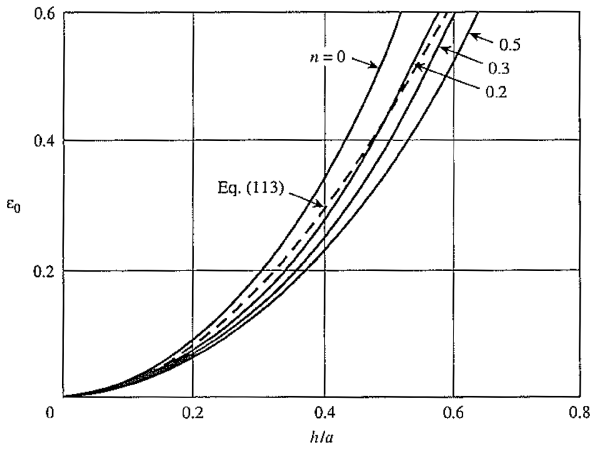

Fig. 2.24 Variation of the polar thickness strain with polar height during the bulging of a circular diaphragm

pole but at some distance away from it, and fracture eventually occurs at this site. In a typical cupping test, known as the Erichsen test, a hardened steel ball is used as the punch head, and the height of the cup when the specimen splits is regarded as the Erichsen number, which is an indication of the formability of the sheet metal. The process has been investigated experimentally by Keeler and Backofen (1963) and theoretically by Woo (1968), Chakrabarty (1970a), Kaftanoglu and Alexander (1970), and Wang (1970), among others. Finite element methods for the analysis of the stretch-forming process have been discussed by Wifi (1976), Kim and Kobayashi (1978), and Wang and Budiansky (1978).

In the theoretical analysis of the forming process, the coefficient of friction μ will be taken as constant over the entire surface of contact. The radius of the punch head, denoted by R, is somewhat smaller than the radius of the die aperture, Fig. 2.25. Let t denote the local thickness of an element currently at a radius r and at an angular distance ϕ from the pole, the initial radius to the element being denoted by r_0.

Over the region of contact, the equations of tangential and normal equilibrium are

$$\frac{\partial}{\partial r}\left(rt\sigma_\phi\right) = t\sigma_\theta + \mu pR\tan\phi, \quad t\left(\sigma_\theta + \sigma_\phi\right) = pR, \tag{2.101}$$

where p is the normal pressure exerted by the punch, and $r = R\sin\phi$. The elimination of pR between the above equations gives

$$\frac{\partial}{\partial r}\left(rt\sigma_\phi\right) = t\sigma_\theta\left(1 + \mu\tan\phi\right) + \mu t\sigma_\phi\tan\phi.$$

If the material obeys the von Mises yield criterion, the stresses are given by (2.93). In terms of the dimensionless variables $\xi = r_0/a$ and $s = \sigma/C$, where C is a constant stress, the above equation becomes

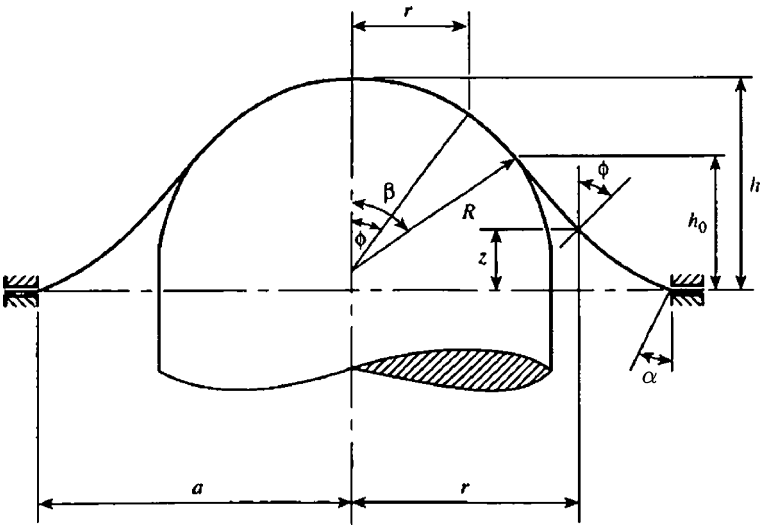

Fig. 2.25 Stretch forming of a circular blank of sheet metal over a hemispherical-headed punch

$$\frac{\partial}{\partial \xi}\left[\xi s \cos\psi \exp\left(-\varepsilon_\phi\right)\right] = s\left[(\cos\phi + \mu \sin\phi)\sin\left(\frac{\pi}{6}+\psi\right) + \mu \sin\phi \cos\psi\right]\exp\left(-\varepsilon_\theta\right),$$

where $\sin\phi = (a/R)\xi \exp(\varepsilon_\theta)$. In view of (2.93) and the second equation of (2.101), the pressure distribution over the punch head is given by

$$\frac{pR}{t_0 C} = s\left(\sin\psi + \sqrt{3}\cos\psi\right)\exp\left(-\varepsilon_\theta - \varepsilon_\phi\right). \tag{2.103}$$

The geometrical relation $r = R \sin\phi$ furnishes $\dot{\phi} = \dot{\varepsilon}_\theta \tan\phi$ over the contact region. Substituting into the compatibility equation (2.92), and using (2.93) for the components of the strain rate, we get

$$\frac{\partial}{\partial \xi}\left[\xi \dot{\varepsilon} \sin\psi \exp(\varepsilon_\theta)\right] = \dot{\varepsilon} \cos\phi\left[\cos\left(\frac{\pi}{6}+\psi\right) - \tan^2\phi \sin\psi\right]\exp\left(\varepsilon_\phi\right).$$

When the stresses and strains are known at the mth stage of the process, (2.104) can be solved using the condition $\dot{\varepsilon} = 1$ at $\xi = 0$, the polar compressive thickness strain ε_0 being taken as the time scale. The computed distribution of $\dot{\varepsilon}$ and an assigned increment of ε_0 furnish the quantities ε_θ, ε_ϕ, and ϕ, while s follows from the given stress–strain curve. Equation (2.102) is then solved for ψ at the $(m+1)$th stage under the boundary condition $\psi = \pi/6$ at $\xi = 0$, and the stresses are finally obtained from (2.93).

Over the unsupported surface of unknown geometry, the equation of meridional equilibrium is given by (2.101) with $p = 0$. Since the circumferential and meridional curvatures at any point are $\sin\phi/r$ and $(\partial\phi/\partial r)\cos\phi$, respectively, the equation of normal equilibrium is

$$\frac{\sigma_\theta}{r}\sin\phi + \frac{\partial\phi}{\partial r}\sigma_\phi\cos\phi = 0.$$

Using the relations (2.91) and (2.93), this may be rewritten as

$$r_0 \cos ec\,\phi \frac{\partial\phi}{\partial r_0} = -\frac{1}{2}\left(1+\sqrt{3}\tan\psi\right)\exp\left(\varepsilon_\phi - \varepsilon_\theta\right).$$

If the angle of contact is denoted by β, then $\xi = \xi^* = (R/a)\sin\beta\exp(-\varepsilon_\theta^*)$ at $\phi = \beta$, where the asterisk refers to the contact boundary. The integration of the above equation results in

$$\ln\left\{\frac{\tan(\phi/2)}{\tan(\beta/2)}\right\} = -\frac{1}{2}\int_{\xi^*}^{\xi}\left(1+\sqrt{3}\tan\psi\right)\exp\left(\varepsilon_\phi - \varepsilon_\theta\right)\frac{d\xi}{\xi}. \tag{2.105}$$

The remaining equilibrium equation and the compatibility equation in the dimensionless form are identical to (2.94) and (2.96), respectively.

To continue the solution from a known value of β at the mth stage, and the corresponding distributions of ψ and s, (2.96) is solved numerically for ε using the condition of continuity across $\xi = \xi^*$, the distribution of $\dot{\phi}$ being obtained from the previous values of ϕ. The distribution of ϕ for the $(m+1)$th stage is then obtained from (2.105), assuming a value of β and the previous distribution of ψ. The correct value of β is that for which the continuity condition for ψ across $\xi = \xi^*$ is satisfied, when (2.94) is solved for ψ with the boundary condition $\psi = 0$ at $\xi = 1$. The total penetration h of the punch at any stage can be computed from the formula

$$\frac{h}{a} = \frac{R}{a}(1-\cos\beta) + \int_{\xi^*}^{1}\sin\phi\exp\left(\varepsilon_\phi\right)d\xi. \tag{2.106}$$

in view of the relation $\partial z/\partial\xi = -\mathrm{a}\tan\phi$, where ϕ is given by (2.105) over the unsupported region. The resultant punch load is $P = 2\pi Rt^*\sigma_\phi^*\sigma\pounds\sin^2\beta$, and the substitution for t^* and σ_ϕ^*, furnishes

$$\frac{P}{2\pi Rt_0 C} = s^*\sin^2\beta\sin\left(\frac{\pi}{6}+\psi^*\right)\exp\left[-\left(\varepsilon_\theta^* + \varepsilon_\phi^*\right)\right]. \tag{2.107}$$

Equations (2.106) and (2.107) define the load–penetration relation parametrically through β. When the load attains a critical value, a local neck is formed at the thinnest section (leading to fracture) due to some kind of instability of the biaxial stretching.

If the strain hardening is expressed by the power law $s = \varepsilon^{\mathrm{n}}$, the Hencky theory may be used for the solution of the initial problem. Assuming $\sqrt{3}\tan\psi \approx 1 - \mathrm{n}\,\xi^2$ as a first approximation, and omitting the negligible friction terms in (2.102), it is found that s is given by the first equation of (2.98) throughout the deformed sheet. Furthermore, $\phi = \mathrm{a}\,\xi/R$ for $0 \le \xi \le \xi^*$, and

$$\phi = \frac{a\xi^{*2}}{\xi R} \exp\left\{\frac{n}{4}\left(\xi^2 - \xi^{*2}\right)\right\}, \quad \xi^* \le \xi \le 1,$$

in view of (2.105). The strain compatibility equation (2.99), which is the same as that for the stretch-forming process, gives

$$\frac{\partial}{\partial\xi}\left[\varepsilon\left(1 - n\xi^2\right)^{3/4}\sin\psi\right] = -\frac{\phi^2}{2\xi}\left(1 - n\xi^2\right)^{3/4}. \tag{2.108}$$

Substituting for ϕ, and using the conditions of continuity of ε and ψ across $\xi = \xi^*$, we obtain the expression for the polar thickness strain as

$$\varepsilon_0 = \frac{\beta^2}{2}\left\{1 + \int_{x^*}^{1}\left(\frac{\xi^*}{x}\right)^2 (1 - nx)^{3/4}\exp\left[\frac{n}{2}\left(x - x^*\right)\right]dx\right\}, \tag{2.109}$$

where $x = \xi^2$ and $x^* = \xi^{*2} = (RB/a)^2$. The distribution of ψ is now obtained by the integration of (2.108). By (2.106), the polar height is

$$h = \tfrac{1}{2}R\beta^2\left\{1 + \int_{x^*}^{1}\exp\left[n\left(\frac{x - x^*}{4}\right)\right]\frac{dx}{x}\right\}, \tag{2.110}$$

while the punch load is easily found from (2.107). Starting with a sufficiently small value of ε_0, for which a complete solution has just been derived, the analysis can be continued by considering (2.104) and (2.96) as explained before. The distribution of thickness strain and the load–penetration relationship are shown graphically in Figs. 2.26 and 2.27 for a material with $n = 0.2$, assuming $R = a$ and $\mu = 0.2$.

The theory seems to be well supported by available experimental results. It is found that the punch load required for a given depth of penetration is affected only slightly by the coefficient of friction.

2.7.3 Solutions for a Special Material

The solution to the stretch-forming problem becomes remarkably simple when the material is assumed to have a special strain-hardening characteristic. From the practical point of view, such a solution is extremely useful in understanding the physical behavior of the forming process and in predicting certain physical quantities with reasonable accuracy. The stress–strain curve for the special material is represented by

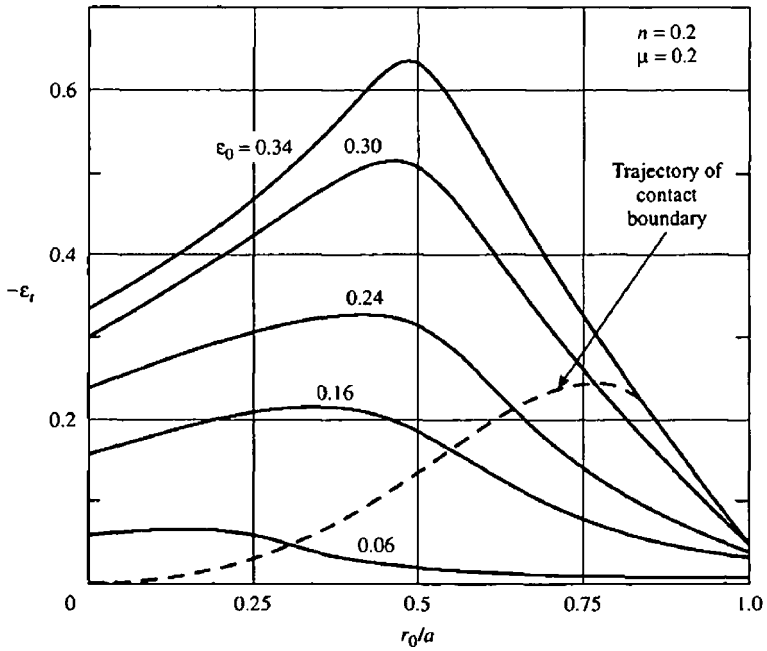

Fig. 2.26 Distribution of thickness strain in the stretch-forming process using a hemispherical punch with $R = a$ (after N.M. Wang, 1970)

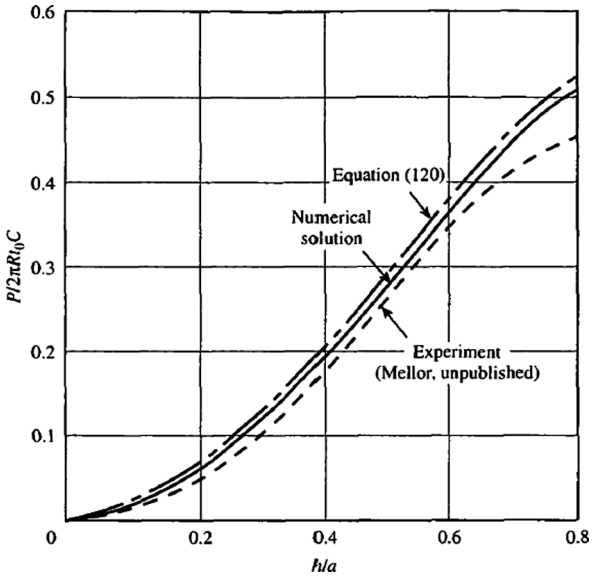

Fig. 2.27 Dimensionless load–penetration behavior in the punch stretching process using $R = a$ ($n = 0.2$, $\mu = 0.2$)

$$\sigma = Y \exp(\varepsilon),$$

where Y is the initial yield stress. The stress–strain curve is unlike that of any real metal, but the solution based on it should provide a good approximation for sufficiently prestrained metals (Hill, 1950b).

Considering the hydrostatic bulging process, it is easy to see that the assumed strain-hardening law requires the bulge to be a spherical cap having a radius of curvature ρ, which is given by simple geometry as

$$\rho = \frac{h^2 + a^2}{2h} = a \operatorname{cosec} \alpha, \tag{2.111}$$

where α is the semiangle of the cap. Indeed, it follows from (2.90a) that $\sigma_\theta = \sigma_\phi = \sigma = p\rho/2t$ when $\rho_\theta = \rho_\phi = \rho$, indicating that $t\sigma$ is a constant at each stage. Since $t = t_0 \exp(-\varepsilon)$, we recover the assumed stress–strain curve. Substituting from (2.91) into the relation $\varepsilon_\theta = \varepsilon_\phi = \varepsilon/2$ given by the flow rule, and using the fact that $r = \rho \sin \phi$, we get

$$r_0 \frac{\partial \phi}{\partial r_0} = \sin \phi \quad \text{or} \quad \frac{r_0}{a} = \frac{\tan(\phi/2)}{\tan(\alpha/2)}$$

in view of the condition $r_0 = a$ at $\phi = \alpha$. The strain distribution over the bulge is therefore given by

$$\varepsilon = 2 \ln \frac{r}{r_0} = 2 \ln \left(\frac{1 + \cos \phi}{1 + \cos \alpha} \right) = 2 \ln \left(1 + \frac{hz}{a^2} \right). \tag{2.112}$$

It follows from (2.112) that $\varepsilon = 0$ at $\phi = \alpha$, indicating that there is no straining at the clamped edge, which merely rotates to allow the increase in bulge height. The magnitude of the polar thickness strain is

$$\varepsilon_0 = 4 \ln \sec \frac{\alpha}{2} = 2 \ln \left(1 + \frac{h^2}{a^2} \right). \tag{2.113}$$

This relation is displayed by a broken curve in Fig. 2.24 for comparison. To obtain the velocity distribution, we consider the rate of change of (2.112) following the particle, as well as that of the geometrical relation $r = a(\sin \phi / \sin \alpha)$, taking α as the time scale. The resulting pair of equations for v and $\dot{\phi}$ may be solved to give

$$\frac{v}{r} = \frac{\cos \phi - \cos \alpha}{\sin \alpha} = \frac{z}{a}, \quad \dot{\phi} = \frac{\sin \phi}{\sin \alpha} = \frac{r}{a}.$$

The rate of change of the above expression for z and the substitution for $\dot{\phi}$ furnish the result $\dot{z} = v \cot \phi$, which shows that the resultant velocity of each particle is along the outward normal to the momentary profile of the bulge.

The relationship between the polar strain and the polar radius of curvature obtained for the special material provides a good approximation for a wide variety of metals. From (2.111) and (2.113), it is easily shown that

$$\frac{a}{\rho} \approx \sqrt{2\varepsilon_0} \exp\left(-\tfrac{3}{8}\varepsilon_0\right).$$

to a close approximation. When the pressure attains a maximum, the parameter $t\sigma/\rho$ has a stationary value at the pole, giving

$$\frac{1}{\sigma_0}\frac{d\sigma_0}{d\varepsilon_0} = 1 + \frac{1}{\rho}\frac{d\rho}{d\varepsilon_0} \approx \frac{11}{8} - \frac{1}{2\varepsilon_0}$$

in view of the preceding expression for ρ as a function of ε_θ. For the simple power law $\sigma_0 = C\varepsilon_0^n$, the polar strain at the onset of instability therefore becomes

$$\varepsilon_0 = \tfrac{4}{11}\,(+2n)\,.$$

The instability strain is thus equal to $\frac{4}{11}$ for a nonhardening material ($n = 0$). This explains the usefulness of the bulge test as a means of obtaining the stress–strain curve of metals for large plastic strains.

The special material is also useful in deriving an analytical solution for stretch forming over a hemispherical punch head, provided friction is neglected (Chakrabarty, 1970). The stress–strain curve is then consistent with the assumption of a balanced biaxial state of stress throughout the deforming surface. We begin with the unsupported region, for which the equilibrium in the normal direction requires

$$\frac{\sigma_\phi}{\sigma_\theta} = -\frac{\rho_\phi}{\rho_\theta} = -\frac{1}{r}\frac{\partial r}{\partial \phi}\tan\phi$$

in view of the first equation of (2.90a) with $p = 0$. The assumption $\sigma_\theta = \sigma_\phi$ therefore implies $\rho_\theta = -\rho\phi$ over the unsupported region, giving

$$\frac{\partial r}{\partial \phi} = -r\cot\phi \quad \text{or} \quad \frac{r}{a} = \frac{\sin\alpha}{\sin\phi}, \tag{2.114}$$

in view of the boundary condition $\phi = \alpha$ at $r = a$. Since $r = R\sin\beta$ at $\phi = \beta$, the angles β and α are related to one another by the equation

$$\sin\alpha = \frac{R}{a}\sin^2\beta \tag{2.115}$$

It may be noted that the meridional radius of curvature changes discontinuously from $-R$ to R across $\phi = \beta$. The shape of the unsupported surface is given by the differential equation

$$\frac{\partial z}{\partial \phi} = -\tan\phi \frac{\partial r}{\partial \phi} = a\left(\frac{\sin\alpha}{\sin\phi}\right),$$

which is integrated under the boundary condition $z = 0$ at $\phi = \alpha$ to obtain

$$\frac{z}{a} = \sin\alpha \ln\left\{\frac{\tan(\phi/2)}{\tan(\alpha/2)}\right\}. \tag{2.116}$$

The unsupported surface is actually a minimal surface since the mean curvature vanishes at each point. It is known from the geometry of surfaces that the only minimal surface of revolution is the catenoid. Indeed, the elimination of ϕ between (2.114) and (2.116) leads to the geometrical relation

$$\frac{r}{a} = \sin\alpha \cosh\left(\frac{z}{a}\cos ec\alpha + \ln\tan\frac{\alpha}{2}\right)$$

which is the equation of a catenoid. The flow rule requires $\varepsilon_\theta = \varepsilon_\phi = \varepsilon/2$, and the substitution from (2.91) and (2.114) gives

$$r_0 \frac{\partial \phi}{\partial r_0} = -\sin\phi \quad \text{or} \quad \frac{r_0}{a} = \frac{\tan(\alpha/2)}{\tan(\phi/2)},$$

in view of the boundary condition $r_0 = a$ at $\phi = \alpha$. The expressions for r and r_0 furnish the compressive thickness strain as

$$\varepsilon = 2\ln\frac{r}{r_0} = 2\ln\left(\frac{1+\cos\alpha}{1+\cos\phi}\right), \quad R\sin\beta \le r \le a. \tag{2.117}$$

Since $t\sigma$ is constant at each stage due to the assumed strain-hardening law, and the fact that $\varepsilon = \ln(t_0/t)$, the first equation of (2.90) is identically satisfied.

Over the region of contact, $\rho_\theta = \rho_\phi = R$, and equilibrium requires $\sigma_\theta = \sigma_\phi = \sigma$ in the absence of friction, giving $p = 2\sigma t/R$. In view of the relations $\varepsilon_\theta = \varepsilon_\phi$ and $r = R\sin\phi$, the initial radius r_0 to a typical particle is given by

$$r_0 \frac{\partial \phi}{\partial r} = \sin\phi \quad \text{or} \quad \frac{r_0}{a} = \frac{\tan(\alpha/2)\tan(\phi/2)}{\tan^2(\beta/2)},$$

in view of the condition of continuity across $\phi = \beta$. The compressive thickness strain therefore becomes

$$\varepsilon = 2\ln\frac{r}{r_0} = 2\ln\left\{\frac{(1+\cos\alpha)(1+\cos\phi)}{(1+\cos\beta)^2}\right\}, \quad 0 \le r \le R\sin\beta, \tag{2.118}$$

The continuity of the strains evidently ensures the continuity of the stresses across the contact boundary. The thickness has a minimum value at the pole when there is no friction between the material and the punch head.

The total penetration of the punch at any stage is obtained from (2.116) and the fact that the height of the pole above the contact boundary is equal to R(1–cos β).

Hence

$$\frac{h}{R} = (1 - \cos\beta) + \sin^2\beta \ln\left\{\frac{\tan(\beta/2)}{\tan(\alpha/2)}\right\} \tag{2.119}$$

in view of (2.115). Available experimental results indicate that the relationship between h/R and β is practically independent of the material properties when the punch is well lubricated. It is therefore a good approximation to assume that the relationship between h/R and $P/2Rt_0C$ is independent of the strain-hardening characteristic. Then, for the simple power law $\sigma = C\varepsilon^n$, the load–penetration relationship is given parametrically through β by (2.119) and the formula

$$\frac{P}{2\pi Rt_0C} = \left(\frac{1+\cos\beta}{1+\cos\alpha}\right)^2 \sin^2\beta \left\{2\ln\left(\frac{1+\cos\alpha}{1+\cos\beta}\right)\right\}^n. \tag{2.120}$$

This expression is obtained from the fact that $t^*\sigma^*$ is equal to $t_0C(\varepsilon^*)^{\mathrm{n}}\exp(-\varepsilon^*)$, where ε^* is given by (2.117) with $\phi = \beta$. It is easily shown that the punch load given by (2.120) does not have a stationary value in the interval $0 < \beta < \pi/2$, a result that is in agreement with experiment. A graphical plot of (2.120) is included in Fig. 2.27 for comparison. An application of the preceding results to the hydrodynamic lubrication in stretch forming has been discussed by Wilson and Hector (1991).

2.8 Deep Drawing of Cylindrical Cups

2.8.1 Introduction

In the simplest deep-drawing operation, a fiat circular blank of sheet metal is formed into a cylindrical cup having a flat or hemispherical base. The blank is placed over a die with a circular aperture, Fig. 2.28, and a blank holder is generally used to prevent wrinkling of the flange. A cylindrical punch is forced on the blank, either hydraulically or mechanically, to draw the outer annulus of the blank forming the cup wall. The blank-holding pressure is provided either by spring loading or by bolting down to a fixed clearance. Due to the elasticity of the apparatus, the latter method effectively generates a spring loading of very high intensity. In commercial deep drawing, the clearance between the punch and the die is slightly greater than the metal thickness, so that the thickness change that occurs through the die is unconstrained.

As the punch penetration increases from zero, the material in a central part of the blank is wrapped around the punch head and is therefore subjected to bending under tension. The deformation in the outer portion of the blank remains at the elastic order of magnitude until the punch load is sufficient to render the flange completely plastic. The outer annulus is then drawn radially inward, and its thickness progressively increases so long as the element remains on the flat part of the die. As the material passes over the die lip, it is first bent and then straightened under tension, resulting

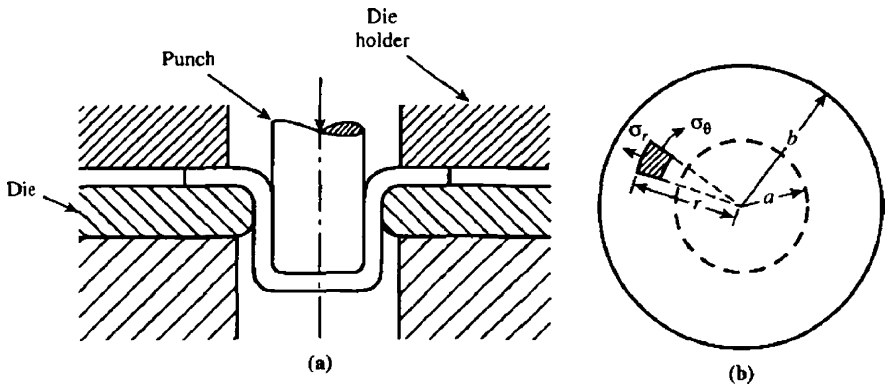

Fig. 2.28 Deep drawing of a cylindrical cup from a circular blank of sheet metal. (**a**) Schematic diagram and (**b**) stresses in an element

in a decrease in thickness. There is a narrow band of relatively thicker metal that has never been in contact with either the die or the punch. In the case of a flat-headed punch, the greatest thinning occurs over the punch profile radius due to bending and friction under biaxial tensile stresses. The load attains a maximum at some intermediate stage of the drawing and falls to zero at the end of the process (Johnson and Mellor 1983). An experimental method of estimating the die profile friction in deep drawing has been discussed by Tsutsumi and Kato (1994).

A complete solution for the deep-drawing process, taking into account the effects of bending and friction over the die and punch, does not seem to have been carried out with sufficient rigor. The early theoretical and experimental results on deep drawing have been reported by Chung and Swift (1951) and reviewed by Alexander (1960a) and Alexander et al. (1987). A numerical solution for deep drawing with a hemispherical headed punch has been obtained by Woo (1968) and Wifi (1976), neglecting the bending effects. Numerical solutions based on the finite element method have been presented by Kobayashi et al. (1989) and Saran et al. (1990). The main contribution to the drawing load is due to the radial drawing of the flange, which will be considered in what follows.

2.8.2 Solution for Nonhardening Materials

Since the blank thickens most at the outer radius, all the blank-holding force is exerted at the rim, but its effect is generally small and may be neglected as a first approximation. The material therefore deforms effectively under conditions of plane stress, the nonzero principal stresses being σ_r and σ_θ in the radial and circumferential directions, respectively. If the local thickness of the blank is denoted by h, the equation of radial equilibrium is

$$\frac{\partial}{\partial r}(h\sigma_r) = \frac{h}{r}(\sigma_\theta - \sigma_r), \tag{2.121}$$

where σ_r is tensile and σ_θ compressive. We begin with a nonhardening material with a uniaxial yield stress Y, and approximate the von Mises yield criterion by the modified Tresca criterion

$$\sigma_r - \sigma_\theta = mY,$$

where m is a constant, equal to 1.1 approximately. It is found that the thickness variation across the blank at any stage can be neglected in the equilibrium equation without significant errors. Equation (2.121) is then immediately integrated on substitution from the yield criterion to obtain the stress distribution

$$\sigma_r = mY \ln\frac{b}{r}, \quad \sigma_0 = -mY\left(1 - \ln\frac{b}{r}\right), \tag{2.122}$$

in view of the boundary condition $\sigma_r = 0$ at the current external radius $r = b$, the initial radius of the blank being b_0.

If v denotes the radial velocity of a typical particle, with respect to the rim displacement $b_0 - b$ taken as the time scale, the relationship between the radial and circumferential strain rates according to the Lévy–Mises flow rule may be written as

$$\frac{\partial v}{\partial r} = \left(\frac{2\sigma_r - \sigma_\theta}{2\sigma_\theta - \sigma_r}\right)\frac{v}{r} = -\left\{\frac{1 + \ln(b/r)}{2 - \ln(b/r)}\right\}\frac{v}{r}$$

in view of (2.122). Using the boundary condition $v = -1$ at $r = b$, the above equation is readily integrated to

$$v = -\frac{dr}{db} = -\frac{r}{b}\left(1 - \tfrac{1}{2}\ln\frac{b}{r}\right)^{-3}. \tag{2.123}$$

This equation can be further integrated with the substitution $\ln(b/r) = \rho$, which on differentiation following the particle gives

$$\frac{dr}{r} = -\frac{d\rho}{1 - (1 - \rho/2)^3} \approx -\frac{4d\rho}{3\rho(2 - \rho)}$$

in view of (2.123), the result being a close approximation over the relevant range. If r_0 denotes the initial radius to a typical particle, the initial condition is $r = r_0$ when $b = b_0$, and the integration of the above equation results in

$$\frac{r_0}{r} = \left\{\frac{\ln(b/r)\left[2 - \ln(b_0/r_0)\right]}{\ln(b_0/r_0)\left[2 - \ln(b/r)\right]}\right\}^{2/3}. \tag{2.124}$$

Equation (2.124) furnishes b/r as a function of b_0/r_0 for any given value of b/b_0. The relationship between r/b_0 and r_0/b_0 is thus obtained for a selected value of b/b_0. The flow rule gives the incremental thickness change in any element as

$$\frac{dh}{h} = -\left(\frac{\sigma_r + \sigma_\theta}{2\sigma_\theta - \sigma_r}\right)\frac{dr}{r} = -\left\{\frac{1 - 2\ln(b/r)}{2 - \ln(b/r)}\right\}\frac{dr}{r}.$$

Inserting the approximate expression for dr/r, and using the initial condition $h = h_0$ when $b = b_0$, the formula for the thickness variation is obtained as

$$\frac{h}{h_0} = \sqrt{\frac{b_0}{b}}\exp\left\{-\frac{\left[\ln(b/r)\right]^2}{4 - 2\ln(b/r)} + \frac{\left[\ln(b_0/r_0)\right]^2}{4 - 2\ln(b_0/r_0)}\right\}. \tag{2.125}$$

Equations (2.124) and (2.125) enable us to determine the thickness contour at any given stage of the drawing. Since the external radius $r = b$ is always stressed in simple compression, the thickness of the outside edge is $h_0\sqrt{b_0/b}$ irrespective of the stress–strain curve of the metal. The initial radius to the element that is currently at the die throat $r = a$ is given by (2.124). For a given element, the ratio b/r steadily increases from its initial value b_0/r_0.

A closed-form solution is also possible when the von Mises yield criterion is used, provided the thickness variation in the equilibrium equation is disregarded. It is convenient to express the yield criterion parametrically through an angle ψ as

$$\sigma_r = \frac{2Y}{\sqrt{3}}\sin\psi, \quad \sigma_\theta = -\frac{2Y}{\sqrt{3}}\cos\left(\frac{\pi}{6} + \psi\right), \tag{2.126}$$

where ψ lies between 0 and $\pi/3$. Substituting into the equilibrium equation (2.121), where h is omitted, we get

$$\cos\psi\frac{\partial\psi}{\partial r} = -\frac{1}{2r}\left(\sin\psi + \sqrt{3}\cos\psi\right).$$

The integration of this equation under the boundary condition $\psi = 0$ at $r = b$ results in

$$\frac{r^2}{b^2} = \frac{\sqrt{3}}{2}\sec\left(\frac{\pi}{6} - \psi\right)\exp\left(-\sqrt{3}\psi\right). \tag{2.127}$$

It is interesting to note that ψ depends only on the ratio r/b. Turning now to the Lévy–Mises flow rule, we have the velocity equation

$$\frac{\partial v}{\partial r} = \left(\frac{2\sigma_r - \sigma_\theta}{2\sigma_\theta - \sigma_r}\right)\frac{v}{r} = -\left(1 + \sqrt{3}\tan\psi\right)\frac{v}{2r},$$

where the external displacement $b_0 - b$ is taken as the time scale. Using the expression for $\partial\psi/\partial r$, the above equation is reduced to

$$\frac{\partial v}{\partial \psi} = \left(\frac{1 + \sqrt{3} \tan \psi}{\sqrt{3} + \tan \psi} \right) v.$$

In view of the boundary condition $v = -1$ at $r = b$, this equation is integrated to

$$v^2 = \frac{\sqrt{3}}{2} \sec \left(\frac{\pi}{6} - \psi \right) \exp \left(\sqrt{3} \psi \right).$$

The quantities ψ and v^2 increase as r decreases. It follows from (2.127) and the above equation for v^2 that

$$v = -\frac{dr}{db} = -\frac{r}{b} \exp \left(\sqrt{3} \psi \right). \tag{2.128}$$

Considering the rate of change of (2.127) following the particle, and substituting from above, we obtain an equation for $d\psi/db$, which is integrated to give

$$\int_{\psi_0}^{\psi} \left\{ \frac{\sqrt{3} + \tan (\pi/6 - \psi)}{\exp \left(\sqrt{3} \psi \right) - 1} \right\} d\psi = 2 \ln \left(\frac{b_0}{b} \right), \tag{2.129}$$

where ψ_0 is the initial value of ψ for a typical particle. The integral must be evaluated numerically to determine ψ for a given ψ_0. For small values of ψ, it is sufficiently accurate to use the approximate expression

$$\frac{\psi}{\psi_0} \left(\frac{\sqrt{3} + \psi}{\sqrt{3} + \psi_0} \right)^2 \left(\frac{2 + \sqrt{3} \psi_0}{2 + \sqrt{3} \psi} \right)^3 = \left(\frac{b_0}{b} \right)^{3/2}, \psi < 0.3.$$

The ratio r_0^2/b_0^2 is given by the right-hand side of (2.127) with ψ_0 written for ψ. Consequently,

$$\frac{r_0}{r} = \frac{b_0}{b} \sqrt{\frac{\cos (\pi/6 - \psi)}{\cos (\pi/6 - \psi_0)}} \exp \left[\frac{\sqrt{3}}{2} (\psi - \psi_0) \right]. \tag{2.130}$$

This expression furnishes the total hoop strain whose magnitude at any stage is $\ln(r_0/\mathrm{r})$. The thickness change is given by the differential equation

$$\frac{dh}{h} = -\left(\frac{\sigma_r + \sigma_\theta}{2\sigma_\theta - \sigma_r} \right) \frac{dr}{r} = -2 \frac{dr}{r} - \frac{\sqrt{3} \exp \left(\sqrt{3} \psi \right) d\psi}{\exp \left(\sqrt{3} \psi \right) - 1}$$

in view of (2.126) and (2.128), and the fact that $-2db/b$ is equal to the expression in the integral of (2.129). Using the initial condition $h = h_0$ when $r = r_0$ and $\psi = \psi_0$, the above equation is integrated to

$$\frac{h}{h_0} = \left(\frac{b_0}{b}\right)^2 \left\{\frac{1 - \exp\left(-\sqrt{3}\psi_0\right)}{1 - \exp\left(-\sqrt{3}\psi\right)}\right\} \left\{\frac{\cos\left(\pi/6 - \psi\right)}{\cos\left(\pi/6 - \psi_0\right)}\right\}. \tag{2.131}$$

The solution is relevant only over the range of $0 \leq \psi \leq \psi_a$, where ψ_a corresponds to the die throat $r = a$ and is obtainable from (2.127) at any stage of the drawing. The solutions based on the von Mises and modified Tresca criteria are compared with one another in Figs. 2.29 and 2.30, which display the positions of particles and thickness profiles at various stages of the process for a drawing ratio $b_0/a = 2.0$.

The blank will neck at $r = a$ if the radial stress there is equal to Y at the beginning of the drawing. Setting $\psi = \pi/3$ in (2.127), the corresponding drawing ratio is found to be

$$\frac{b_0}{a} = \exp\left(\frac{\pi}{2\sqrt{3}}\right) \approx 2.477.$$

In actual practice, failure would occur over the punch head, where bending and frictional effects are responsible for lowering the limiting drawing ratio to somewhat smaller values. A detailed analysis for the limiting drawing ratio will be given in Section 6.6, including the effect of anisotropy of the sheet metal.

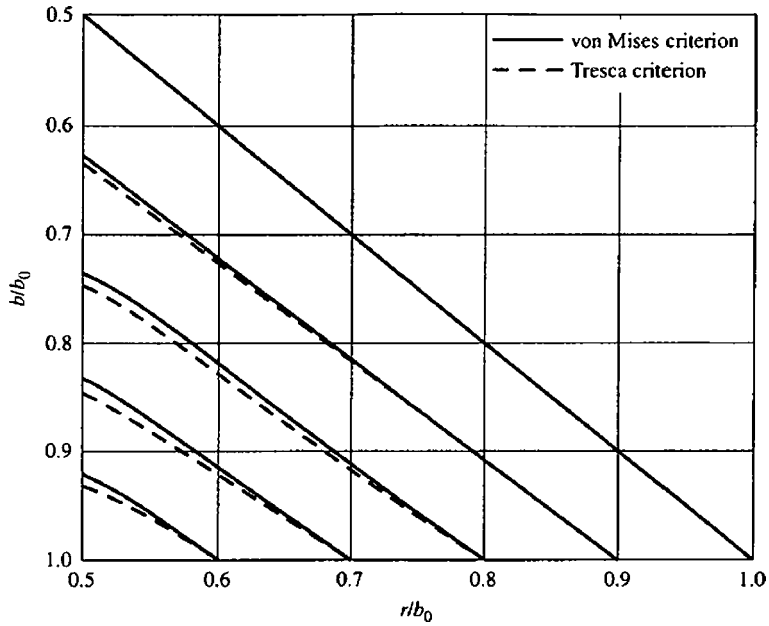

Fig. 2.29 Trajectories of the paths of particles during the progressive radial drawing of a circular blank (no work-hardening)

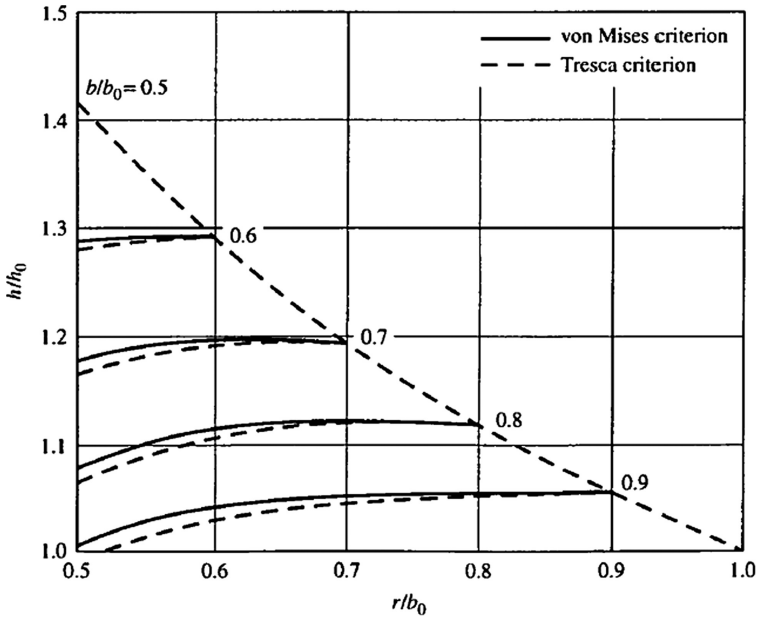

Fig. 2.30 Thickness profile at different stages of radial drawing of a circular blank (no work-hardening)

2.8.3 Influence of Work-Hardening

The overall effect of work-hardening is to increase the drawing load and reduce the variation of thickness across the blank at any given stage of the drawing. When the rate of work-hardening is sufficiently high, the drawing stress and the drawing load attain their maximum values at different stages of the process. The paths of the particles are, however, found to be only marginally affected by the work-hardening characteristic of the material. It is therefore a useful approximation to assume that the total equivalent strain at any stage is independent of the rate of work-hardening. By the Lévy–Mises flow rule, the increment of equivalent strain ε in the absence of hardening is

$$d\varepsilon = \left(\frac{2mY}{2\sigma_\theta - \sigma_r}\right) d\varepsilon_\theta = -\left\{\frac{2mY}{2 - \ln(b/r)}\right\} \frac{dr}{r} \approx \frac{8d\rho}{3\rho\,(2-\rho)^2},$$

where $\rho = \ln(b/r)$. Since $\varepsilon = 0$ in the initial state $\rho = \rho_0$, the integration of the above equation furnishes

$$\varepsilon = \frac{2}{3}\left\{\ln\left[\frac{\rho(2-\rho_0)}{\rho_0(2-\rho)}\right] + \frac{2(\rho-\rho_0)}{(2-\rho)\,(2-\rho_0)}\right\}. \tag{2.132}$$

Equations (2.124), (2.125), and (2.132) indicate that the relationship between the equivalent strain, hoop strain, and thickness strain is

$$\varepsilon = \frac{2}{3}\left(2\ln\frac{r_0}{r} - \ln\frac{h}{h_0}\right).$$

The equivalent strain is therefore significantly higher than the magnitude of the local hoop strain, equal to $\ln(r_0/r)$, in a region near the die throat $r = a$.

The relationship between b/r and b_0/r_0 at any stage may be obtained, to a close approximation, on the basis of a uniform flange thickness equal to $h_0\sqrt{b_0/b}$ at each stage of the drawing. Then by the condition of constancy of volume, we get

$$b_0^2 - r_0^2 = \sqrt{\frac{b_0}{b}}\left(b^2 - r^2\right),$$

this relation furnishes r_0/r explicitly as a function of b/r and b_0/b, the result being

$$\frac{r_0}{r} = \left(\frac{b_0}{b}\right)^{1/4}\left\{1 + \left[\left(\frac{b_0}{b}\right)^{3/2} - 1\right]\frac{b^2}{r^2}\right\}^{1/2}, \tag{2.133}$$

from which the ratio b_0/r_0 can be found for any given values of b/r and b_0/b, in view of the identity $b_0/r_0 = (b_0/b)(b/r)(r/r_0)$. The ratio b_0/b can be expressed in terms of b/r and $b_0 r_0$ as

$$\frac{b_0}{b} = \left\{\frac{\left(b_0^2/r_0^2\right)\left(b^2/r^2 - 1\right)}{\left(b^2/r^2\right)\left(b_0^2/r_0^2 - 1\right)}\right\}^{2/3}$$

in view of (2.133). The ratio r_0/r can be similarly expressed in terms of b/r and b_0/r_0 using the preceding relation, to establish the variation of the hoop strain in a given element as the drawing proceeds.

Consider now the stress and velocity distributions in a work-hardening blank. If the current uniaxial yield stress of the material is denoted by σ, the modified Tresca criterion in the presence of hardening may be written as

$$\sigma_r - \sigma_\theta = m\sigma = mF(\varepsilon).$$

The function F is defined by the stress–strain curve of the material in simple compression. The substitution in the equilibrium equation (2.121), with the thickness variation disregarded, gives the radial stress as

$$\sigma_r = m\int_r^b \sigma\frac{dr}{r} = m\int_0^\rho F(\varepsilon)\,d\rho. \tag{2.134}$$

The integration can be carried out numerically for any given stage specified by the ratio b/b_0, the integrand being a known function of ρ in view of (2.132) and

(2.133). Initially, however, $\sigma_r = mY\rho$, as in the case of a nonhardening material. The radial velocity v of a typical particle is governed by the differential equation

$$\frac{1}{v}\frac{\partial v}{\partial \rho} = -\frac{2\sigma_r - \sigma_\theta}{2\sigma_\theta - \sigma_r} = \frac{m\sigma + \sigma_r}{2m\sigma - \sigma_r}.$$

In view of the boundary condition $v = -1$ at $\rho = 0$, the solution to the above equation may be expressed in the form

$$v = -\exp\left\{\int_0^\rho \left(\frac{m\sigma + \sigma_r}{2m\sigma - \sigma_r}\right) d\rho\right\}, \tag{2.135}$$

which furnishes the velocity distribution at any given stage of the drawing. Since $v = -dr/db$, the variation of ρ following the particle is

$$d\rho = \frac{db}{b} = \frac{dr}{r} = -\left(1 + \frac{r}{bv}\right)\frac{dr}{r}.$$

The change in thickness of a given element is finally obtained by the integration of the equation

$$\frac{dh}{h} = -\left(\frac{\sigma_r + \sigma_\theta}{2\sigma_\theta + \sigma_r}\right)\frac{dr}{r} = -\left(\frac{m\sigma - 2\sigma_r}{2m\sigma - \sigma_r}\right)\frac{dr}{r}$$

along the path of the particle. Substituting for dr/r, and using the initial condition $h = h_0$ at $\rho = \rho_0$, we obtain the thickness strain as

$$\ln\left(\frac{h}{h_0}\right) = \int_{\rho_0}^\rho \left(\frac{m\sigma - 2\sigma_r}{2m\sigma - \sigma_r}\right)\frac{v d\rho}{v + e^{-\rho}}, \tag{2.136}$$

where the integrand is a known function of ρ and ρ_0. The numerical integration is based on a fixed value of ρ_0 and varying values of ρ, which increases with increasing b_0/b. Figure 2.31 shows the computed results for the drawing stress and flange thickness at $r = a$, for a drawing ratio of 2, based on the power law $F(\varepsilon) = \sigma_0\varepsilon^n$ for the strain hardening.

A numerical analysis of the radial drawing process for a work-hardening blank, based on the von Mises yield criterion, can be carried out in a manner similar to that for the stretch-forming process. In terms of an auxiliary angle ψ, the stresses and strains rates may be expressed as

$$\left.\begin{aligned} \sigma_r &= \frac{2\sigma}{\sqrt{3}}\sin\psi, & \sigma_\theta &= -\frac{2\sigma}{\sqrt{3}}\cos\left(\frac{\pi}{6} + \psi\right), \\ \dot{\varepsilon}_r &= \dot{\varepsilon}\,\sin\left(\frac{\pi}{6} + \psi\right), & \dot{\varepsilon}_\theta &= -\dot{\varepsilon}\,\cos\,\psi, \end{aligned}\right\} \tag{2.137}$$

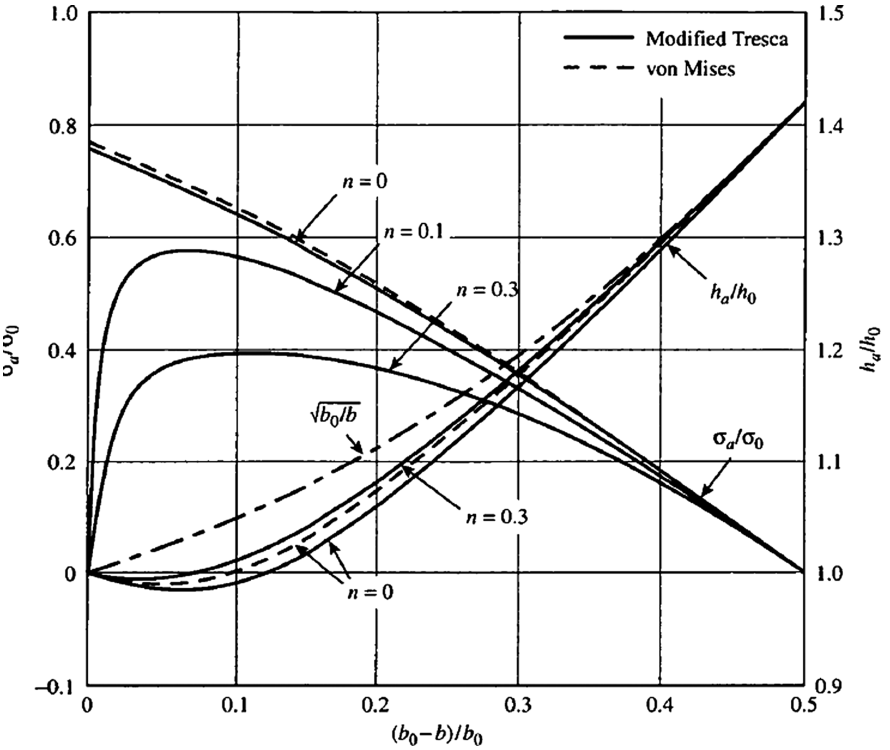

Fig. 2.31 Influence of work-hardening on the drawing stress and flange thickness at the die throat during radial drawing ($b_0/a = 2$)

where σ and $\dot{\varepsilon}$ are the equivalent stress and strain rate, respectively. The relevant differential equations are the equilibrium equation (2.121) and the compatibility equation

$$\frac{\partial \dot{\varepsilon}_\theta}{\partial r} = \frac{\dot{\varepsilon}_r - \dot{\varepsilon}_\theta}{r} \tag{2.138}$$

obtained by eliminating v between the expressions $\dot{\varepsilon}_r = \partial v / \partial r$ and $\dot{\varepsilon}_\theta = v / r$. The substitution from (2.137) into (2.121) and (2.138) results in

$$\left.\begin{aligned} \frac{\partial}{\partial \xi}\left[s \sin\psi \exp(\varepsilon_z)\right] &= -\frac{s}{\xi}\cos\left(\frac{\pi}{6} - \psi\right)\exp(-2\varepsilon_\theta), \\ \frac{\partial}{\partial \xi}\left(\dot{\varepsilon} \cos\psi\right) &= -\frac{\sqrt{3}\dot{\varepsilon}}{\xi}\cos\left(\frac{\pi}{6} - \psi\right)\exp(\varepsilon_r - \varepsilon_\theta), \end{aligned}\right\} \tag{2.139}$$

where ε_z is the thickness strain equal to $-(\varepsilon_r + \varepsilon_\theta)$, while ξ and s are dimensionless variables defined as

$$\xi = \frac{r_0}{b_0}, \quad s = \frac{\sigma}{\sigma_0} = f(\varepsilon),$$

with σ_0 denoting a constant stress. The boundary conditions are $\psi = 0, s = f\left[\ln(b_0/b)\right]$ and $\dot{\varepsilon} = 1/b$ at $\xi = 1$. The solution at any stage is relevant only over the range $\xi^* \le \xi \le 1$, where $\xi^* = (a/b_0)\exp\left(-\varepsilon_\theta^*\right)$, with the asterisk specifying quantities at the die throat $r = a$.

In order to start the solution, an initial distribution of ψ and s must be found. If we adopt the power law $s = \varepsilon^n$ for strain hardening, the Hencky theory may be used for the solution of the initial problem. Then $\dot{\varepsilon}$ may be replaced by ε in the preceding relations, and (2.139) becomes

$$\frac{n}{\varepsilon}\frac{\partial \varepsilon}{\partial \xi} + \cot\psi \frac{\partial \psi}{\partial \xi} = -\frac{1}{2\xi}\left(1 + \sqrt{3}\cot\psi\right),$$
$$\frac{1}{\varepsilon}\frac{\partial \varepsilon}{\partial \xi} - \tan\psi \frac{\partial \psi}{\partial \xi} = -\frac{\sqrt{3}}{2\xi}\left(\sqrt{3} + \tan\psi\right),$$

to a sufficient accuracy. This is a pair of simultaneous differential equations for ε and ψ, and the elimination of $\partial\varepsilon/\partial\xi$ and $\partial\psi/\partial\xi$ in turn leads to

$$\frac{\partial \psi}{\partial \xi} = -\frac{\left(1 - \sqrt{3}n\tan\psi\right)\left(\sqrt{3} + \tan\psi\right)}{2\xi\left(1 + n\tan^2\psi\right)}, \quad \frac{\partial \varepsilon}{\partial \xi} = -\frac{\varepsilon\left(\sqrt{3} + \tan\psi\right)^2}{2\xi\left(1 + n\tan^2\psi\right)}. \tag{2.140}$$

The first equation of (2.140) is readily integrated to obtain ξ as a function of ψ, using the boundary condition $\psi = 0$ at $\xi = 1$, the result being

$$\xi^2 = \frac{\sqrt{3}}{2}\sec\left(\frac{\pi}{6} - \psi\right)\left(\cos\psi - \sqrt{3}n\,\sin\psi\right)^{4n/\left(1+3n^2\right)} \exp\left\{-\sqrt{3}\left(\frac{1-n^2}{1+3n^2}\right)\psi\right\}. \tag{2.141}$$

The elimination of ξ between the two equations of (2.140) furnishes the differential equation for ε as

$$\frac{\partial \varepsilon}{\partial \psi} = \varepsilon\left(\frac{\sqrt{3}\cos\psi + \sin\psi}{\cos\psi - \sqrt{3}n\sin\psi}\right).$$

Integrating and using the boundary condition $\varepsilon = \ln(b_0/b)$ at $\psi = 0$, we obtain the solution

$$\varepsilon = \left(\ln\frac{b_0}{b}\right)\left\{\frac{\exp\left[\sqrt{3}\left(1-n^2\right)\psi/\left(1+3n^2\right)\right]}{\cos\psi - \sqrt{3}n\sin\psi}\right\}^{(1+3n)/\left(1+3n^2\right)} \tag{2.142}$$

Equations (2.141) and (2.142) provide the complete solution for the stresses and strains for an arbitrary small value of $\ln(b_0/b)$. To continue the solution, the second equation of (2.139) is solved for $\dot{\varepsilon}$ using the boundary condition $\dot{\varepsilon} = 1/b$ at $\xi = 1$.

The last two equations of (2.137) then furnish the components of strain increment for an assumed small change in b. Using the hardening law $s = \varepsilon^n$, the first equation of (2.139) is next solved to obtain the corresponding distribution of ψ. The distribution of the radial stress at different stages and the variation of the drawing load with the amount of drawing for $n = 0.4$ are displayed in Fig. 2.32.

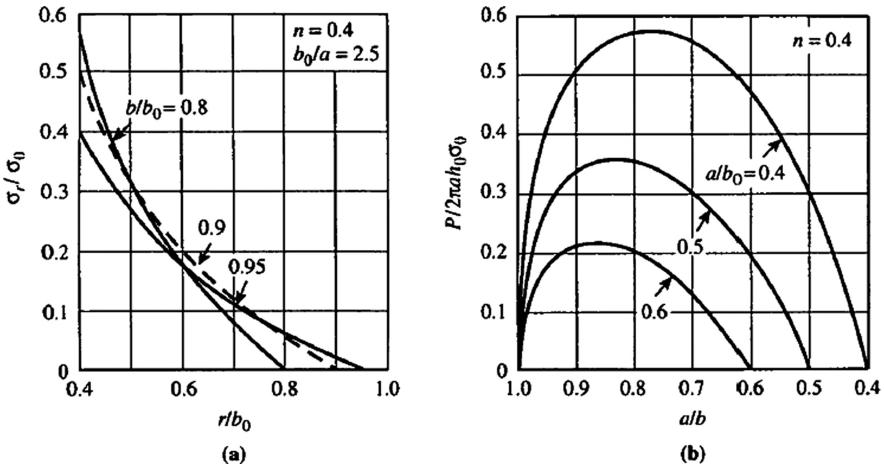

Fig. 2.32 Results for radial drawing of a work-hardening circular blank. (**a**) Distribution of radial stress at different stages and (**b**) variation of drawing load with amount of drawing (after Chiang and Kobayashi, 1966)

Experiments have shown that the limiting drawing ratio in conventional deep drawing with a flat-headed punch is practically independent of the strain-hardening characteristic of the material (Wallace, 1960). The theoretical limiting drawing ratio using a flat-headed punch is therefore about 2.48 for isotropic metals. This ideal value can be approximately realized by lubricating the die and making the punch rough enough to prevent sliding of the material over its surface. Work-hardening has a significant effect, however, on the limiting drawing ratio in the case of pressure-assisted deep drawing, where a high-pressure fluid holds the material against the punch and inhibits fracture over the punch head, as has been demonstrated by Kasuga and Tsutsumi (1965) and El-Sebaie and Mellor (1973). The hydrodynamic deep-drawing process has been further investigated by Yossifon and Tirosh (1985).

2.8.4 Punch Load and Punch Travel

We begin by considering a nonhardening material for which the punch load has its greatest value at the beginning of the drawing. If Tresca's yield criterion is adopted, the radial velocity v_a at $r = a$ is given by (2.123). Since the material entering the die cavity is of length $v_a\, db$ during a small change in the flange radius b, the amount of punch travel z at any stage of the drawing is given by

$$\frac{z}{a} = \int_{b_0}^{b} \left(\frac{va}{a}\right) db = \frac{4 \ln (b_0/b) \left[4 - \ln \left(b_0 b/a^2\right)\right]}{\left[2 - \ln (b_0/a)\right]^2 \left[2 - \ln (b/a)\right]^2}, \tag{2.143}$$

which should be sufficiently accurate for the practical range of values of b_0/a. Setting $b = a$ in (2.143), we obtain the length l of the drawn cup as

$$\frac{l}{a} = \frac{\left[4 - \ln (b_0/a)\right] \ln (b_0/a)}{\left[2 - \ln (b_0/a)^2\right]}.$$

As representative values, l/a is equal to 1.342 when $b_0/a = 2$ and equal to 2.406 when $b_0/a = 2.5$. These lengths are of the same order as those experimentally observed. If the effect of bending over the die profile is disregarded, the punch load P acting at any stage of the drawing is equal to the radial drawing load $2\pi a h_a \sigma_a$. Using (2.122) and (2.125), the punch load can be expressed as

$$\frac{\rho}{2\pi a h_0 Y} = m \sqrt{\frac{b_0}{b} \ln \left(\frac{b}{a}\right)} \exp \left\{ \frac{\left[\ln (b_0/a_0)\right]^2}{4 - 2 \ln (b_0/a_0)} - \frac{\left[\ln (b/a)\right]^2}{4 - 2 \ln (b/a)} \right\}, \tag{2.144}$$

where a_0 is the initial radius to the element that has currently reached the die throat and can be found by setting $r = a$ and $r_0 = a_0$ in (2.133). The right-hand side of (2.144) progressively decreases from its initial value of $\ln(b_0/a)$ and becomes zero at the end of the drawing process. The thickness distribution in the drawn cup is obtained from the fact that the wall thickness is equal to h_a at a distance z from the bottom of the cup.

When the rate of hardening is sufficiently high, the punch load increases with the punch travel until the load attains a maximum. There is a critical rate of hardening below which the load has its greatest value at the beginning of the drawing (Chakrabarty and Mellor, 1968). The punch load at any stage is given by

$$P = 2\pi a h_a \sigma_a = 2\pi a m \int_a^b hF(\varepsilon) \frac{dr}{r} \tag{2.145}$$

in view of the equilibrium equation and the modified Tresca criterion. Considering the rate of change of the above equation with respect to $b_0 - b$, and then setting $b = b_0$, the initial rate of change of P is obtained as

$$\frac{\dot{P}}{2\pi a m} = F(0) \left\{ -\frac{h_0}{b_0} + \int_a^{b0} \dot{h} \frac{dr}{r} \right\} + h_0 F'(0) \int_a^{b0} \dot{\varepsilon} \frac{dr}{r},$$

since $\partial h/\partial r = 0$ in the initial stage. The condition for $\dot{P}$ to be initially positive may therefore be written as

$$b_0 F'(0) \int_a^{b_0} \dot{\varepsilon} \frac{dr}{r} - F(0) \left\{ 1 - \frac{b_0}{h_0} \int_a^b \dot{h} \frac{dr}{r} \right\} > 0.$$

The expressions for $\dot{h}$ and $\dot{\varepsilon}$ in the initial stage are identical to those for a non-hardening material with a uniaxial yield stress $Y = F(0)$. Using (2.122) and (2.123), and the Lévy–Mises flow rule, it is easily shown that

$$\dot{\varepsilon} = \frac{1}{b_0}\left(1 - \frac{1}{2}\ln\frac{b_0}{r}\right)^{-4}, \quad \dot{h} = h_0\left(\frac{1}{2} - \ln\frac{b_0}{r}\right)\dot{\varepsilon},$$

when $b = b_0$. Inserting these expressions into the preceding integrals and integrating, we obtain the required condition as

$$\frac{F'(0)}{F(0)} > \frac{4 - \ln\alpha\,(2 - \ln\alpha)\,(4 - \ln\alpha)}{2\ln\alpha\,(2 - \ln\alpha) + (\ln\alpha)^3/3}, \tag{2.146}$$

where α is the drawing ratio b_0/a. The right-hand side of (2.146) decreases as α increases and approaches infinity as α tends to unity. When the strain hardening is represented by the power law $F(\varepsilon) = \sigma_0\varepsilon^n$, which will be assumed in what follows, the above inequality is satisfied for all values of α.

During the continued drawing of a work-hardening blank, the stretching of the flange material that enters the die cavity is usually small and may be disregarded. However, the contribution to the punch travel, made by the stretching of the sheet material over the punch head, must be taken into consideration. Assuming a flat-headed punch, and neglecting the effects of bending and friction, the state of stress over the punch head may be taken as one of balanced biaxial tension of increasing intensity. Since the thickness of the sheet decreases uniformly from h_0 to $h_0\exp(-\varepsilon)$, where ε is the compressive thickness strain at a generic stage, the contribution to the cup length due to the biaxial stretching of the material is

$$d = \frac{a}{2}\left(e^{\varepsilon} - 1\right), \quad \varepsilon^n e^{-\varepsilon} = \left(\frac{h_a}{h_o}\right)\left(\frac{\sigma_a}{\sigma_o}\right). \tag{2.147}$$

The first relation of (2.147) results from the constancy of volume of the material over the punch head, while the second relation follows from the condition of overall longitudinal equilibrium of the partially formed cup. Equation (2.147) holds only for $b \geq b^*$, where b^* denotes the flange radius when the punch load attains its maximum.

During a small time interval represented by db, an annular element of the flange at $r = a$ enters the die cavity to form an elemental ring of length $v_a\,db$. The amount of punch travel due to the combined effects of metal flow into the die, and stretching over the punch, is

$$z = d + \int_{b_0}^{b} v_a db = \frac{a}{2}\left(e^{\varepsilon} - 1\right) + \int_{b_0}^{b} v_a db, \quad b^* \leq b \leq b_0, \tag{2.148}$$

where v_a is given by (2.135) with $\rho = \ln(b/a)$ for the upper limit of integration. Once the punch load has reached its maximum, there is no further stretching of material over the punch head, and the punch travel is then given by

$$z = \frac{a}{2}\left(e^{\varepsilon^*} - 1\right) + \int_{b_0}^{b} v_a db, \quad a \le b \le b^*.$$

The punch load at any stage can be determined approximately from the relation $P = 2\pi a h_a \sigma_a$, or more accurately from (2.145) using (2.136). In Fig. 2.33, the punch load is plotted against the punch travel in dimensionless form for a flat-headed punch, using $b_0/a = 2.0$ and $m = 1.1$. The computed results for the maximum drawing load P^* may be expressed with reasonable accuracy by the empirical equation

$$\frac{P^*}{2\pi a h_0 \sigma_0} = \frac{m}{1+n}\left(\frac{1}{\sqrt{3}}\right)^n \left(\ln \frac{b_0}{a}\right)^{1+\sqrt{n}}, \quad 1 \le \frac{b_0}{a} < 2.5 \tag{2.149}$$

where $m = 1.10$. Due to the effects of friction and bending, which are neglected here, the actual load will be somewhat higher than that predicted by the theory.

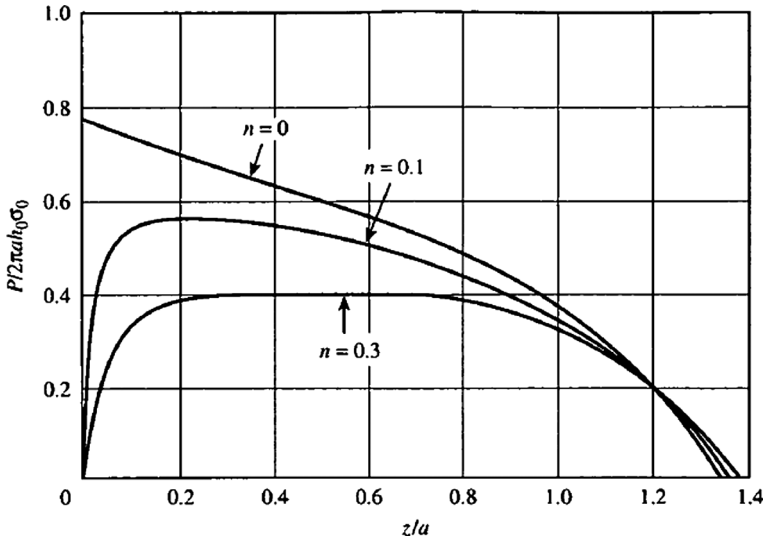

Fig. 2.33 Variation of punch load with punch travel in the deep-drawing process using a flat-headed punch ($b_0/a = 2$)

In the industrial stamping of sheet metal, drawbeads are often used to control the metal flow into the die cavity, thereby suppressing or minimizing the possibility of wrinkling. A drawbead generally consists of a semicylindrical projection on the inner face of the blank holder, designed to fit into a groove provided on the die face, the blank holding force being sufficient to bend the sheet plastically before it is drawn into the die. The restraining force produced by the drawbead is due partly to the bending and unbending of the sheet as it moves over the drawbead, and partly to the friction between the material and the surfaces of contact. The details

of the method and its analysis have been discussed by Nine (1978), Wang (1982), Triantafyllidis et al. (1986), and Sanchez and Weinmann (1996).

2.9 Ironing and Flange Wrinkling

2.9.1 Ironing of Cylindrical Cups

In the ironing process, the wall thickness of a deep-drawn cup is reduced by restricting the clearance between the die and the punch. We consider the situation where the internal diameter of the cup is held constant during the process (Hill, 1950a), and the reduction in thickness is achieved by forcing the cup axially through a die as shown in Fig. 2.34a. The circumferential strain imparted to the cup is zero at the punch surface and is negligible elsewhere when the initial wall thickness H is sufficiently small in relation to the cup diameter d. Since the cup is elongated during the ironing, frictional forces arise not only between die and cup but also between cup and punch. If the latter is neglected, the problem is identical to the plane strain drawing of a sheet between rough tapered dies, the surface of the punch being regarded as the center line of the sheet, Fig. 2.34b. The longitudinal force exerted by the punch on the cup wall is

$$P = \pi h\,(d + h)\,t',$$

where h is the final wall thickness, and t' the mean tensile stress in the ironed wall. By the plane strain theory of sheet drawing (Chakrabarty, 2006), we have

$$t' = t\left\{1 + \left(1 - \frac{1}{2}\ln\frac{1}{1-r}\right)\mu\cot\alpha\right\}$$

to a close approximation, where t is the mean drawing stress for frictionless drawing, μ the coefficient of friction, α the die angle, and $r = (H - h)/H$ the fractional

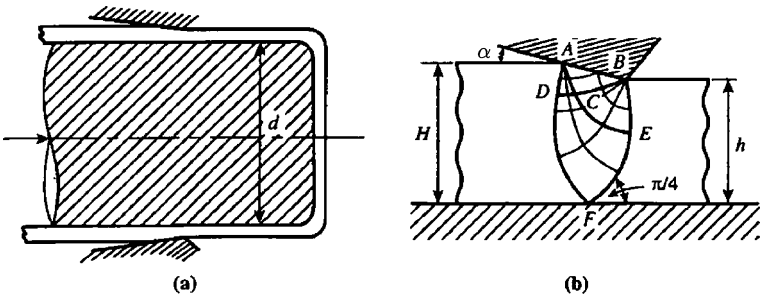

Fig. 2.34 Ironing of a thin-walled cup without friction, together with the associated slipline field

reduction in thickness. Neglecting h/d in comparison with unity, the punch load may be expressed in the nondimensional form

$$\frac{P}{2\pi kdH} = (1-r)\left\{1+\left(1-\frac{1}{2}\ln\frac{1}{1-r}\right)\mu\cot\alpha\right\}\frac{t}{2k}, \tag{2.150}$$

where k is the yield stress in pure shear. In terms of a parameter $\lambda = (2/r-1)\,\alpha$, the ratio $t/2k$ for a nonhardening material is given by the empirical formulas

$$\left.\begin{aligned}\frac{t}{2k} &= \left(0.93+0.07\beta\lambda^2\right)\ln\left(\frac{1}{1-r}\right), \quad 1.0\le\lambda\le 2.5,\\ \frac{t}{2k} &= 0.85\lambda^{0.52}\ln\left(\frac{1}{1-r}\right), \qquad\qquad 2.5\le\lambda\le 8.0.\end{aligned}\right\} \tag{2.151}$$

Figure 2.35 shows the variation of the dimensionless punch force with the fractional reduction for different values of α, when $\mu = 0$. Each solid curve passes through a maximum and approaches zero load. The lower broken curve corresponds to $t/2k = -\ln(1-r)$, representing the ideal drawing stress. This curve has a maximum ordinate of $1/e \cong 0.368$ at a fractional reduction of $1 - e^{-1} \cong 0.632$. The upper broken curve on the left represents the bulge limit and is given by the relation

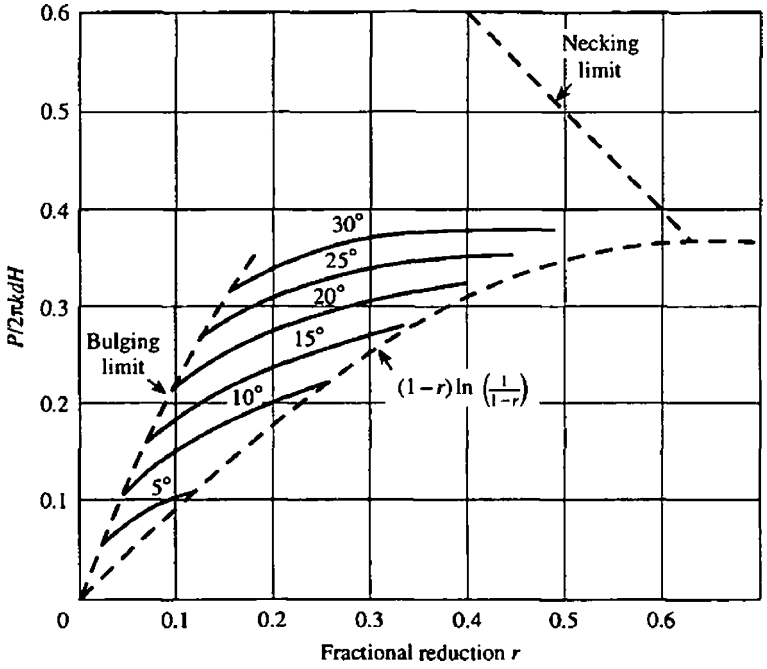

Fig. 2.35 Variation of dimensionless ironing load with fractional reduction in thickness of the cup wall

$r = \alpha\,(0.23 + \alpha/9)$ to a close approximation. The broken straight line on the right-hand side represents $t = 2k$, which corresponds to necking of the ironed wall. The influence of the friction factor in (2.150) is to make the solid curves cross due to the existence of an optimum die angle for which the punch load is a minimum with a given reduction in thickness. The optimum die angle is

$$\alpha_0 \approx 1.49 \left(\frac{\mu r^2}{2 - r} \right)^{1/3} - 0.08\mu\,(2 - r) \tag{2.152}$$

to a close approximation. The influence of work-hardening on the ironing load has been investigated by Fukui and Hansson (1970). An analysis for the redrawing of deep-drawn cups through conical dies has been given by Fogg (1968). The redrawing operation in one or more stages is necessary for producing cups of larger drawing ratio than can be achieved in a single drawing operation.

When the punch is rough, frictional stresses are induced in the cup wall to the left of point F due to the relative motion between the wall and the punch. The frictional stresses are obviously absent over the ironed wall which is carried along with the punch. The effect of punch friction may be approximately estimated by considering the frictional force to be equivalent to a negative back pull, the punch speed being higher than that of the sliding wall. The resultant tension in the ironed wall is thereby reduced by the amount $(1 — \eta)F$, where F denotes the frictional force, and η is the back-pull factor equal to $r(1 + \mu \cot \alpha)$ approximately. The punch load is therefore increased by the amount ηF, where F is an unknown to be determined by experiment.

2.9.2 Flange Wrinkling in Deep Drawing

During the deep-drawing operation, the compressive hoop stress induced in the flange may exceed a certain critical value causing the flange to collapse into waves or wrinkles. When no blank holder is employed to provide lateral support, the critical blank size is generally too small for practical purposes. The development of wrinkles of large amplitude can be prevented by using a blank holder which exerts a lateral pressure on the blank. The effect of the constraint around the inner boundary may be simulated by assuming the flange to be clamped at this radius and subjected to a line load along the circumference of the mean radius $c = (b+a)/2$. An analysis for the associated elastic bending problem reveals that the load per unit circumference is equal to $\beta E\omega$, where ω is the lateral deflection at the mean radius, and

$$\beta \approx \frac{8I}{(b-a)^4} = \frac{2}{3}\left(\frac{h}{b-a}\right)^3, \quad I = \frac{1}{12}\,(b-a)\,h^3, \tag{2.153}$$

over the relevant range, where E is Young's modulus, and I is the second moment of area of the flange section about a radial line through the center. The analysis of

the flange wrinkling process in the plastic range is most conveniently carried out by the energy method commonly used in the elastic buckling of columns, if we replace Young's modulus E by a mean value of the reduced modulus

$$E_r = \frac{4ET}{\left(\sqrt{E} + \sqrt{T}\right)^2},$$

where T is the tangent modulus at the current state of hardening. The analysis given below is essentially due to Senior (1956), who extended an earlier treatment by Geckeler (1928), for the flange wrinkling process.

The number of waves m in the wrinkled flange is assumed large enough for each half-wave of the segment to be considered as having a length $l = \pi c/m$ measured along the mean radius $r = c$. For simplicity, the transverse displacement w is assumed to be independent of r, the wave form being expressed as

$$\omega = \delta \sin \frac{\pi s}{l} = \delta \sin \frac{ms}{c}, \tag{2.154}$$

where δ is the amplitude of the half-wave, and s is the distance along the mean circumference. If the radial displacement is assumed to vanish during the formation of wrinkles, the strain energy of bending of a typical flange segment into a half-wave is given by

$$U_1 = \frac{1}{2} E_r I \int_0^l \left(\frac{d^2 w}{ds^2}\right)^2 ds = \pi E_r I \left(\frac{\delta^2 m^3}{4c^3}\right),$$

where I is given by (2.153), the current blank thickness h being taken as uniform. For a spring-type blank holder having a stiffness ka, the lateral force acting at the crown of each half-wave is $ka\delta^2/2m$, giving an energy component equal to $ka\delta^2/4m$. In view of the additional lateral force $\beta E_r w$ per unit circumference acting at the mean radius c, the energy stored in the flange segment due to the lateral loading is

$$U_2 = \frac{ka\delta^2}{4m} + \frac{\beta E_r}{2} \int_0^1 w^2 ds = \left(\beta c + \frac{ka}{\pi E_r}\right) \frac{\delta^2}{4m},$$

where β is given by (2.153). Since there are $2m$ half-waves in the wrinkled flange, the total energy of distortion is

$$U = 2m\,(U_1 + U_2) = \frac{\pi}{3} E_r h^3 \delta^2 \left\{ \frac{(b-a)\,m^4}{(b+a)^2} + \frac{b+a}{2\,(b-a)^3} \right\} + \frac{1}{2} ka\delta^2. \tag{2.155}$$

It may be noted in passing that the pressure exerted by the blank holder is confined near the periphery $r = b$, where the flange thickness is actually the greatest.

Since w does not depend on r according to (2.154), no work is done by the radial stress distribution during the wrinkling. To obtain the work done by the hoop stress σ_θ due to the circumferential shortening, it is convenient to take the hoop stress

distribution approximately in the form

$$\sigma_\theta = -\sigma\left(1 - \ln\frac{b}{r}\right), \quad a \le r \le b,$$

where σ denotes the mean uniaxial yield stress at the considered stage of the flange drawing. The required work is therefore given by

$$W = -\frac{1}{2}\iint h\sigma_\theta\left(\frac{1}{r}\frac{dw}{d\theta}\right)^2 r dr\, d\theta.$$

Substituting for σ_θ, and noting that $w = \delta \sin m\theta$ according to (2.154), it is easily shown that

$$W = \frac{\pi}{4}\sigma h m^2 \delta^2\left(2 - \ln\frac{b}{r}\right)\ln\frac{b}{r}.$$

The critical condition for the wrinkling of the flange is $W = U$. In view of (2.155) and the preceding relation for W, this condition furnishes the critical stress in the form

$$\begin{aligned}\frac{\sigma}{E_r}\left(2 - \ln\frac{b}{a}\right)\ln\frac{b}{a} = \frac{2h^2}{3a^2}\left(\frac{b-a}{b+a}\right)\Bigg\{2\left(\frac{ma}{b+a}\right)^2 \\ + \left(\frac{a}{b-a}\right)^4\left(\frac{b+a}{ma}\right)^2\Bigg\} + \frac{2k}{\pi E_r}\left(\frac{a}{hm^2}\right).\end{aligned} \tag{2.156}$$

This is the required relationship between the various physical parameters affecting the wrinkling process. The value of m that makes σ/E_r a minimum, the remaining quantities being given, is easily shown to be

$$m = 0.841\left(\frac{b+a}{b-a}\right)\left\{1 + \frac{3k}{\pi E_r}\left(\frac{a}{b+a}\right)\left(\frac{b-a}{h}\right)^3\right\}^{1/4}. \tag{2.157}$$

It should be noted that E_r is a function of σ and is defined by the stress–strain curve of the material. When the blank holder is absent ($k = 0$), the preceding results reduce to

$$m = 0.841\left(\frac{b+a}{b-a}\right), \quad \frac{E_r h^2}{\sigma a^2} = 0.531\left(\frac{b^2}{a^2} - 1\right)\left(2 - \ln\frac{b}{a}\right)\ln\frac{b}{a}. \tag{2.158}$$

For a given drawing ratio b_0/a, and a given blank holding pressure defined by k, the critical value of σ/E can be calculated from (2.156) for any stage of the drawing using the relation $h = h_0\sqrt{b_0/b}$. The failure by wrinkling will not occur if the corresponding critical value of σ is greater than the actual mean yield stress in the flange, which may be taken as the arithmetic mean of the yield stresses at $r = a$

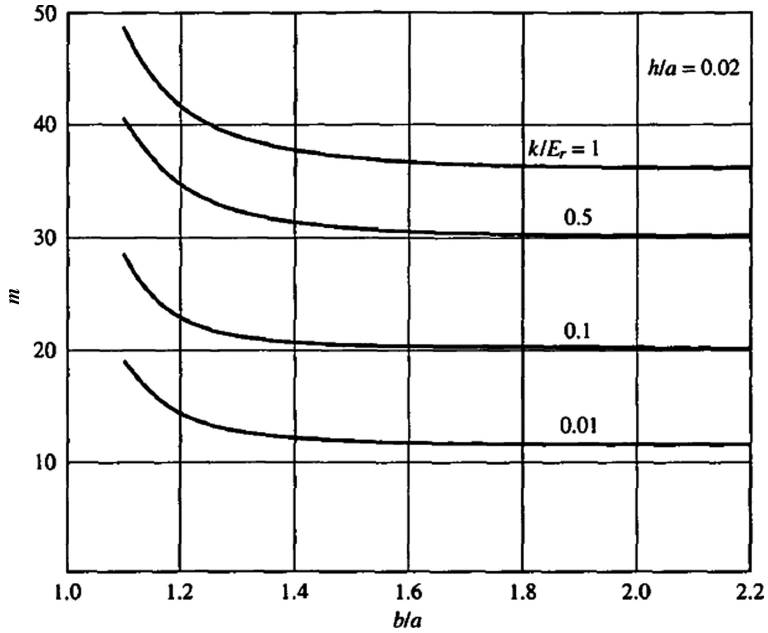

Fig. 2.36 Number of waves in a wrinkled flange as a function of the current radius ratio for different vales of the stiffness parameter

and $r = b$. Figure 2.36 shows the variation of the number of waves of the wrinkled flange with the radius ratio of the flange for various values of the stiffness parameter k/E_r, using a representative value of h/a. The theoretical results are consistent with the observed wrinkling behavior.

The overall effect of the blank holding pressure is to increase the number of waves in the wrinkled flange while reducing their amplitude. In the deep-drawing operation, the number of waves developed by wrinkling should be fairly large so that the wave amplitude is small enough to permit ironing out of the wave tips without unduly raising the punch load. An analysis for flange wrinkling that includes a variation of w with r has been given by Yu and Johnson (1982). A solution based on the consideration of the elastic/plastic bifurcation has been discussed by Chu and Xu (2001). The problem has been treated both analytically and numerically by Carreia et al. (2003). The wrinkling in sheet metal forming has been investigated by Wang and Lee (1989), Hassani and Neale (1991), and Kim et al. (2000).

Problems

2.1 A plane sheet of metal is subjected to biaxial tensile loading in its plane, the strain-hardening exponent of the material being n. Show that the effective strain at the onset

of plastic instability, which occurs when the applied loads attain their maximum, is given by

$$\bar{\varepsilon} = \frac{2n\left(1+3\alpha^2\right)^{3/2}}{1+15\alpha^2}, \quad \alpha = \frac{\sigma_1 - \sigma_2}{\sigma_1 + \sigma_2}$$

Suppose that the load ratio is held constant during the loading, which makes α vary from an initial value α_0. Setting $\lambda_0 = \left(1+3\alpha_0^2\right)^{1/2}$, and assuming a state of plane strain at instability, show that

$$\left(\frac{\lambda_0 - 1}{\lambda_0 + 1}\right)\left(\frac{2+\lambda_0}{2-\lambda_0}\right)^2 = \exp\left(-2\sqrt{3}n\right)$$

Compute the numerical values of λ_0 and α_0 in the special case when $n = 0.3$.

2.2 A square plate, whose sides are of length $2a$, has a central circular hole of radius ρa, and is brought to the yield point state by the application of tensile and compressive stresses, each of magnitude σ, in orthogonal directions normal to the edges. Using the stress discontinuity pattern shown in Fig. A, in which the stresses in regions 4, 5 , and 6 are equal in magnitude but opposite in sign to those in regions 1, 2, and 3 respectively, and assuming $\rho + \xi > 1$, obtain the lower bounds for a Tresca material as

$$\frac{\sigma}{Y} = \frac{(1-\rho)(1-\xi)}{\rho+\xi-1}, \qquad \frac{\xi}{1-\xi} = \frac{2\sqrt{\rho^2+\xi^2}}{\rho+\xi-1}, \ \rho \le 0.48$$

$$\frac{\sigma}{Y} = -\rho + \sqrt{1-2\rho+2\rho^2}, \ 2\xi = 1 + \sqrt{1-2\rho+2\rho^2}, \ \rho \ge 0.48$$

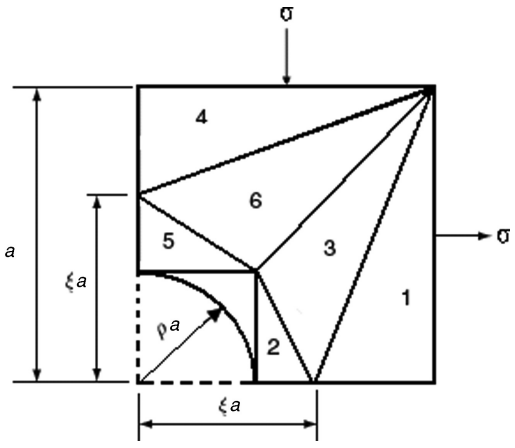

Fig. A

Fig. B

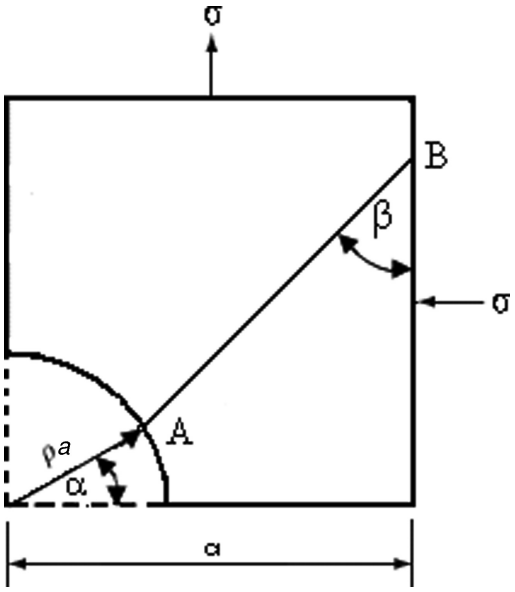

2.3 For sufficiently small values of ρ, a fairly close upper bound solution for the yield point state of the square plate of the preceding problem is obtained by using the velocity discontinuity pattern indicated in Fig. B, where the tangential velocity is discontinuous across the neck *AB*. Assuming the Tresca criterion, show that the best upper bound is given by

$$\frac{2\sigma}{Y} = \frac{1 - \rho\cos\alpha}{\sin 2\beta - \rho\sin\beta\cos(\alpha+\beta)}, \quad \tan\beta = \frac{\sin\alpha}{\cos\alpha - \rho}.$$

$$4\rho\cos^3\alpha - 4\left(1+\rho^2\right)\cos^2\alpha + \rho\left(1+\rho^2\right)\cos\alpha + 2 = 0$$

Verify that for $\rho \geq 0.37$, an improved upper bound is obtained by setting $\lambda = -1$ in (2.71), which coincides with the preceding lower bound for $\rho \geq 0.48$.

2.4 A circular hole in an infinite plate is expanded from zero radius by the application of a uniform radial pressure, the stress–strain curve of the material being given by

$$\sigma = \sigma_0\left[1 - m\exp(-n\varepsilon)\right]$$

where σ_0, m, and n are constants. Show that the work done in expanding the hole to any radius a for a Tresca material is equal to $\pi\ a\ \rho\ h_0\ Y$, where Y is the initial yield stress, h_0 is the initial plate thickness, and ρ is the radius to the rigid/plastic boundary. Using (2.88), show that the formula

$$\frac{a}{\rho} = \frac{1-m}{nm^{2/n}} \ln\left\{\frac{2+(n-2)\,m^{2/n}}{2\left(1-m^{2/n}\right)}\right\}, \quad 2 \le n \le 5$$

is exact for $n = 2$ and $n = 4$ but can be used as a good approximation for other values of n.

2.5 An infinite plate of uniform initial thickness h_0, and containing a circular hole of initial radius a_0, is expanded by the application of an increasing radial pressure p. The material obeys Tresca's yield criterion and its associated flow rule, and strain-hardens according to the law $\sigma = Y \exp(n\varepsilon)$, where n is a constant. Show that the current thickness h in the deformed plate varies with the initial radial distance r_0 according to the formula

$$\frac{h_0}{h} = \frac{1}{2+n}\left\{\left(\frac{\rho}{r_0}\right)^{n/(1+n)} + (1+n)\left(\frac{r_0}{\rho}\right)^{2/(1+n)}\right\}, \quad a \le r \le \rho$$

where ρ is the radius to the rigid/plastic boundary. Denoting the current radius of the hole by a, derive the expression

$$\frac{a}{\rho} = \frac{1}{2+n}\left\{1 + (1+n)\left(\frac{a_0}{\rho}\right)^{(2+n)/(1+n)}\right\}, \quad \frac{1}{2} \le \frac{a}{\rho} \le 1$$

2.6 In the hydrostatic bulging of circular diaphragm using a die aperture of radius a, let the shape of the bulge at each stage be assumed as a spherical cap of angular span equal to 2α. Show that this assumption is consistent with Tresca's associated flow rule for an arbitrary strain-hardening characteristic of the material when the thickness of the bulge is uniform at each stage. Obtain the associated strain distribution in the form

$$\varepsilon_\theta = \frac{1}{2}\ln\left(\frac{1+\cos\phi}{1+\cos\alpha}\right) \quad \varepsilon_\phi = \frac{1}{2}\ln\left\{\left(\frac{2}{1+\cos\alpha}\right)\left(\frac{2}{1+\cos\phi}\right)\right\}$$

Verify that the magnitude of the polar thickness strain is exactly one-half of that given by (2.125). Derive the expressions for the associated strain rates at a generic stage of the bulge, using the angle α as the time scale.

2.7 In the radial drawing of a circular blank, it is generally a good approximation to assume the total effective strain ε at any radius as equal to the magnitude of the hoop strain, which is given by equation (2.133). If the material yields according to the modified Tresca criterion, and strain-hardens according to the power law $\sigma = \sigma_0 \varepsilon^n$, show that the radial drawing stress at any stage is given by

$$\frac{\sigma_a}{\sigma_0} = m\int_{\varepsilon_b}^{\varepsilon_a} \frac{\varepsilon^n d\varepsilon}{1-\sqrt{\beta}\exp(-2\varepsilon)}, \quad \beta = \frac{b_0}{b}$$

where $\varepsilon_b = \ln(b_0/b)$, and ε_a follows from (2.133). Obtain a graphical plot of the ratio σ_a/σ_0 against $1 - b/b_0$ when $b_0/a = 2$, using $m = 1.1$ and $n = 0.1$, 0.3, and 0.5.

2.8 For determining the paths of the particles in the radial drawing of a circular blank, a good overall approximation is achieved by writing $dr/r = -d\rho/\rho$, where $\rho = \ln(b/r)$. Show that the thickness variation based on this approximation for the Tresca criterion is given by

$$\frac{h}{h_0} = \left(\frac{\rho}{\rho_0}\right)^{1/2} \left(\frac{2-\rho}{2-\rho_0}\right)^{3/2}, \quad \frac{r_0^2}{b_0^2} = 1 - \left(\frac{b}{b_0}\right)^{3/2} \left(1 - \frac{r^2}{b^2}\right)$$

where $\rho_0 = \ln(b_0/r_0)$, the last equation being based on the assumption of a uniform blank thickness at each stage. Taking $b_0/a = 2$, make a graphical comparison of the variation of h_a/h_0 with $1 - b/b_0$ given by the preceding relations with that predicted by the more exact solution based on the Tresca criterion presented in Section 2.7 (ii).

2.9 Consider a thin plate in the form of a ring sector defined by concentric circular arcs of radii a and b, where $b > a$. The plate is brought to the yield point state by the application of terminal couples that tend to increase the curvature. The radial and hoop stresses may be expressed in the form

$$\sigma_r = 2k \sin\alpha. \quad \sigma_\theta = \pm 2k \cos\left(\frac{\pi}{6} \mp \alpha\right)$$

which satisfies the von Mises yield criterion parametrically through α. The upper sign applies to $r \le c$, and the lower sign to $r \ge c$, where c is the radius to the neutral surface which corresponds to $\alpha = \alpha_0$. Using the equilibrium equation, show that

$$\frac{b^2}{c^2} = \frac{2}{\sqrt{3}} \cos\left(\frac{\pi}{6} - \alpha_0\right) \exp\left(\sqrt{3}\alpha_0\right), \quad \frac{c^2}{ab} = \left(1 - \frac{4}{3}\sin^2\alpha_0\right)^{-1/2}$$

2.10 For usual values of the b/a ratio in the preceding problem, the auxiliary angle α is fairly small, so that α^2 is generally negligible compared to unity. Show that the value of α at $r = c$, and the associated yield couple M_0, is given approximately by

$$\alpha_0 = \frac{\sqrt{3}}{4} \ln\left(\frac{b}{a}\right), \quad \frac{c^2}{ab} \approx 1 + \frac{1}{8}\left(\ln\frac{b}{a}\right)^2, \quad M_0 \equiv \frac{\sqrt{3}}{4} kh\,(b-a)^2$$

The last expression may be obtained by taking the hoop stress distribution approximately as

$$\sigma_\theta = k\left(\sqrt{3} + \alpha\right), \quad a \le r \le c; \quad \sigma_\theta = -k\left(\sqrt{3} - \alpha\right), \quad c \le r \le b$$

where α in the two regions is expressed in the way similar to that for α_0 .

http://www.springer.com/978-0-387-77673-6

Applied Plasticity, Second Edition
Chakrabarty, J.
2010, XVIII, 756 p., Hardcover
ISBN: 978-0-387-77673-6